INSTITUTE
OF HUMAN GENETICS
POLISH ACADEMY OF SCIENCES

mgr Agnieszka Nadel

The establishment of human iPSCs -derived chamber-specific Engineered Heart Tissues for deciphering the cardiac development and for pharmacological studies

Doctoral dissertation was conducted at

The Institute of Human Genetics PAS

Department of Molecular Pathology

Under supervision of

dr hab. n. med. i n. o zdr. Tomasz Kolanowski

Poznań, 2024

I would like to thank my supervisor, dr hab. n. med. Tomasz Kolanowski for support and guidance during my scientific development - a friendly atmosphere in which I could admit my mistakes and doubts, and meetings/calls on the way, after which I left with the attitude "I can do it!". Thank you also for introducing me to tissue engineering and organ-on-chip technology.

Furthermore, I would like to thank the Molecular Pathology team and the head of the Department - dr hab. n. med. Natalia Rozwadowska, for all the help and support. Especially: mgr Agata Barszcz, dr n. med. i n. o zdr. Marta Kasprzyk, dr n. biol. Weronika Sura for endless supplies of chocolates, mugs of tea, and motivation to act (when the experiments were falling). Also, former members of FIBROdrive team - dr Ewelina Kalużna and mgr Katarzyna Hubert, for countless hours at Dziupla (C21) in an amiable atmosphere.

I would also like to acknowledge members of my PhD Advisory Board: dr hab. n. med. Natalia Rozwadowska and dr hab. n. med. Urszula Mackiewicz, prof. CMKP for all comments and suggestions always in an incredibly friendly atmosphere.

Lastly, to my wonderful family and friends, I owe a debt of gratitude for being the pillars of support during my moments of doubt. Your belief in my potential has been a driving force behind my accomplishments. There are no words to express my gratitude.

I want to dedicate my doctoral thesis to my grandfather - Mirosław Markiewicz, who fervently believed in my journey to become a doctor. I wish you could see it.

FUNDING

This research was funded by the National Science Centre, Poland: grant no. 2018/31/D/NZ3/01719 (awarded to T. J. Kolanowski)

TABLE OF CONTENTS

ABBREVIATIONS

α-MHC - α-myosin heavy chain, protein

α-SMA - smooth muscle actin, protein

β-MHC - β-myosin heavy chain, protein

AERP - atrial effective refractory period

APD - action potential duration

ARL6IP5 - Ribosylation Factor Like GTPase 6 Interacting Protein 5, protein

AV - atrioventricular node

BSA - Bovine Serum Albumin

BPM - beats per minute

cDNA - complementary DNA

CFs - cardiac fibroblasts

chEHT – chamber-specific Engineered Heart Tissue comprising of chamber-specific cardiomyocytes and fibroblasts

CMs - cardiomyocytes

c-MYC - MYC Proto-Oncogene, BHLH Transcription Factor, gene

CVDs - cardiovascular diseases

cTNT - Cardiac troponin T, protein

Cx43 - connexin 43, protein encoded by *GJA1* gene

Cx45 - connexin 45, protein encoded by *GJC1* gene

DEG - differentially expressed genes

EB - embryoid body

EC_{50} - half maximal effective concentration

ECM - extracellular matrix

EGTA - Ethylene glycol-bis (2-aminoethylether)-N, N, N’, N'-tetraacetic acid

EHT - Engineered Heart Tissue

EMT - epithelial-to-mesenchymal transition

EndoMT - endothelial-to-mesenchymal transition

EPDCs - epicardium-derived cells

FAK - focal adhesion kinase

FOC – the force of contraction

GO - Gene Ontology

HEY1 - Hes Related Family BHLH Transcription Factor with YRPW Motif 1

HEY2 - Hes Related Family BHLH Transcription Factor with YRPW Motif 2

IC_{50} - half maximal inhibitory concentration

ISO - isoprenaline

iPSCs - induced pluripotent stem cells

GJA1 - gap junction protein alpha 1, gene coding Cx43 protein

GJC1 - gap Junction Protein Gamma 1, gene coding Cx45 protein

gDNA - genomic DNA

hiPSCs – human-induced pluripotent stem cells

KCNA5 - Potassium Voltage-Gated Channel Subfamily A Member 5, gene

KCNJ3/5 - Potassium Inwardly Rectifying Channel Subfamily J Member 3/5, gene

KEGG - The Kyoto Encyclopedia of Genes and Genomes

KLF4 - Kruppel-like factor 4, gene

MLC2a - Myosin Light Chain 2 atrial, protein encoded by *MYL7* gene

MLC2v - Myosin Light Chain 2 ventricular, protein encoded by*MYL2*gene

MYL2 - Myosin Light Chain 2, gene coding MLC2vprotein

MYL7 - Myosin Light Chain 7, gene coding MLC2aprotein

MYH6 - myosin heavy chain 6, gene

MYH7 - myosin heavy chain 7, gene

OCT4 – octamer-binding transcription factor 4, gene

OXPHOS - oxidative phosphorylation

PCA - principal component analysis

RA - retinoic acid

RMP - resting membrane potential

ROCK-Rho - associated coiled-coil containing protein kinase

SA - sinoatrial node

SK2 - small conductance calcium-activated potassium channels, gene

SOX2 - SRY (sex determining region Y)-box 2, gene

SFBM - serum-free basal medium

SFMM - serum-free maturation medium

STAR - spliced transcripts alignmentTGF-β - Transforming growth factor beta, protein

TNNI3 - troponin I3, gene

TRP - transient receptor potential channels, protein

qRT-PCR - Quantitative Real-Time Polymerase Chain Reaction

WHO - World Health Organization

VGCC - voltage-gated calcium channel

STRESZCZENIE

Zgodnie z najnowszymi statystykami WHO, choroby układu sercowo - naczyniowego, są główną przyczyną śmierci, przyczyniającą się do około 18,6 miliona zgonów rocznie. Ze względu na narastający problem, aby zapewnić nowe metody leczenia, kluczowe jest zrozumienie przyczyn chorób i tego, stąd konieczne jest opracowanie odpowiedniego modelu ludzkiego.

Jednym z najbardziej zaawansowanych modeli sercowych jest makroskopowy model serca (ang. Engineered Heart Tissue, EHT) o strukturze i funkcji podobnej do prawdziwej tkanki sercowej. Składa się on z kardiomiocytów, fibroblastów oraz macierzy zewnątrzkomórkowej i umożliwia zaawansowaną ocenę czynności i fizjologii tkanek sercowych *in vitro*.

W niniejszej pracy skupiliśmy się na realizacji 3 celów: 1) zwiększenia stopnia zaawansowania modelu poprzez utworzenie, komorowo-specyficznego EHT (chEHT, ang. chamber-specifc Engineered Heart Tissue), 2) potwierdzeniu przydatności wcześniej opracowanego modelu chEHT do testowania leku (AP14145) o znanej aktywności klinicznej, specyficznej dla przedsionków serca, oraz 3) udowodnieniu wpływu fibroblastów sercowych na różnicowanie kardiomiocytów w kierunku przedsionkowym i komorowym z wykorzystaniem modelu EHT.

Pierwszy etap naszych badań skutkował opracowaniem metodologii wykorzystania w pełni komorowo-specyficznego modelu tkankowego chEHT, jest on znaczącym postępem w dotychczas wykorzystywanych modelach tkankowych i pozwala na odwzorowanie funkcjonalnych różnic między przedsionkami i komorami serca, w tym częstotliwości czy czasu trwania skurczu.

W drugim etapie, udowodniono, iż przedsionkowy chEHT różni się od komorowego chEHT nie tylko ekspresją genów i parametrami fizjologicznymi, ale również pozwala na różnicowanie funkcjonalne obu typów tkanek. Wykorzystano w tym celu przedsionkowo-specyficzny inhibitor kanałów potasowych zależnych od wapnia – AP14145. Specyficzność przedsionkowa AP14145 nie została udowodniona w niektórych

modelach zwierzęcych, co wskazuje na lepsze odwzorowanie fizjologii serca człowieka przez opracowany model.

Mechanizmy leżące u podstaw terminalnego różnicowania serca człowieka wciąż pozostają niejasne. Jedna z hipotez sugeruje, że kluczową rolę w tym procesie odgrywają fibroblasty sercowe, choć nie zostało to dotychczas udowodnione. Model EHT miał na celu określenie czy fibroblasty sercowe kierunkują końcowe etapy różnicowania kardiomiocytów w podtypy przedsionkowe i komorowe. Podczas naszych badań zaobserwowaliśmy, że fibroblasty przedsionkowe mogą wpływać na różnicowanie i zmieniać charakterystykę kardiomiocytów komorowych w kierunku fenotypu kardiomiocytów przedsionkowych.

Podsumowując, przeprowadzone doświadczenia pozwoliły na opracowanie i zademonstrowanie potencjału komorowo-specyficznego modelu chEHT w badaniach farmakologicznych oraz w badaniach biologii serca. Model EHT zapewnia unikalną platformę do badania mikrośrodowiska komórkowego oraz interakcji międzykomórkowych, wspierając strukturalną i funkcjonalną dojrzałość kardiomiocytów. Nasze wyniki sugerują, że fibroblasty sercowe odgrywają znaczącą rolę w terminalnym różnicowaniu kardiomiocytów, podkreślając znaczenie modelu EHT w poszerzaniu wiedzy na temat rozwoju serca i mechanizmów chorób układu sercowo-naczyniowego.

ABSTRACT

According to the latest WHO statistics, cardiovascular diseases are the leading cause of death, contributing to approximately 18.6 million deaths annually. Due to the growing problem, it is crucial to understand the causes of these diseases in order to provide new treatment methods. The development of an appropriate human model is necessary.

One of the most advanced heart models is Engineered Heart Tissue (EHT) with a structure and function similar to real cardiac tissue. It consists of cardiomyocytes, fibroblasts, and extracellular matrix, enables advanced assessment of cardiac tissue function and physiology *in vitro*.

In this study, we focused to achieve three aims: 1) to enhance the model by creating a chamber-specific EHT (chEHT), 2) to confirm the usefulness of the previously developed chEHT model for testing a drug (AP14145) with known clinical activity specific to the atria, and 3) to prove cardiac fibroblasts influence on the differentiation of cardiomyocytes towards atrial and ventricular, using the EHT model.

The first part of our research resulted in the development of the methodology for using a fully chamber-specific tissue model, chEHT, which represents a significant advancement over previously used tissue models. It allows for the replication of functional differences between the atria and ventricles of the heart, including contraction frequency and duration.

In the second part, we demonstrated that atrial chEHT differs from ventricular chEHT not only in gene expression and physiological parameters but also allows for the functional differentiation of both tissue types. This was achieved using the atrial-specific inhibitor of calcium-activated potassium channels – AP14145. The atrial specificity of AP14145 had not been demonstrated in some animal models, which indicates a better representation of human heart physiology by the developed model.

The mechanisms underlying the terminal differentiation of the human heart are still unclear. One hypothesis suggests that cardiac fibroblasts play a key role in this process, although this has not yet been proven. The EHT model aimed to determine whether cardiac fibroblasts direct the final stages of cardiomyocyte differentiation into atrial and ventricular subtypes. During our research, we observed that atrial fibroblasts can

influence the differentiation and change the characteristics of ventricular cardiomyocytes towards an atrial cardiomyocyte phenotype.

In conclusion, the conducted experiments allowed us to develop and demonstrate the potential of the ventricular-specific chEHT model in pharmacological and in cardiac biology studies. The EHT model provides a unique platform for studying the cellular microenvironment and intercellular interactions, supporting the structural and functional maturation of cardiomyocytes. Our results suggest that cardiac fibroblasts play a significant role in terminal differentiation of cardiomyocytes, highlighting the importance of the EHT model in expanding our knowledge of heart development and mechanisms of cardiovascular diseases.

In conclusion, the conducted experiments allowed for the development and demonstration of the potential of the chamber-specific chEHT model in pharmacological studies and heart biology studies. The EHT model provides a unique platform for studying the cellular microenvironment and intercellular interactions, supporting the structural and functional maturation of cardiomyocytes. Our results suggest that cardiac fibroblasts play a significant role in the terminal differentiation of cardiomyocytes, highlighting the importance of the EHT model in expanding our understanding of heart development and the mechanisms of cardiovascular diseases.

1. INTRODUCTION

1.1. Cardiovascular diseases as the global problem

Cardiovascular diseases (CVDs) are a group of disorders of the heart and blood vessels, commonly referring to various types of conditions, among others: stroke, heart failure, arrhythmias, heart valve disease and atherosclerosis. According to the World Health Organization (WHO) (World Health Organization, 2021). CVDs are the leading cause of global death. An estimated 19.9 million people died from CVDs in 2021, reflecting a 72% increase compared to 1990 (Martin et al., 2024). All the available statistics, present CVD as a significant global problem, which is likely to continue to increase due to multiple factors such as population growth, ageing, and lifestyle changes. Therefore, to improve the effectiveness of the treatment, it is important to understand better the causes underlying CVDs.

1.2. The complexity of the human heart

The human heart is an essential organ maintaining blood circulation and is responsible for delivering oxygen and nutrients to all parts of the organism. It contracts approximately 2.5 billion times over a lifetime (Shaffer *et al.*, 2014) and can pump 5 - 6 liters of blood per minute (Joyner & Casey, 2015). Such an unusual and efficiently designed pump consists of numerous structures and shows unique muscle-related features.

1.2.1. General structure of human heart

The heart of mammals consists of four chambers - the right and left atrium and the right and left ventricle (Tirziu *et al.*, 2010).

The atria are responsible for receiving blood from either the lungs or the rest of the body, while the ventricles are responsible for pumping blood out to these areas. To ensure proper circulation, the heart also contains four valves - the tricuspid and pulmonary valves on the right side, and the mitral and aortic valves on the left side. They

prevent the backflow of blood by opening and closing in response to pressure changes (Buckberg *et al.*, 2018).

1.2.2. Components of myocardium

The human heart wall is composed of three layers: the epicardium (outer layer), the myocardium (middle layer), and the endocardium (inner layer lining the heart chambers) (Iaizzo, 2005).

As the thickest layer, the myocardium is responsible for generating the force needed for heart contractions. While cardiomyocytes are considered the key functional cell type within the myocardium, they are not the only cells found in the heart. The myocardium also includes cardiac fibroblasts, which are located in between cardiomyocytes, endothelial cells, smooth muscle cells, and others, contributing to its complex microenvironment (Herum *et al.*, 2017) (Figure 1).

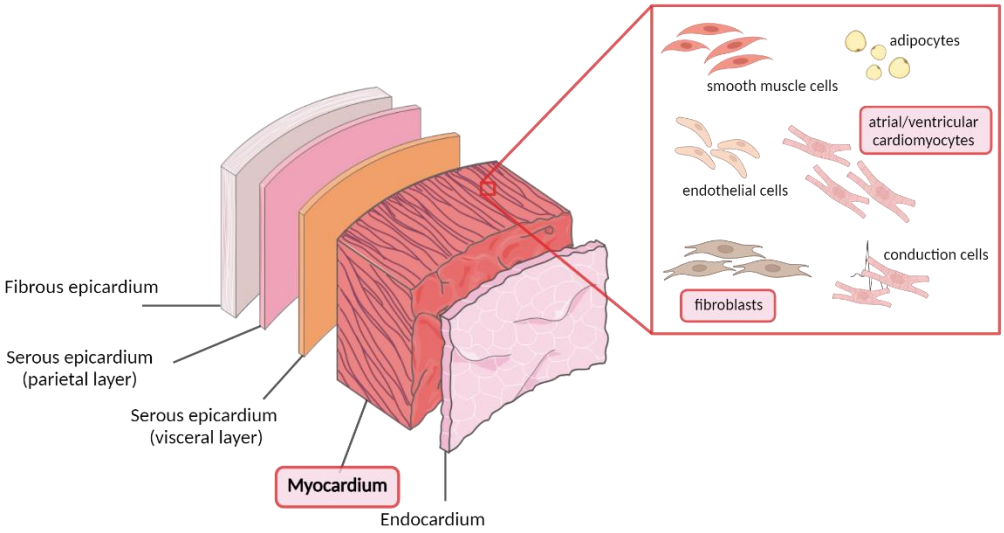

Figure 1 Heart wall structure. Heart walls consist of three main layers: epicardium, myocardium, and endocardium. The thicker layer- myocardium is composed from variety of cells, however the majority obtained: cardiomyocytes and cardiac fibroblasts. Modified from (Id *et al.*, 2022). Created with BioRender.com.

1.2.3. Sarcomere

The sarcomere is the basic unit of a heart muscle cell and is key to heart muscle contraction. It is composed of organized filaments - actin and myosin, that slide between each other. Troponin regulates the formation of cross-bridges between these filaments in response to calcium levels.

As actin and myosin slide together, the sarcomere shortens, and as a consequence, generates the force needed for heart contraction (Crocini, 2021).

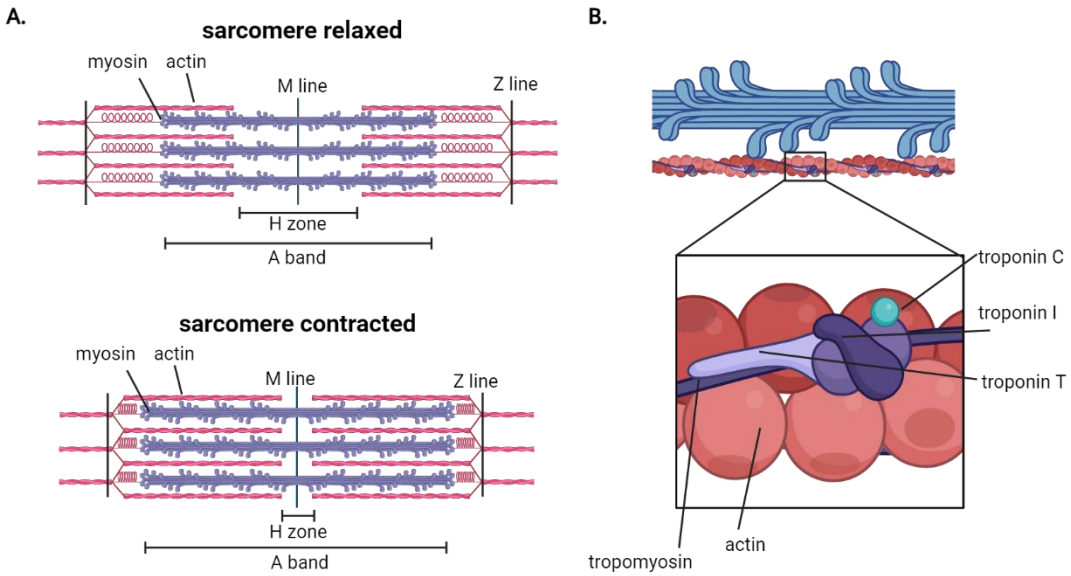

Figure 2 Sarcomere structure. A. It consists of organized filaments of actin and myosin that slide between each other during contraction. B. Troponin is a complex of three proteins (troponin C, troponin I, and troponin T) that is part of the actin filament. Modified from (Crocini, 2021). Created with BioRender.com.

1.2.4. Cardiac conduction system – action potential propagation

1.2.4.1. Signal propagation in the heart

Heart possesses a signal automatization, which means that it is independent from nervous system to produce signals for contraction. The system responsible for controlling the synchronous contraction force of the heart is called cardiac conduction system (Figure 3A). The electrical signals originate in the upper part of the right atrium, in the sinoatrial (SA) node. The SA node is a group of cells, which act as the natural pacemaker of the heart. They are producing regular electrical impulses that spread through the atria, into deeper parts of the atrium and heart, at the end causing the heart contraction. Signal propagation in the atrium is dependent upon not - well defined cells and multiple paths, though any damages in the atrial tissue is often a cause for abnormalities in contractility pattern which can lead to atrial fibrillation (AF) (Nattel, 2002).

Next, impulses pass through the atrioventricular (AV) node, which is an organized structure located at the base of the right atrium. By delaying the electrical impulses before further way to the ventricles, AV ensures that atria have fully contracted and pumped all the blood into the relaxed ventricles.

After the ventricles are filled, the contraction is possible thanks to electrical impulses transmission through a bundle of His and Purkinje fibers consisting of modified cardiomyocytes with fast signal transduction velocities (Maass *et al.*, 2015). The ventricles contract and the blood is pumped out from the heart into the circulatory system (Park & Fishman, 2014).

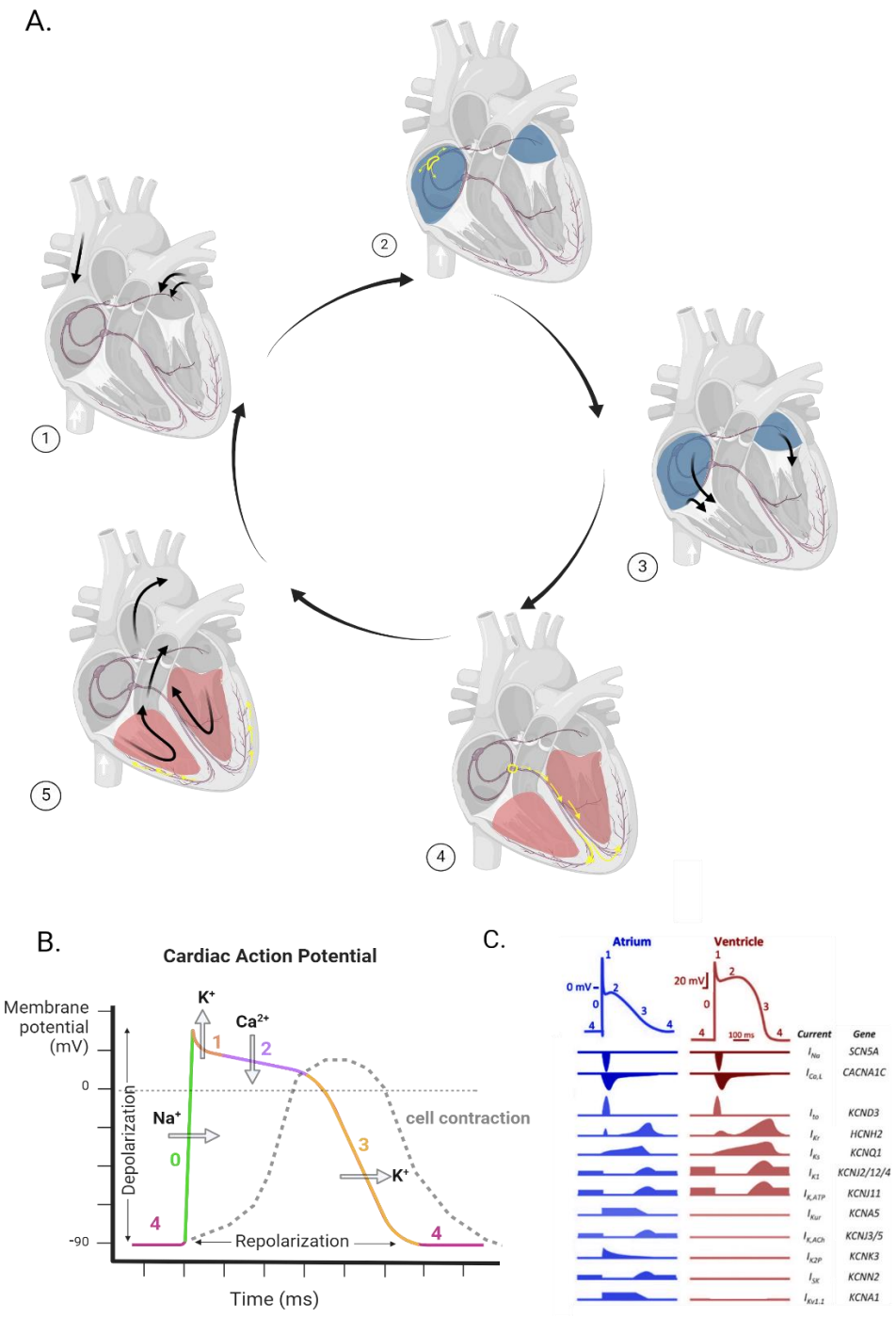

Figure 3 Propagation of action potential in the cardiac conduction system. A. (1) The SA node and the rest of the conduction system are in a resting state, (2) The SA node initiates an action potential that spreads across the atria, (3) The impulse reaches AV node and allows for complete atrial contraction, (4) The impulse travels through the AV bundle and bundle branches to the Purkinje fibers, (5) The impulse spreads to the contractile fibers of the ventricle. Ventricular contraction begins. Modified from (Park & Fishman, 2014). B. Cardiac action potential is a sequence of ion movements across the cell membrane that results in the depolarization and repolarization of cardiac cells. Modified from (Santana et al., 2010). C. Differences in the ion

channels activity of atrial and ventricular cardiomyocytes, determine their unique action potential. Modified from (Grant, 2009; Shaffer *et al.*, 2014; Voigt & Dobrev, 2016). Created with BioRender.com.

1.2.4.2. Molecular mechanisms of the action potential propagation in cardiomyocyte subtypes

This electrical system is a network of more - or less - specialized cells which generate and conduct electrical signals (Munshi, 2012). Brief and reversible changes in a potential (voltage) across the cardiomyocytes cell membrane, which lead to CM contraction is known as an action potential (Figure 3B). Depending on the location in the heart, the action potential dynamics have a chamber or cell-specific pattern (Santana *et al.*, 2010). Below, a subtype-specific biology of the action potential has been described.

Pacemaker's cardiomyocytes (which initiate the heartbeat):

- Phase 0 (Depolarization Phase): Triggered by the opening of voltage-gated calcium channels (Ca^{2+}), leading to a rapid influx of calcium ions, causing depolarization. No distinct sodium channels are involved here, unlike other cardiac cells (Pinnell *et al.*, 2007);
- Phase 1: (Repolarization Phase): Absent (Baruscotti *et al.*, 2010);
- Phase 2 (Plateau Phase): Absent (Baruscotti *et al.*, 2010);
- Phase 3 (Repolarization Phase): Calcium channels close, and potassium channels open, allowing potassium ions to leave the cell, restoring the membrane potential;
- Phase 4 (Resting Phase): Slow depolarization occurs due to the "funny" current (mixed sodium and potassium ions), gradually bringing the membrane potential closer to the threshold for the next action potential (Pinnell *et al.*, 2007).

Atrial Cardiomyocytes (which contract to pump blood from the atria to the ventricles) (Figure 3C):

- Phase 0 (Depolarization Phase): Sodium channels open, allowing a rapid influx of Na^{+}, causing the membrane potential to become positive quickly;

- Phase 1 (Repolarization Phase): The opening of transient potassium channels, leading to a small outward flow of K^+;
- Phase 2 (Plateau Phase): A balance between the inward flow of calcium ions through calcium channels and the outward flow of potassium ions maintains the membrane potential;
- Phase 3 (Rapid Repolarization): Calcium channels close, while potassium channels remain open, allowing K^+ to leave the cell, which restores the membrane potential;
- Phase 4 (Resting Phase): The membrane potential stabilizes as the ion balance between inside and outside the cell is maintained (Ehra et al., 2016).

Ventricular Cardiomyocytes (which pump blood from the heart) (Figure 3C):

- Phase 0 (Depolarization Phase): Voltage-gated sodium channels open, causing a rapid influx of sodium ions, leading to a sharp rise in membrane potential;
- Phase 1 (Early Repolarization): Short-term potassium channels open, allowing K^+ to exit the cell, leading to partial repolarization;
- Phase 2 (Plateau Phase): A prolonged phase where inward calcium currents (Ca2+) balance the outward potassium currents (K^+), maintaining the membrane potential and allowing sustained contraction;
- Phase 3 (Rapid Repolarization): The calcium channels close, and the potassium channels open, causing a rapid outward flow of K+ and bringing the cell back to its resting membrane potential;
- Phase 4 (Resting Phase): The cell reaches its resting membrane potential due to the equilibrium between ion inflow and outflow, remaining stable until the next depolarization (Ehra et al., 2016).

1.2.5. Atrial and ventricular cardiomyocytes

Based on the location and function in the human heart, different types of cardiomyocytes can be distinguished. While all cardiomyocytes have similar basic structures and functions, there are some discrete differences between the chamber-specific cardiac cells.

For instance, ventricular cardiomyocytes are larger and can generate more force than atrial (Nakano *et al.*, 2012), as the left ventricle needs to pump blood all over the body. Also, the pattern of electrical conduction, and as a consequence - contraction is different due to the specific distribution of gap junctions and ion channels.

The differences between atrial and ventricle cardiomyocytes could be divided into three levels: regulatory network, structural and electrophysiological features.

The expression profile of transcription factors that are involved in the regulation of cardiac development and function is chamber-specific. Hes Related Family BHLH Transcription Factor With YRPW Motif 1 (*HEY1*) and Motif 2 (*HEY2*) have distinct expression patterns in different regions of the heart (Ihara *et al.*, 2020). Both *HEY1* and *HEY2* have been shown to regulate the expression of genes involved in cardiac development, such as transcription factors, structural proteins and ion channels. However, *HEY1* is preferentially expressed in the atria, while *HEY2* is highly expressed in the ventricles (Watanabe *et al.*, 2020, 2023).

Other examples are Myosin light chain 2 isoforms, specific for atrial - MLC2a (also known as *MYL2A*, *MYL7*) and ventricular – MLC2v (also known as *MYL2*) cardiomyocytes (Bizy *et al.*, 2013) that show structural differences between CMs subtypes. Myosin light chain 2 (MLC2) protein is a component of the thick filament in sarcomeres, which is responsible for myosin-actin filaments interactions and, as a consequence, plays an important role in the contractile apparatus of cardiac muscle. In all fetal cardiomyocytes - atrial and ventricular, mainly the *MYL7* is expressed, however within the maturation process, *MYL7* becomes dedicated to atrial cardiomyocytes, and in mature ventricular cardiomyocytes it switches to *MYL2* isoform (Guo & Pu, 2020).

Further examples of differences on the structural level are genes coding myosin heavy chain (MHC) a major contractile protein in cardiac muscle e.g. *MYH6* and *MYH7* genes. *MYH6* encodes for the alpha isoform of MHC (α-MHC), while *MYH7* encodes for the beta isoform of MHC (β-MHC) (England & Loughna, 2013). *MYH6* and *MYH7* are expressed in different areas of the heart. *MYH6* is predominantly expressed in the atria, while *MYH7* is predominantly expressed in the ventricles (Razmara & Garshasbi, 2018; Walklate *et al.*, 2021; Warkman *et al.*, 2012). The differences between *MYH6* and *MYH7* are not only

in their expression patterns but also in functional properties. For instance, β-MHC might affects physiological processes beyond muscle contraction - slower action potential duration (APD) and generate a larger force, compared to α-MHC, which may reflect the physiological differences between atria and ventricles (Barrick & Greenberg, 2021).

On top of that, MHC expression pattern reflects the developmental changes that occur during growth and maturation in heart. *MYH6* is expressed in the myocardium during early cardiac development and decreases within the time in the ventricles, to be replaced by *MYH7*. After birth, *MYH6* remains dominant atrial isoform (Anfinson *et al.*, 2022).

The crucial difference between chamber-specific cardiomyocytes is based on electrophysiological properties shown in alternate ion channels expression, which activity is reflected in the action potential (Figure 3C). Among them, KCNJ3/5 can be mentioned:

- KCNJ3/5, also known as the inward rectifier potassium channels - ion channels which allow the flow of potassium ions into the cell. They are primarily expressed in atrial cardiomyocytes and help to maintain the resting membrane potential of these cells (Yamada *et al.*, 2019);
- KCNA5, also known as the voltage-gated potassium channel $K_v1.5$ - another type of ion channel that regulates the flow of potassium ions across the cell membrane. Specific for atrial cardiomyocytes (Marczenke *et al.*, 2017);
- SK2, also known as the small-conductance calcium-activated potassium channel - a type of ion channel that is activated by increases in intracellular calcium levels. Recently presented as a target for atrial fibrillation treatment in many animal models (Weisbrod, 2020);
- Cav1.2, also known as voltage - gated L-type calcium channel, is involved promoting muscle contraction, by regulating influx of calcium ions during the plateau phase. In ventricular cardiomyocytes, Cav1.2 is the sole voltage-gated calcium channel (VGCC) responsible for calcium currents. However, in atrial cardiomyocytes, both Cav1.2 and Cav1.3 channels are expressed (Harvey & Hell, 2013).

CMs biology alterations influence the function of the heart chambers. Those differences are crucial for the distinct contractile properties of the atria and ventricles. However, cardiomyocytes are not the only chamber-specific cell population.

1.2.6. Cardiac fibroblasts

Cardiac fibroblasts (CFs) are non-muscle cell population with mesenchymal phenotype, which plays a crucial role in functional integrity of human heart and maintenance of the extracellular matrix (ECM). By producing proteins such a as collagen, fibronectin, and laminin, CFs provide structural tissue coherence, support and the heart tissue elasticity (Hall, Gehmlich, Denning, et al., 2021; Manabe et al., 2002).

Cardiac fibroblasts can also modulate the electrophysiology of the heart. Primarily, CFs are presented as an insulator for cardiomyocytes, presented as 'zero-coupled' state. However, it was proven that they are possible to remain as a passive load in 'one-sided coupled' state or as a passive conductor of electrical activity 'two-sided coupled' (Ongstad & Kohl, 2016). This CF-CM coupling is possible by expressing define types of connexins, connexin 43 (Cx43, encoded by *GJA1*) and connexin 45 (Cx45, encoded by *GJC1*). Thanks to gap junction formation CFs can couple with CMs (Vasquez *et al.*, 2011).

CFs are able to sense and respond to mechanical stimuli within the cardiac tissue through specialized mechanosensitive proteins, among others: integrins, focal adhesion kinase (FAK), talin or transient receptor potential (TRP) channels. These sensors are associated with the cytoskeleton or presented on cell surface and activate signaling pathways, regulating the diversity of processes, including ECM modeling, gene expression or protein synthesis (Pesce *et al.*, 2022).

Cardiac fibroblasts can also play a crucial role in heart repair and wound healing while transformed into activated form of contractile myofibroblasts while expressing the smooth muscle actin (α-SMA) (Hall, Gehmlich, Denning, et al., 2021). CFs are involved in the inflammatory response, promote proliferation of other cells and angiogenesis by cytokines and grow factors. This makes the wound more flexible and reduces the consequences associated with a fibrotic structure of healed tissue.

One of the classifications of cardiac fibroblasts consider chamber-specificity. Similar to CMs, there can be recognized atrial and ventricular fibroblasts. The differences can be

indicated in terms of morphology (atrial are smaller) or ion channels and ECM components expression (Thomsen & Calloe, 2016), further differentiating chamber functionalities. In particular, it have been shown, that presence of inward rectifier K^+ current, voltage-dependent outward K^+ current and non-selective cation current in ventricular fibroblasts might influence their resting membrane potential (Vasquez *et al.*, 2011). On the other hand, the depolarization or repolarization of the resting membrane potential in atrial fibroblasts depends on compression or stretching of the mechano-dependent cation channels (Kamkin *et al.*, 2003). These differences implicate that atrial and ventricular fibroblasts might have specific functions and contribute differently to the heart chambers electrophysiology and mechanical properties.

Another difference is the expression of extracellular matrix components. Ventricular fibroblasts produce more collagen type I, fibronectin and fibrillin than atrial fibroblasts. Atrial fibroblasts indicates higher expression of fibulin and collagen type IV (Litviňuková *et al.*, 2020). Different ECM compositions in the heart lead to distinct mechanical properties - being stiffer for forceful pumping in ventricles and compliant for blood filling in atria.

Differences in chamber-specific CFs may play a crucial role in shaping the tissue's mechanical and structural characteristics. The enhanced production of collagen type I by ventricular CFs contributes to the increased stiffness of the ventricular chambers. Meanwhile, the elevated fibulin levels in atrial fibroblasts may enhance the elasticity of the atrial tissue (Burstein et al., 2008; Papke & Yanagisawa, 2015; Querejeta et al., 2004).

Overall, cardiac fibroblasts are essential for maintaining the structure and function of the heart. Understanding their role is essential for identifying the mechanisms underlying both cardiac development and pathological changes in heart tissue.

1.2.7. Origins of fibroblasts during heart development

The origins of cardiac fibroblasts remain a topic of ongoing research. It is well known that fibroblasts arise from the epicardium during development, however there is evidence that suggests alternative sources also exist. For now, we believe that CFs are derived from three different pools of progenitor cells:

- 80% from epicardial cells, located on the outermost layer of the heart and give rise, among others: fibroblasts, smooth muscle cells, and endothelial cells;
- 18% from endocardial cells, located in the innermost layer of the heart;
- 2% from neural crest, located in outflow region of the heart and also contribute to the valve mesenchyme (Doppler *et al.*, 2017; Moore - Morris *et al.*, 2014).

The epicardium arises from a transient extra-cardiac cell cluster known as the proepicardial organ (PEO). It forms as an outgrowth of the coelomic mesothelium at the ventro-caudal base of the developing heart. By embryonic day 10.5 in mice, proepicardial cells migrate and cover the entire embryonic myocardium as a single cell layer (Dueñas *et al.*, 2017). A subset of these cells undergoes epithelial-to- mesenchymal transition (EMT) and migrates into the myocardium, giving rise to epicardium-derived cells (EPDCs) (Vega - Hernández *et al.*, 2011). These cells invade the cardiac jelly and begin to occupy the space between the epicardium and myocardium. This invasion process plays a key role in remodeling the extracellular matrix and shaping the structure and function of the developing heart. Around embryonic day 12.5, fibroblasts are detected in the mouse embryo (Kovacic *et al.*, 2019; Lajiness & Conway, 2014).

Another source of cardiac fibroblasts is the endothelial-to-mesenchymal transition (EndoMT) of a subset of endocardium cells. During the process they lose their endothelial characteristics and acquire mesenchymal properties. These cells are thought to constitute a component of the primitive valves during early development and contribute to cardiac valve development (O'Donnell & Yutzey, 2020).

Finally, a small subset of cardiac fibroblasts arises from neural crest progenitor cells originating from the dorsal region of the neural tube. These fibroblasts undergo EMT and contribute to the development of the outflow region of the heart. However, they constitute only a minor subgroup of the cardiac fibroblasts population (Camelliti *et al.*, 2005; Moore-Morris *et al.*, 2015) (Figure 4).

The processes of EMT and EndoMT are essential for the development of different populations of cardiac fibroblasts. While EMT occurs in the heart wall regions and EndoMT occurs in cardiac valves, both transitions play essential roles in heart development.

Further research is needed to understand better the mechanisms that regulate the differentiation of cardiac fibroblasts and to answer the question of how important the EMT and EndoMT processes are in the development of the heart and chamber-specification.

Cardiac fibroblasts are more often presented as an essential part of cardiac tissue and heart formation. Further insight might affect the perception of the cardiac fibroblast and cardiomyocyte relation in the development of the heart in humans and lead to the questioning of the accepted hierarchy of the cells in the heart tissue.

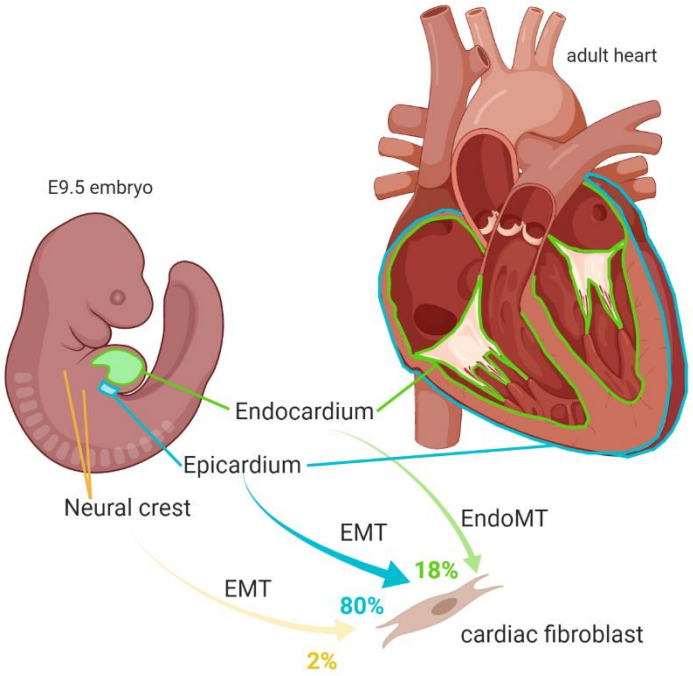

Figure 4 The origins of cardiac fibroblasts. Cardiac fibroblasts are primarily generated from mesenchymal cells via epithelial-to-mesenchymal transition (EMT) and endothelial-to-mesenchymal transition (EndoMT) processes. The epicardium is the main origin of fibroblasts, accounting for approximately 80% of the total, while the endocardium contributes to around 18%, and only a small number of fibroblasts are derived from neural crest cells. Modified from (Moore - Morris et al., 2014). Created with BioRender.com.

1.3. Limitations of animal models in CVDs research

Depending on the aim of the study and the availability of resources, there are several animal models used in the research to better investigate CVDs. The most common models applied in CVDs development and progression studies are mice and rats (Egido

et al., 2011). They are also used to test the efficacy of numerous therapeutic agents. Due to their similarities with human cardiovascular physiology, rabbits are generally used to study atherosclerosis and restenosis (Pogwizd & Bers, 2008). However, to study cardiac electrophysiology, by reason of similar structure and ion channel composition to the human heart, the guinea pig is leading model (Morrison *et al.*, 2018; von Bibra *et al.*, 2022). Large animals such as dogs and pigs are used to increase knowledge about CVDs, in particular, the effects of heart disease on exercise performance and the mechanisms of heart failure (Gabriel *et al.*, 2021; Shull *et al.*, 2021; Toyoda *et al.*, 1998).

Animal models have provided valuable insights into the pathophysiology, nevertheless neither model is able to fully replicate the complexity of human CVD, and each has its own limitations. Animal models may have significant differences in anatomy, physiology, and metabolism compared to humans, which may limit their applicability to human disease (Mukherjee *et al.*, 2022). Additionally, the ratio of cardiomyocytes to fibroblasts in animal hearts may differ from that in human hearts (Banerjee *et al.*, 2007; Vliegen *et al.*, 1991). This can affect the response of the heart to injury or the ability to regenerate.

It should also be remembered, that establishing and maintain the animal model is an expensive process, which also depend on specialized facilities and equipment and it raises ethical concerns.

Due to ethical concerns, a new legislature in the US signed in December 2022 eliminated the need for animal tests in the drug development process. The law intended to minimalize the suffering of animal test subjects and provide safer, more effective drugs to market, by using alternative testing methods (Wadman, 2023).

1.4. iPSCs-derived cardiomyocytes differentiation

To provide an alternative for animal tests in research and in the pharmaceutical field, the source of human cardiomyocytes is necessary. Over the last decade, iPSCs have become an extraordinary option. iPSCs can be derived from numerous, cell types by using reprogramming factors: *OCT4*, *SOX2*, *KLF4*, and *c-MYC* (Takahashi & Yamanaka, 2006). The process of generating iPSCs was first demonstrated in 2006, and it resulted in The Nobel Prize award in 2012 for Shinya Yamanaka (Press release.NobelPrize.org,

2012). iPSCs cells possess the potential to differentiate into any cell type of adult organism, so scientists have gained access to unlimited sources of relevant cell models.

1.4.1. iPSCs - a common source of ventricular and atrial cardiomyocytes (CMs)

There are many protocols in the literature that allow to obtain iPSCs-derived cardiomyocytes. iPSCs are first differentiated into mesoderm cells, which are then directed to become cardiac progenitor cells. The cardiac progenitor cells are then further differentiated into ventricular cardiomyocytes by culturing them in specific conditions that promote the development of the ventricular lineage (Batalov & Feinberg, 2015). The inhibition of the WNT signaling pathway has been shown to promote the differentiation of pluripotent stem cells into ventricular cardiomyocytes. WNT signaling inhibition can be achieved through the use of small molecules, such as CHIR99021 or IWP2 (Lian *et al.*, 2013). To generate atrial cardiomyocytes, after the differentiation of iPSCs into cardiac progenitors, retinoic acid (RA) signaling is used. RA has been found to promote the formation of atrial cardiomyocytes (Cyganek *et al.*, 2018; Zhang *et al.*, 2011), however the precise mechanism of RA action still needs to be revealed (Figure 5).

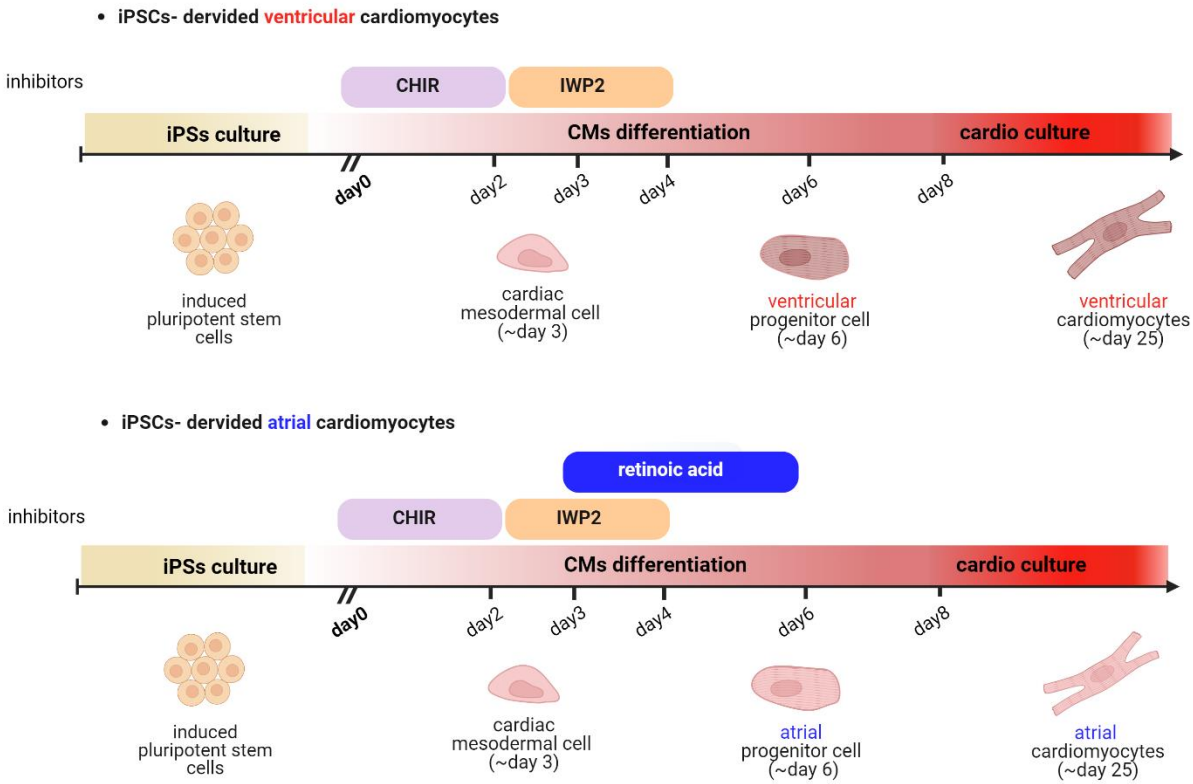

Figure 5 CMs differentiation process. The differentiation involves a series of steps, including the cardiac mesoderm induction, and cardiac progenitor cell specification. This process can be enhanced by various small molecules, leading to the generation of functional cardiomyocytes (Lian *et al.*, 2013). To obtain atrial-specific cardiomyocytes, incubation with RA is necessary (Cyganek *et al.*, 2018). Modified from (Cyganek *et al.*, 2018). Created with BioRender.com.

1.4.2. CMs maturation

The maturity of iPSCs-derived CMs depends on the differentiation protocols used and the time allowed for maturation (Guo & Pu, 2020). In general, compared to adult cardiomyocytes, are considered to be immature on various levels, including structural, electrical, metabolic, and functional (Kolanowski *et al.*, 2017).

Structural maturation refers to the development of the structural components of the cardiomyocytes, such as the contractile units, which are invaginations of the cell membrane that play a critical role in the propagation of electrical signals (Skorska *et al.*, 2022). For instance, in iPSCs-derived CMs, the length of the sarcomere exhibits approximately 1.7 µm, whereas in adult CMs, it expands to 2.2 – 2.3 µm. In iPSCs-derived CMs, a lack of transverse tubules (T-tubules) occurs (Van Den Heuvel *et al.*, 2014; Yang, Pabon, *et al.*, 2014).

Electrical maturation is defined as the expression of ion channels that regulate the flow of ions across the cell membrane, which is crucial for the generation and propagation of electrical impulses in the heart. Currents critical for iPSC-CMs depolarization phase and stabilization of the resting membrane potential (RMP) - I_{K1} are often diminished or even absent. In conjunction with immature I_{Na} and I_{Kr}, these alterations results in changes in APDs, greater RMP and lower maximum velocity (Vmax) (Kolanowski *et al.*, 2017). Compared to mature cardiomyocytes, iPSCs-CMs generally present a less negative and stable resting membrane potential, typically ranging from -57 to -70 mV rather than the more negative - 85 mV (Goversen *et al.*, 2018).

Metabolic maturation refers to the substitution of energy sources by cardiomyocytes from glycolysis to oxidative phosphorylation, which is more efficient and provides the energy required for the realization of the contractile function (Lopaschuk & Jaswal, 2010). The transition from glycolysis to fatty acid β-oxidation results in a greater production of oxidative energy, making iPSCs-CMs more similar to mature cardiomyocytes in their dependence on oxidative phosphorylation (OXPHOS) (Kolanowski *et al.*, 2017).

Functional maturation - the most rigorous criterium, refers to the development of the contractile function of the cardiomyocytes, including the ability to generate force and respond to changes in mechanical load (Lundy *et al.*, 2013). Mature CMs respond to β-adrenergic signaling in a dose-dependent manner, involving β1 and β2 receptors, in contrast, immature CMs primarily respond to β2 receptors. Additionally, mature CMs possess a significantly greater capacity (around 10-fold higher) to maintain - retain or hold onto electric charges on their cell membranes compared to iPSCs-derived CMs. Last but not least, intracellular calcium dynamics, mostly based on NCX together with activity of T-(early) and L-type (late) Ca^{2+} channels are also important indicators of CM maturity (Dolnikov *et al.*, 2006; Polak & Fijorek, 2012; Wu *et al.*, 2015).

Key indicators of cardiomyocyte's maturation are presented in Figure 6.

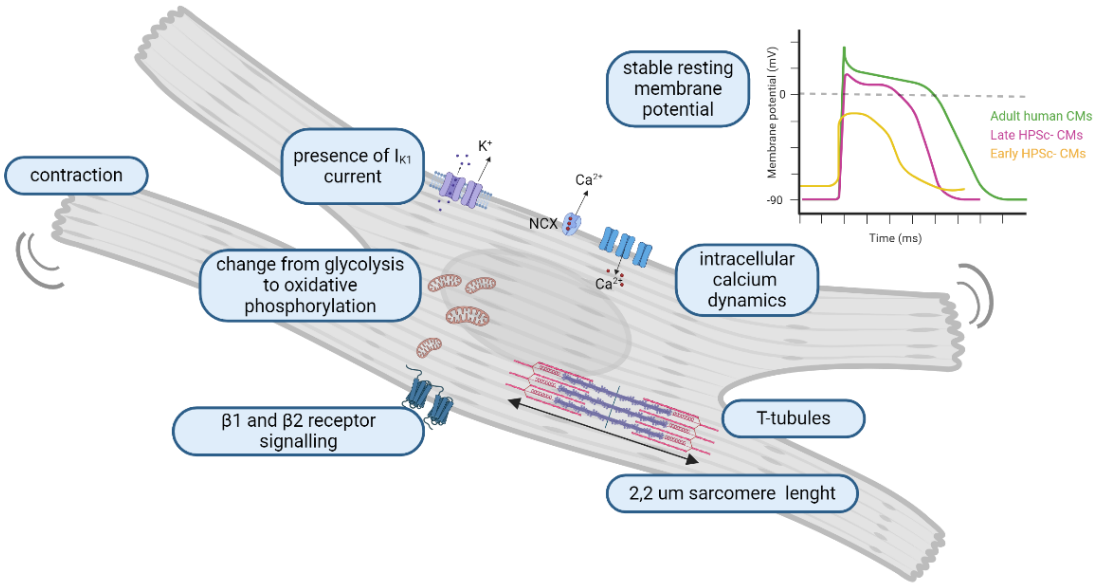

Figure 6 Mature cardiomyocytes. Features examples that allow maturity determination. Based on (Aigha & Raynaud, 2016; T Kolanowski *et al.*, 2017). Modified from (T Kolanowski *et al.*, 2017). Created with BioRender.com.

In order for cardiomyocytes to be considered mature, they must present above mentioned features. There are several approaches to enhance CMs maturation:

- Cell culture prolongation (Kamakura *et al.*, 2013);
- Co-culture with other cells, such as fibroblasts, endothelial cells, and immune cells to provide paracrine signals that promote cardiomyocyte maturation (Ahmed et al., 2020);
- Small molecules, growth factors, and hormones (Yang, Rodriguez, *et al.*, 2014);
- Mechanical and electrical stimulation to mimic the mechanical force and electrical signals that occur in the heart (Ahmed et al., 2020);
- Genetic engineering by overexpression of genes involved in e.g. potassium handling (Saito *et al.*, 2022);
- 3D cultures, to mimic the biological environment - structure, stiffness and ECM composition (Kałużna et al., 2022).

1.5. Available 3D culture systems to study heart development

In the recent studies, three-dimensional (3D) culture systems are presented as a powerful tool for studying cardiac development and disease. 3D models allows for the creation of more complex and physiologically relevant environments for cells to grow, which allow them to mimic better the complex architecture and mechanical properties of the heart (Kałużna *et al.*, 2022) (Figure 7).

One of the most widely used 3D culture systems are organoids. A self-organizing 3D structure, formed from pluripotent stem cells, can contain multiple cell types, including cardiomyocytes, fibroblasts, endothelial cells, and immune cells, and can present features of the developing or adult heart. Nevertheless, they include contractile cardiomyocytes and vascular networks, they may not fully reflect the complexity and structure of the heart (Forte *et al.*, 2018; Richards *et al.*, 2020).

Step further in structure organization are cell sheets. They are created by culturing cells on temperature-responsive polymer sheets, which can be detached and layered onto each other to form a 3D structure (Augustine *et al.*, 2021). This approach allows to generate functional cardiac patches with aligned cardiomyocytes and well-organized ECM (Xiao *et al.*, 2014).

The more advanced system that has shown promise in mimicking heart structure is the engineered heart tissue (EHT) model (Fink *et al.*, 2000). This model involves the mixing cardiomyocytes with collagen or fibrin and also other cell types such as cardiac fibroblasts, to improve cells ability to organize themselves into a more mature tissue structure, complete with organized sarcomeres and functional calcium handling mechanisms (Goldfracht *et al.*, 2019).

Another model, that pays attention to the architectural features aspect are decellularized heart scaffolds. This approach involves the removal of cells from a heart tissue sample, leaving behind only the ECM scaffolding. This ECM scaffold can then be used to seed new cells. It allows the creation of a more mature and physiologically relevant tissue structure (Taylor *et al.*, 2018). Decellularized heart scaffolds have been

used to generate functional heart tissue in vitro, as well as to study the effects of various mechanical and electrical stimuli on cardiac development (Song & Ott, 2011).

A further approach involves the combination of tissue models with microfluidic platform. Organ-on-a-chip (OOC) allows for precise control over the cellular microenvironment, including fluid flow, chemical gradients, and mechanical forces. By providing the flow, it introduces the sheer forces of the human heart (Kolanowski *et al.*, 2020), as a consequence, it can be used to study cellular behavior and interactions, as well as drug screening (Sakamiya *et al.*, 2020).

While each of these 3D culture systems has its advantages and limitations, they have all provided valuable insights into cardiac development and disease progression (Figure 7). Each model differs in its complexity and applicability, however compared to two-dimensional (2D) cultures, all of 3D culture systems offer a more physiologically relevant approach to studying heart disease and new therapeutics.

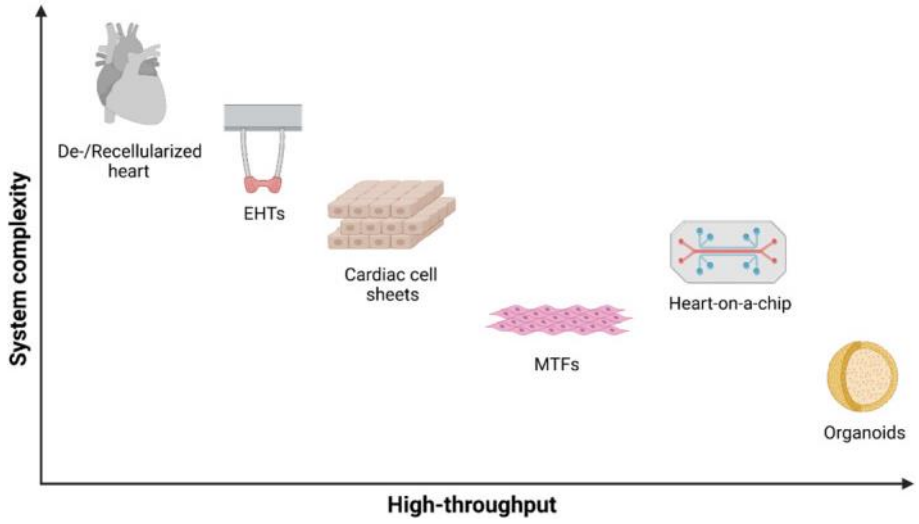

Figure 7 Characteristics of 3D culture systems. Visual representation of the relationship between model complexity and high throughput. Adapted from Kałużna *et al.*, 2022.

1.5.1. Engineered Heart Tissue model

One of the complex 3D culture system, and yet with a high potential for application, is the EHT model, which allows the generation of cardiac tissue composed of cardiomyocytes, fibroblasts, and components of extracellular matrix (Tiburcy, 2014).

EHTs have several advantages over other 3D culture systems for studying cardiac development. One of them is the implementation of other cells into the system, such as fibroblasts (Goldfracht *et al.*, 2019). As mentioned earlier CFs are crucial for proper tissue function and maturation, giving an advantage to the system to shape ECM into more mature states.

Another advantage is the control of mechanical and electrical stimulation, which can improve cardiomyocyte maturation and functionality. By applying electrical stimulation to the EHT and measuring the resulting force, the precise monitoring of major parameters of heart function can be performed (Goldfracht *et al.*, 2019). Including contractility force, contraction/relaxation kinetics, and responses to pharmacological stimuli, e.g. isoprenaline or ion channels inhibits. For example, the model can be used to evaluate cardiac contractility and tissue extracellular matrix changes by measuring response curves and calculating parameters such as EC_{50} or IC_{50} (Saleem *et al.*, 2020).

The EHT model allows for the investigation of several advanced physiological phenomena, specific only to cardiac tissue. These includes the Frank-Starling mechanism (Asnes *et al.*, 2006) and calcium response mechanics, and provides a way to study the microenvironment and interactions between cells.

The first attempts to generate chamber -specific EHT (chEHT), were performed in 2020 (Diness *et al.*, 2020) however proposed tissues, have been composed of atrial and ventricular cardiomyocytes only, with no fibroblast specificity. Nevertheless, the differences between atrial and ventricular EHT have been demonstrated at multiple levels, including gene and protein expression, electrophysiology, and ion channel activities. Until now no full chEHT has been developed.

The EHT model is a powerful tool for studying cardiac development, disease, and regeneration. It opens new avenues for applying heart regenerative therapies, however, to replicate the myocardium's complex cell composition, additional EHT improvements were necessary.

2. SCIENTIFIC AIM

The aim of this study is to develop a chamber-specific Engineered Heart Tissue (chEHT) model based on chamber-specific iPSCs-derived cardiomyocytes and cardiac fibroblasts able to recapitulate the human heart's physiology in developmental and drug-response aspect and to prove chEHT functional and physiological effectiveness.

This aim has been realized by three tasks (Figure 8):

1. Establishment of full chamber-specific EHT (chEHT), using iPSCs-derived chamber specific cardiomyocyte, cardiac fibroblast and extracellular matrix component with adequate gene expression pattern and contraction features
2. Evaluation of chEHT model through pharmacological-grade studies of atrial-specific AP14145 inhibitor of small-conductance calcium-activated potassium channel.
3. Investigation of the role of cardiac fibroblasts in the terminal cardiomyocyte differentiation process.

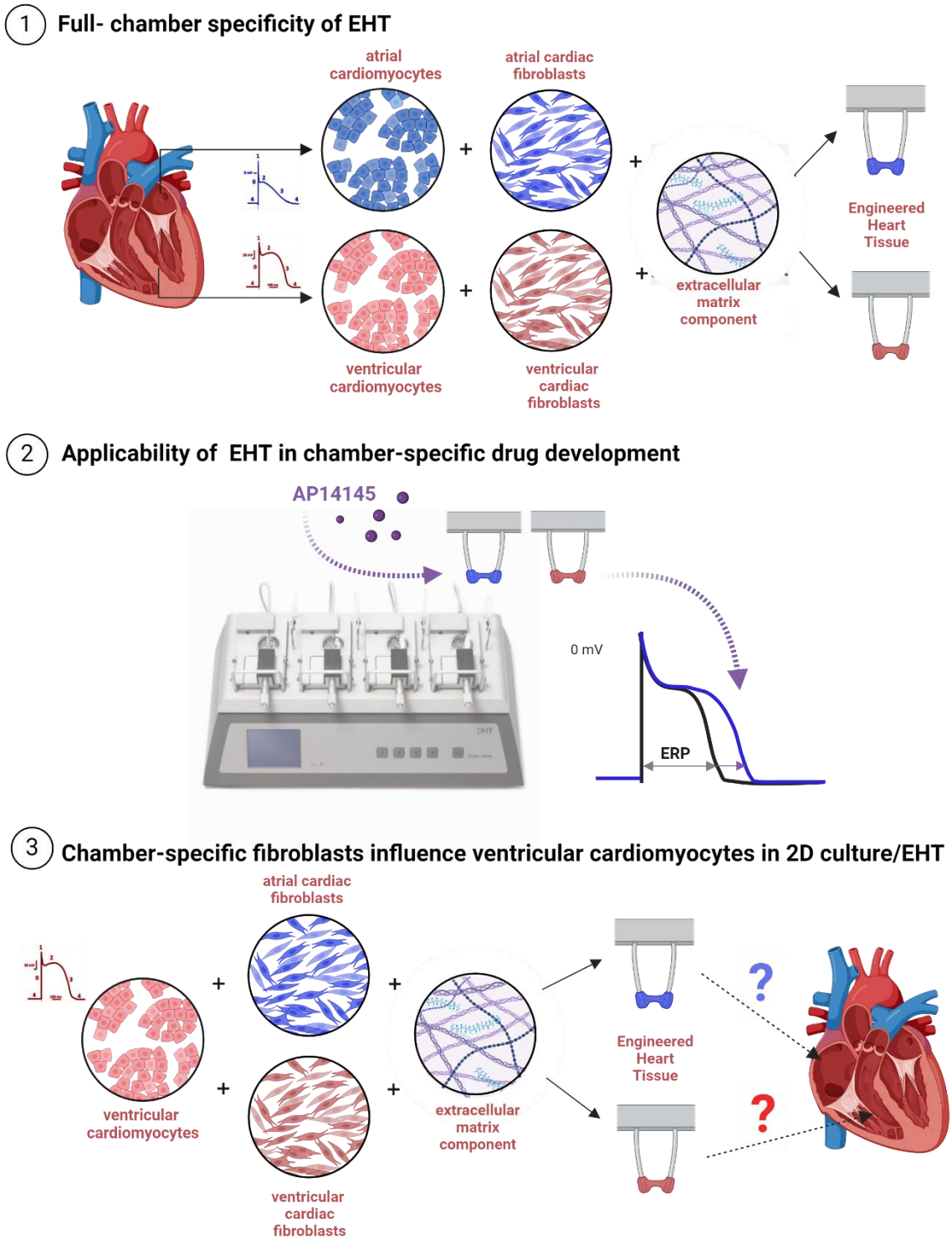

Figure 8 Experimental approach scheme. Created with BioRender.com.

3. MATERIALS AND METHODS

3.1. Materials

3.1.1. Cell lines

- **iBM76.3** – Parental cell line iBM76.3 was derived from bone marrow cells by using the STEMCCA lentivirus system in Prof. Kaomei Guan-Schmidt group, Technische Universität Dresden, Dresden Germany. Described in Cyganek *et al.* and Streckfuss-Bömeke *et al.* (Cyganek *et al.*, 2018; Streckfuss-Bömeke *et al.*, 2013). Throughout all the dissertation, was name as **iPSC_1**.
- **iWTD2.3** – Parental cell line iWTD2.3 was derived from dermal fibroblasts by using the STEMCCA lentivirus system in Prof. Kaomei Guan-Schmidt group, Technische Universität Dresden, Dresden Germany. Described in Cyganek *et al.* and Streckfuss-Bömeke *et al.* (Cyganek *et al.*, 2018; Streckfuss-Bömeke *et al.*, 2013). Throughout all the dissertation, was name as **iPSC_2**.
- **HAF - Human Atrial Fibroblasts** - parental cell line HAF was a gift from Prof. Ali El-Armouche from Technische Universität Dresden, Dresden Germany. Described in Künzel *et al.* ((Künzel *et al.*, 2020).
- **HVF - Human Ventricular Fibroblasts** - commercially available cell line, Human Primary Cardiac Fibroblasts, Cat. 74038, Lot. HC7947, Company: Applied Biological Materials Inc.

3.1.2. Heart tissue

Human heart tissue obtained from healthy donors was used as a reference. It was acquired based on bioethical consent under Permission Number: 778/23 dated 9th November 2023.

3.1.3. Reagents and media for cell lines culture

Table 1 Reagents used during iPSCs culture and EB formation.

Reagent	Company	Catalogue number
Geltrex™ LDEV-Free, hESC-Qualified, Reduced Growth Factor Basement Membrane Matrix	Thermo Fisher Scientific	A1413302
DMEM/F-12, GlutaMAX™ supplement	Thermo Fisher Scientific	1056501
Essential 8™ Medium	Thermo Fisher Scientific	A1517001
Versene® EDTA, 0.02%, 0.53mM in DPBS, without calcium or magnesium	Lonza	BE17-711E
Thiazovivin ≥98% (HPLC)	Sigma	SML1045-25MG
CryoStor® CS10, 10% DMSO	Stemcell technologies	07930
Cryogenic Vials	CryoKING	88-021X
BioCision CoolCell LX	BioCision	4929014
Essential 6™ Medium	Thermo Fisher Scientific	A1516401
HyClone™ Fetal Bovine Serum, South American Origin, Research Grade	Cytiva	HYCLSV30160.03
AggreWell™400	StemCell Technologies	34411
Anti-Adherence Rinsing Solution	StemCell Technologies	07010

Table 2 Reagents used during cardiomyocytes differentiation.

Reagent	Company	Catalogue number
Geltrex™ LDEV-Free, hESC-Qualified, Reduced Growth Factor Basement Membrane Matrix	Thermo Fisher Scientific	A1413302
RPMI 1640 Medium, GlutaMAX™ Supplement, HEPES	Thermo Fisher Scientific	72400047
Albumin, human recombinant	Sigma	A9731-10G
L-Ascobic Acid 2-Phosphate	Sigma	A8960-5G

CHIR99021	StemCell Technologies	72054
IWP2	Merck Millipore	681671-10MG
Retinoic acid ≥98% (HPLC)	Sigma	R2625
B-27™ Supplement (50X), serum free	Thermo Fisher Scientific	17504044
Fetal Bovine Serum	Sigma	F7524
Collagenase II	Thermo Fisher Scientific	17101-015
Trypsin 2.5%, no phenol red, 10x	Thermo Fisher Scientific	15090-046
RPM1 1640 without Glucose without HEPES	Thermo Fisher Scientific	11879020
HEPES	Sigma	H0887-20ML
DPBS	Thermo Fisher Scientific	14190169
L- (+)-Lactic acid	Sigma	L1750-10G
DPBS, calcium, magnesium	Thermo Fisher Scientific	14040117
$MgCl_2$	Sigma	M-0250
Ethylene glycol-bis (2-aminoethylether)-N, N, N', N'-tetraacetic acid (EGTA)	Sigma	E3889

Table 3 Reagents required for the fibroblasts culture.

Reagent	**Company**	**Catalogue number**
Geltrex™ LDEV-Free, hESC-Qualified, Reduced Growth Factor Basement Membrane Matrix	Thermo Fisher Scientific	A1413302
IMDM, GlutaMAX™ Supplement	Gibco	12440053
100 x MEM-NEAA	Gibco	11140035
FBS	Gibco	10270106
Insulin solution human	Sigma	I9278-5ML
DPBS	Thermo Fisher Scientific	14190169
Trypsin-EDTA	Gentaur	171-TM050
Cryopreservation Medium	Gentaur	171-TM024

3.1.4. Reagents and media for Engineered Heart Tissue molding, culture and measurements

Table 4 Equipment and reagents required for EHT dish preparation.

Reagent	Company	Catalogue number
DUROPLAN® Glas Petri Dishes, 60 x 20 mm	Carl Roth	K608.1
Sylgard 184 silicone elastomer Kit	Krayden	4019862
Silicone hoses	PharMed®BPT	070539-03F, 070539-16F

Table 5 Reagents required for EHT molding and culture.

Reagent	Company	Catalogue number
StemPro Accutase	Gibco	A11105-01
Iscove Medium with Glutamax	Gibco	31980-022
100 x MEM-NEAA	Gibco	11140035
TrypLE™ Express Enzyme	Gibco	12604013
L-ascorbic acid 2-phosphate sesquimagnesium salt hydrate	Sigma	A8960
B-27™ Supplement (50X), serum free	Gibco	17504-044
IGF-1	Peprotech	100-11
VEGF-B	Peprotech	100-20B
FGF-2	Peprotech	100-18B
Iscove powder	Gibco	42200014
MOPS	Sigma	M1254-100G
Bovine Collagen Solution, Type I	advancedbiomatrix	#5010
B27 supplement, minus insulin	Gibco	A1895601
NaOH	Sigma	S0899

Steriflip® Filter Units	Milipore	SCGP00525

Table 6 Reagents required for EHT measurements.

Reagent	**Company**	**Catalogue number**
Glucose	POCH	459560117
L-Ascorbic acid	Sigma	A5960-25G
NaCl	POCH	794121116
KCl	Sigma	P5405
$MgCl_2 * 6H_2O$	Sigma	M0250
$CaCl_2$	POCH	87480116
$NaH_2PO_4 * H_2O$	Sigma	S9638
$NaHCO_3$	Sigma	S8875

3.1.5. Reagents required for the molecular evaluation

Table 7 Reagents required for the molecular evaluation - RNA isolation, reverse transcription and real-time PCR.

Reagent	**Company**	**Catalogue number**
RNAlater™ Stabilization Solution	Thermo Fisher Scientific	AM7020
RNeasy Mini Kit	Quigen	74104
Bead-Beat Total RNA Mini	A&A Biotechnology	031-100BB
TURBO DNA-free™ Kit	Thermo Fisher Scientific	AM1907
SuperScript™ IV Reverse Transcriptase	Thermo Fisher Scientific	18090010
PowerUp™ SYBR™ Green Master Mix	Thermo Fisher Scientific	A25742
TRI reagent	Sigma	T9424-100ML
Chloroform	Sigma	T9424-100ML
Isopropanol	POCH	751500111
dNTP Mix (10 mM)	Thermo Fisher Scientific	18427013

RNasin® Ribonuclease Inhibitor	Promega	N251B

Table 8 List of primers used during the molecular evaluation.

Gene target	Forward Primer	Revers Primer	Annealing	Product size
References gene				
GAPDH	CACCATCTTCCAGGAGCGAG	GTTCACACCCATGACGAACA	187	60°C
iPSCs characteristic				
NANOG	AACTCTCCAACATCCTGAACCT	GCCAGTTGTTTTTCTGCCACC	96	53°C
KLF4	TCAAGGCACACCTGCGAAC	ATTTTTGGCACTGGAACGGG	144	52°C
SOX2	GGGGAAAGTAGTTTGCTGCCT	CCGCCGCCGATGATTGTTA	132	60°C
OCT4	CTCACCCTGGGGGTTCTATT	CTGGTTCGCTTTCTCTTTCG	203	60°C
CMs characteristic				
TNNI3	AGGACACCGAGAAGGAAAACC	GCAGTAGGCAGGAAGGCTCA	115	52°C
MYL2	GGCTGATTACGTTCGGGAAATG	CTTCTCCGTGGGTGATGATGTG	144	60°C
MYL7	TGACCCCAGCGGCAAA	GCGAACATCTGCTCCACCTC	102	61°C
ANP	GCTGCTCACTGCCCCTC	GCTTGTCCTCCCTGGCTG	130	66°C
MYH6	CAAGAGCCGTGACATTGGTG	TGGCAAGAGTGAGGTTCCC	77	55°C
MYH7	GCCAAGAGCCGTGACATT	TGCTTTATTCTGCTTCCTCCCA	142	55°C
KCNA5	TAAGGAAGAGCAGGGCACTCA	TCGGGCACTGTCTGCATTCT	127	53°C
SK2	GGAAACTGAATGACCAAGCAAAC	TCCAGGGTAACAATCCTCTTCTC	101	58°C
SK3	GTTCTTTCACCCCCTCTTCTTTC	TTGGCTTGCTTCGGTTCTCT	80	58°C
KCNJ3	GCACGCGGTGATCTCCATGA	TCGAGCTTGACAAGTCATCC	249	57°C
KCNJ2	GTCCCCAACACTCCCCTTTG	ACTGTCGTCTTCCTCTTTGCT	123	60°C

3.1.6. Commercial kits

Table 9 Commercial kits.

Reagent	Company	Catalogue number
RNA isolation		
RNeasy Mini Kit	Qiagen	74104
Bead-Beat Total RNA Mini	A&A Biotechnology	031-100BB
RNA purification		
TURBO DNA-free™ Kit	Thermo Fisher Scientific	AM1907
Reverse transcription		
SuperScript™ IV Reverse Transcriptase	Thermo Fisher Scientific	18090010

3.1.7. Immunostaining and flow cytometry

Table 10 Reagents used for immunostaining procedure.

Reagent	Company	Catalogue number
Paraformaldehyde	Sigma	P6148-500G
DPBS	Thermo Fisher Scientific	14190169
Triton-X-100	Sigma	11332481001
Bovine serum albumin	Sigma	A2153-10G
Goat serum	Sigma	G9023
Donkey serum	Sigma	D9663
Fluoroshield™ with DAPI	Sigma	F6057

Table 11 List of antibodies used for immunostaining procedure for CMs.

1º Ab					2º Ab				Serum
Protein target	**Host**	**Company and Catalog number**	**Class**	**Dilution**	**Name**	**Company and Catalog number**	**Class**	**Dilution**	
EB characteristic									
SOX17	Mouse	Abcam Ab84990	Mono	1:50	Goat anti-mouse Alexa Fluor 594	Thermo Fisher Scientific A-11005P	Poly	1:500	Goat
SMA	Mouse	Thermo Fisher Scientific MA1-06110	Mono	1:200					
TUJ1	Rabbit	Abcam Ab18207	Poly	1:500	Goat anti-rabbit Alexa Fluor 594	Thermo Fisher Scientific A-11012	Poly	1:500	Goat
iPSCs characteristic									
SSEA4	Mouse	Abcam ab16287	Mono	1:200	Goat anti-mouse Alexa Fluor 594	Thermo Fisher Scientific A-11005P	Poly	1:500	Goat
OCT3/4	Mouse	SantaCruz sc-5279	Mono	1:250					
SOX2	Rabbit	Cell Signaling	Poly	1:100	Goat anti-rabbit	Thermo Fisher	Poly	1:500	Goat

		Technologies 3579S			Alexa Fluor 594	Scientific A-11012			
NANOG	Goat	R&D AF1997-sp	Poly	1:200	Donkey anti-goat Alexa Fluor 555	Abcam ab150130	Poly	1:500	Donkey
CMs characteristic									
cTNT	Mouse	Thermo Scientific MS295PABX	Mono	1:200	Goat anti-mouse Alexa Fluor 594	Thermo Fisher Scientific A-11005	Poly	1:500	Goat
MLC2v	Rabbit	Protein tech 10906-1-AP	Mono	1:200	Goat anti-rabbit Alexa Fluor 594	Thermo Fisher Scientific A-11012	Poly	1:500	Goat
α-Actinin	Mouse	Sigma A7811	Mono	1:200	Donkey anti-mouse Alexa Fluor 488	BD Pharmingen 561495	Mono	1:500	Donkey
Vimentin	Mouse	Santa Cruz Biotechnology sc-6260	Mono	1:200					
MLC2a	Mouse	Synaptic System 311 011	Poly	1:200					

3.1.8. Equipment

All equipment used during the study is listed in Table 12.

Table 12 Equipment used during experiments.

Equipment	Type	Producer
Cell culture incubator	CellXpert® C170i	Eppendorf
Laminar airflow cabinet	BIO190 A2	ALPINA
Water bath	BL2/200	WSL
Inverted light microscopes	AxioVert 100, PrimoVert	Zeiss
Camera	Axiocam 305 color	Zeiss
Confocal microscope	DMi8	Leica
Flow Cytometer	V5-B5-R0	Beckman Coulter Life Sciences
Myograph, Muscle Strip System	840MD	DMT
Chamber covers with electrods	300278	DMT
Stimulator	101025	DMT
Force transducers	300277	DMT
Vacuum Package	101019	DMT
Automatic Buffer Filler	101057	DMT
Centrifuges	5417R, 5804R	Eppendorf
Scale	ADJ200-4	KERN
Vortex	Vortex Mixer	Labnet International
Thermocycler for PCR	Tetrad2	Bio-Rad
Thermocycler for qPCR	CFX96 Touch qPCR System	Bio-Rad
Homogenizer	BeadBlaster™ D2400	Benchmark
NanoDrop™ 2000	Thermo Fisher Scientific	ND-2000

3.1.9. Software

To analyze obtained data, software listed in Table 13 was used.

Table 13 Used programs.

Program	Purpose
SnapGene	Primer design
CFX Maestro™ Software	Analysis of qRT-PCR data
GraphPad Prism 9	Statistical analysis of data and charts preparation
BioRender	Figure preparation
LabChart 8	Analysis of physiological data
ZEN 2	Recording 2D cells culture and EHT
Leica Application Suite X (LAS X) software	Confocal pictures processing
MotionVektor	Analysis of 2D CMs contraction

3.2. Methods

3.2.1. iPSCs culture

The cells were grown in plastic 6-well or 12-well plates (surface 9.6 cm^2 or 3.8 cm^2) coated before with a Geltrex (Thermo Fisher Scientific).

All plates, tips, and pipettes used in coating, were cooled down at - 20°C for 10 minutes before the procedure. A box with ice was also prepared. The Geltrex aliquot prepared earlier (16mg/ml, 144µl stock in a 15 ml Falcon tube) was thawed from -80°C and resuspended in 12 ml of cold DMEM-F12 (Thermo Fisher Scientific). Next, 1 ml of the prepared solution was added to each well of the 6-well plates or 0.5 ml to each well of the 12-well plates. The whole procedure was done on the ice. The plates were then placed in the refrigerator for up to two weeks. Before use, the Geltrex-coated plates had to be incubated in 37°C for at least 40 minutes.

iPSCs were cultured in E8 Medium (Thermo Fisher Scientific), which is a specially designed culture medium that has been proven to maintain the pluripotency of iPSCs lines. The iPSCs were incubated at 37°C with 5% CO_2 until they reached a confluence of about 90 - 95%, which usually took about three days. During this time, the E8 medium was changed each day. Once the cells reached an appropriate confluence, a Thiazovivin (Sigma) - a selective inhibitor of Rho-associated coiled-coil containing protein kinase (ROCK) was added to the cells to prevent unwanted differentiation. 2 µM Thiazovivin was added one hour before passage. During the passaging, the cells were first carefully washed twice with Versene® solution (Lonza) and then, for the third time, left in it for 3 minutes incubation at 37°C The cells were checked under the microscope to see if they had started to detach. After incubation, the Versene® solution was aspirated, and 1 ml of E8 Medium was added. The cells on the plate were detached using a 1000 µl pipette, to avoid excessive pipetting to preserve small colonies. The cell suspension was carefully mixed, and the cells were resuspended in the E8 Medium supplemented with 2 µM Thiazovivin. The Geltrex coating was removed, and the desired ratio of cells was plated per well (1:5 up to 1:8). The plate was gently shaken in an "8" motion and place in standard *in vitro* culture condition. (5% CO_2, 37°C). After 24 hours, the medium was changed to E8 Medium without Thiazovivin. To maintain the pattern of passages every 3 days, the 1:5 ratio was implemented.

For iPSCs line freezing procedure, one million cells were counted during passage and centrifuged at 200g for 5 minutes. During centrifugation, the cryo tube was labelled and filled with 0.5ml of cold commercially available cryoprotectant for stem cell cultures - CryoStor® CS10, 10% DMSO (Stemcell technologies). After the centrifugation, the supernatant was aspirated, and the pellet was carefully resuspended in CryCryoStor®. 0.5ml of the cell suspension was transferred into each labeled cryotube. The cells were then placed in cryogenic vials and placed in a freezing container BioCision CoolCell LX for 24 hours at -80°C, to achieve a cooling rate of approximately - 1°C/minute, which is the optimal rate for cell survival. The following day, the vials were transferred to liquid nitrogen Dewar, for long-term storage in LN_2 vapors.

3.2.2. Embryoid bodies (EB) formation

The formation of embryoid bodies (EBs) involves the creation of three-dimensional aggregates through the suspension of pluripotent stem cells. The process of EB formation utilized the AggreWell™ plate (Stemcell technologies). Initially, the Anti-Adherence Rinsing Solution (Stemcell technologies) was applied to the AggreWell™ plate well to prevent cell adhesion. Subsequently, 106 million iPSCs were suspended in E6 medium (Thermo Fisher Scientific), added to the well, and centrifuged for 3 min at RT and 300 g. Over the next 48h, the cells were cultured, with a single medium change to E6, resulting in the formation of spherical aggregates. Next, the formed aggregates were transferred from the AggreWell to Geltrex-coated, 15mm diameter cover glasses placed in a standard 12-well plate. For the next 12 days, for staining purposes, around 20-25 EBs per cover glass were seeded and cultured in E6 medium supplemented with 20% HyClone™ Fetal Bovine Serum (Cytiva), with medium changes every 48h.

3.2.3. Cardiac differentiation and cardiomyocytes sub-culturing

The cardiac differentiation was initiated by seeding iPSCs colonies in a ratio of 1:6 on Geltrex-coated 12-well plates. All differentiation protocols were performed in standard cell culture conditions (5% CO_2, 37°C) As in the iPSCs passage procedure, 2 µM Thiazovivin was added to the medium and incubated for 24 hours after passage (3.2.1. iPSCs **culture**). The cells were cultured as regular iPSCs for approximately 2 days until they reach a confluence of about 90%. At this point, the medium was replaced with a Cardiac Differentiation Medium composed of RPMI1640 with HEPES and GlutaMAX™ (Thermo Fisher Scientific), 0.5 mg/ml human recombinant albumin (Sigma), and 0.2 mg/ml L - ascorbic acid 2-phosphate (Sigma). On Day0, which is considered as a start of the differentiation process, 4µM of CHIR99021 (Stemcell technology) was added to Cardiac Differentiation Medium for 48 hours.

On Day2, the medium was changed again, and dissolved 5µM IWP2 (Merk Milipore) was added to Cardiac Differentiation Medium and left for 48 hours.

To induce atrial CM phenotype On Day3, 1 µM Retinoic acid (Sigma) in the Cardiac Differentiation Medium was added. Cardiac Differentiation Medium without RA

supplementation was expected to differentiate mostly into ventricular subtype cardiomyocytes. The cells were cultured in *in vitro* condition for the next 3 days, until day 6 (Figure 5).

On Day6, all the cells were treated with fresh Cardiac Differentiation Medium without the addition of any small molecules and left for 48 hours.

On Day8, the final day of the differentiation process, Cardiac Differentiation Medium was replaced with Cardio Culture Medium, consisted of RPMI1640 with HEPES and GlutaMAX™ and 2% B27 supplement (Thermo Fisher Scientific). Starting from that day, the medium was refreshed every second day.

Between day 14 and day 16, a cardiomyocyte passage was conducted. Before cardiomyocytes digestion, components needed to be warmed: Cardio Digestion Medium (Medium composed of Cardiac Culture medium, 20% Fetal Bovine Serum (FBS, Sigma), 2 µM Thiazovivin, Versene® solution, Collagenase II (Thermo Fisher Scientific, 400 units/ml RPMI with GlutaMax and HEPES), and 0.25% Trypsin-EDTA (Thermo Fisher Scientific). First, the Cardio Culture medium was aspirated from the cells, and a wash step with 1ml of Versene® solution per well was performed for all wells. After washing, cells were covered with warmed 400 units/ml Collagenase II (0.5 ml per well) and incubated at 37ºC for 20 minutes. After checking the detachment status, the cell clusters were carefully transferred into a 15 ml falcon tube containing 1 ml of 400 units/ml Collagenase II. Then, the next round of incubation for 20 min at 37ºC was performed. The cells were diluted in DPBS (Thermo Fisher Scientific) and centrifuged at 200g for 5 minutes. The medium was aspirated, and 1 ml of 0. 25% Trypsin-EDTA was added to the pellet. Pellet had to be resuspended slowly and gently with one move of a 1 ml pipette. The tube was incubated for 4-6 minutes at 37ºC. Every 2 min, the cell suspension was checked and mixed. If clusters were still present, gentle pipetting was performed with a 1 ml pipette up to a maximum of 3 times. Double the volume of Cardio Digestion Medium was added, and a 10 µl sample was collected for cell counting. Cells were placed in the Neubauer chamber and counted under a microscope from at least 4 squares. The number of cells per unit area is determined and multiplied by 10^4 and general cell suspension volume to obtain the final cell number. After centrifugation at 200g for 5 minutes, the medium was carefully aspirated, and the pellet was resuspended again in Cardio Digestion Medium. Approximately 8.5 x 10^5 cells/well in 1ml Cardiac Digestion

Medium were plated into a pre-coated with Geltrex 6-well plate. After a 40-minute incubation, another 1 ml of Cardio Digestion Medium was added. Depending on the condition of the cells, after 24-48h the medium has to be changed from Cardio Digestion Medium to Cardio Culture. The cell culture medium was changed every 2-3 days.

At approximately day 20, a metabolic selection procedure was performed to purify the cardiomyocytes, by taking advantage of cells' high sensitivity to lactate. The cells were cultured in 2 ml/well Cardiac Selection Medium based on RPMI 1640 without Glucose, supplemented with 0. 5 mg/ml human recombinant albumin, and 0.2 mg/ml L-ascorbic acid 2-phosphate, and 4 mM lactate (Sigma). The selection process lasted 5 days and cardiomyocytes were under constant observation. The Cardiac Selection Medium was changed every 48 hours. In case of bad conditions of the cells, the procedure would be shortened. Following the selection process, the cells were cultured once again using Cardiac Culture medium. All the necessary medium and their components are listed in Table 14.

Table 14 The components of necessary mediums for CMs culture.

Reagent	volume
Cardiac Differentiation Medium	
RPMI1640 with HEPES and GlutaMAX™	50 ml
Human recombinant albumin	25 mg
L-ascorbic acid 2-phosphate	10 mg
Cardiac Culture Medium	
RPMI1640 with HEPES and GlutaMAX™	50 ml
B27 supplement with insulin	1 ml
Cardiac Digestion Medium	
Cardiac Culture Medium	40 ml
Fetal Bovine Serum	10 ml
2 µM Thiazovivin	50 µl
Cardiac Selection Medium	
RPMI1640 with HEPES and GlutaMAX™	50 ml
Human recombinant albumin	25 mg

L-ascorbic acid 2-phosphate	10 mg
1M Lactate/HEPES	200 µl

3.2.4. Fibroblasts culture

The cardiac fibroblasts were cultured on a T75 culture vessel pre-coated with 16mg/ml Geltrex (3ml a mixture of 16mg/ml Geltrex and DMEM-F12/T75 flask) with Iscove Medium consisting of IMDM, GlutaMAX™ Supplement medium (Gibco), 10% of FBS (Gibco), 1% MEM-NEA (100x, Gibco) and 0,5 µg/ml Insulin (Sigma). CFs were incubated at 37°C with 5% CO_2 until reached approximately 70-80% confluency.

The passage procedure started with discarding the culture medium and subsequent washing with 3ml of DPBS at room temperature. DPBS (Thermo Fisher Scientific) was added to the culture vessel three times to ensure thorough washing. Next, 3ml of 0,25% Trypsin-EDTA (Gentaur) was added to detach the cells from the surface. Cells were incubated for 3 minutes at 37°C. Once the majority of the cells had detached, a double volume of Iscove Medium was added to the T75 flask to neutralize the trypsin-EDTA. The culture suspension was gently swirled or pipetted to ensure complete neutralization. Then, the culture suspension was transferred to a fresh falcon and centrifuged at 200g for 5 minutes at RT. The supernatant was aspirated, and the cell pellet was resuspended in a pre-warmed fresh Iscove Medium. A new T75 flask was prepared by adding 10 ml of Iscove Medium, and the cells were seeded at the recommended seeding density. To maintain the pattern of max. two passages per week, with a 1:3 ratio. Medium change with Iscove Medium was performed every 2-3 days.

To keep the cells in the lower passages for future experiments and Engineered Heart Tissue formation, the freezing cells procedure was performed. At the last stage of passaging - centrifugation, the cell pellet was resuspended in Cryopreservation Medium (Gentaur), with the volume adjusted based on the confluence of the cells. For a 90% confluent T75 flask, three cryo stocks could be performed. The cell suspension was dispensed into cryovials. Finally, the cells were frozen at - 80°C in a freezing container BioCision CoolCell LX for 24 hours at -80°C, then stored for long-term in liquid nitrogen.

3.2.5. Molding dish and stretcher preparation

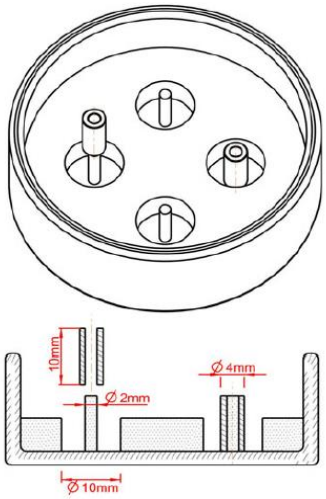

Figure 9 Technical drawing of molding dish. Modified from (Tiburcy *et al.* 2014).

Silicon hoses were cut into approximately 1.5 cm long pieces and put inside the teflon rings. Then, a 10% Silicon Elastomer mixture was prepared and centrifuged to remove air bubbles. By using a 10 ml syringe, the petri dishes were filled. The molding dishes were left in 60-70 °C dry oven for overnight incubation.

The next day, a new 10% Elastomer was prepared. The teflon ring was put back in the hole and the thin silicon hose arranged in the middle of them, previously immersed in Elastomer. The dish was again put in a 70 °C dry oven for 4-5 hours. Once the Elastomer had hardened, the teflon rings were removed, leaving the thin silicon hose glued to the bottom (Tiburcy *et al.* 2014). After the dishes were autoclaved, were ready to use Figure 9.

During EHT maturation, tissues were placed on a customized stainless steel holders - stretchers (Tiburcy *et al.* 2014), to apply isometric exercises, promoting development and strength (Figure 10).

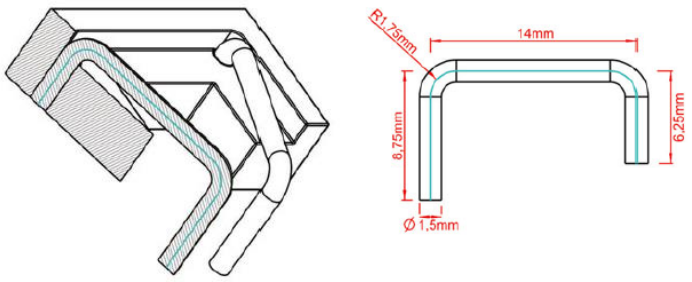

Figure 10 Technical drawing of mechanical stretchers. Modified from (Tiburcy *et al.* 2014).

3.2.6. EHT formation

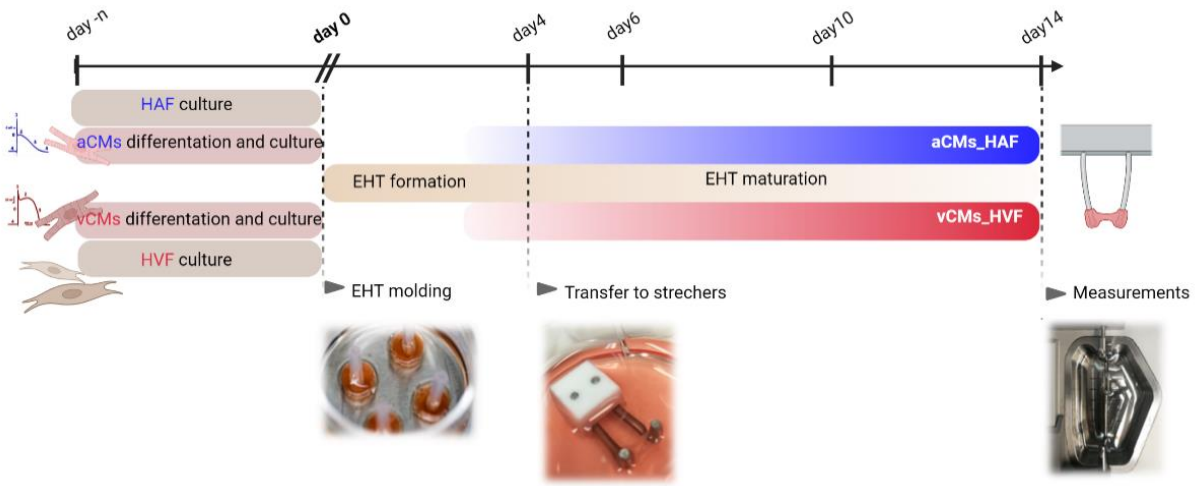

Figure 11 EHT formation and maturation scheme. Graphical representation of EHT procedures over time: from formation through maturation to final measurement. Created with BioRender.com.

To form Engineered Heart Tissue, the preparation of main cell components: human induced pluripotent stem cell-derived cardiomyocytes (iPSC-CMs) and human fibroblast was necessary (Figure 11). All the media necessary for the procedure: Recovery medium, Serum-Free Basal Medium (SFBM), Serum-Free Maturation Medium (SFMM), Serum-Free Maturation Medium (SFMM) with TGF-β and Iscove 2x were prepared fresh before cell passage (Table 15).

Table 15 The components of necessary mediums for EHT formation

Reagent	volume
Iscove Basal Medium	
Iscove Medium with Glutamax	50 ml
100x MEM-NEAA	500 µl
Iscove Recovery Medium	
Iscove Basal Medium	49 ml
Ascorbic acid 2-phosphate sesquimagnesium salt hydrate (200 µM, 60 µg/ml)	50 µl

B27 Supplement with Insulin (2%)	1 ml
Iscove Serum-free Base Medium (SFBM)	
Iscove Basal Medium	49 ml
Ascorbic acid 2-phosphate sesquimagnesium salt hydrate (300 µM, 90 µg/ml)	75 µl
Iscove Serum-free Maturation Medium (SFMM)	
Iscove Basal Medium	49 ml
Ascorbic acid 2-phosphate sesquimagnesium salt hydrate (300 µM, 90 µg/ml)	75 µl
B27 Supplement without Insulin (2%)	1 ml
IGF-1 Stock (=100 ng/ml)	50 µl
VEGF-B Stock (=5 ng/ml)	50 µl
FGF-2 Stock (=10 ng/ml)	50 µl
Iscove Serum-free Maturation Medium (SFMM) + TGF-β	
Iscove Basal Medium	49 ml
Ascorbic acid 2-phosphate sesquimagnesium salt hydrate (300 µM, 90 µg/ml)	75 µl
B27 Supplement without Insulin (2%)	1 ml
IGF-1 Stock (=100 ng/ml)	50 µl
VEGF-B Stock (=5 ng/ml)	50 µl
FGF-2 Stock (=10 ng/ml)	50 µl
TGF-β Stock (=5 ng/ml)	50 µl

First, when fibroblast confluency reached approximately 80%, cells were washed with 3 ml of DPBS to remove any residual media. Then, 3 ml of TrypLe was added, and the cells were incubated for 5 minutes at 37°C. After the incubation, double the amount of Recovery Medium was added to the culture dish, and all cells were collected in a falcon tube. The cells were then counted and centrifuged at 200g for 5 minutes at room temperature. The supernatant was removed, and the cell pellet was resuspended in serum-free basal medium (SFBM) in a concentration of 10^6 cells/ml medium.

To prepare iPSCs-CMs, the cells were washed twice with DPBS at room temperature. Then, 1 ml of Accutase (Gibco) with 10µM Thiazovivin was added to each well from the 6-well plate. The cells were incubated for 15 minutes at 37°C. Following cell detachment, cells were transferred with Accutase to the prepared Recovery Medium with 10µM Thiazovivin. The wells were washed with an additional 1 ml of Recovery Medium, which was also added to the cells. The cells were counted, centrifuged at 200g for 5 minutes at RT, and resuspended in 1mln/ml Recovery Medium without Thiazovivin.

For the cell mix, the appropriate amount of CMs and FBs were mixed and centrifuged at 200g for 5 minutes at room temperature. The resulting cell mix was resuspended in SFBM medium for further use. For one EHT: 1,015 mln of iPSCs-CMs and 0,435 mln Fbs were needed.

Then, all components for the master mix: Bovine collagen (advancedbiomatrix, 5.8 mg/ml), 2x Iscove (Gibco), 0. 1 M NaOH (Signa), and 1M MOPS (Sigma) were sequentially added to reach a mixture with a pH of 7.6. The volume composition of the master mix is presented in Table 16.

Table 16 The components of master mix, necessary for one EHT formation

Reagent	µl per one EHT
Bovine collagen (5.8mg/ml)	80.25
2x Iscove	80.25
0.1 M NaOH	8
1M MOPS	5.25

An appropriate amount of cell mixture was combined with the master mix. 450 µl of the established EHT mixture was transferred to each cavity of the molding dish and incubated for 1 hour at 37°C with 5% CO_2. After the required time, 5ml SFMM-TGFβ medium was added to the dish (day 0). The medium was changed daily until days 4-5, when formed tissues were transferred onto the stretchers. For the following 10 days of isometric exercises, SFMM medium (5ml/well) was provided every day. On day 14, the

measurements were performed. Additionally, every day 6, day 10, and one day before measurements, the videos were recorded for future contraction analysis by using an inverted light microscope Zeiss AxioVert 100 with camera Axiocam 305 color.

3.2.7. EHT measurements and analysis

3.2.7.1. EHT measurements

Before each measurement, the fresh Tyrode solution had to be prepared with a pH of 7.4 (Table 17). Also, the calibration of the 840MD Myograph had to be performed before every use. Calibration was performed using a 10 g weight to check the display for the 49.05 mN force for each transducer. When all equipment was switched on and correctly set to zero, 9ml of Tyrode solution in chambers reached 37°C, measurement could be conducted. EHT was hung on personalized hooks.

The stimulation was switched on, and the EHT have respectively undergone the procedure: 1) optimal force generation - Frank-Starling curve, 2) calcium dose-response relationship, 3) isoprenaline pharmacological stimulation and 4) muscarinic receptor stimulation. The curves were created logarithmically, in accordance with pharmaceutical standards. At least seven points were used on a logarithmic scale.

Between every procedure, EHT was washed twice for 5min with fresh Tyrode solution.

Table 17 The components of Tyrode solution.

Reagent	per 2L of Tyrode
<u>Stock A</u> 296.174 g NaCl 16.103 g KCl 8.539 g $MgCl_2 * 6H_2O$ 1.176 g $CaCl_2 * 2H_2O$ 2L Milipore - H_2O	100 ml
<u>Stock B</u> 2.318 g $NaH_2PO_4 * H_2O$ 73.929 g $NaHCO_3$	100 ml

2L Milipore - H_2O	
Glucose	2 g
Ascorbic acid	200 mg
Milipore - H_2O	1800 ml

3.2.7.1.1. Frank-Starling mechanism

The measurement was started by stretching each tissue to a passive force of contraction (FOC) of 0.13 mN. Subsequently, FOC was quantified following incremental stretches of 0.1 mm in physiological calcium conditions (1.4 mM). FOC exhibited a logarithmic increase in mN with each additional stretch. The elongation process will stop once a plateau phase is reached and the values for active and passive force are noted. For each EHT, the values are determined individually.

3.2.7.1.2. Calcium response

At the beginning of the measurement, the tissue was stretched to the determined passive force during the Frank-Starling mechanism. The initial concentration of calcium in Tyrode's solution was 0.2 mM. Subsequently, it was incrementally increased successively: 0.4 mM, 0.6 mM, 0.8 mM, 1 mM, 1.4 mM, 1.8 mM, 2.2 mM, 2.6 mM, 3.0 mM, 3.4 mM. The concentration changes occurred every 3 minutes.

3.2.7.1.3. Reaction for β-adrenergic stimulation

Initially, the tissue was elongated to achieve the specified passive force in Frank-Starling mechanism measurement. An isoprenaline curve was performed by logarithmically increasing the ISO concentration in a 0.8 mM calcium Tyrode solution (0.1 nM, 0.3 nM, 1 nM, 3 nM, 10 nM, 30 nM, 100 nM, 300 µM, 1 uM, 3 µM). Concentrations were increased every 3 minutes.

3.2.7.1.4. Muscarinic receptor stimulation

The measurements were performed at 0.8 mM Ca^{2+} concentration and consisted of a

sequence of steps. As in the steps before, the EHT was stretched to the determined passive force during the Frank-Starling curve.

The first part consisted of incubation with two doses of carbachol, in order: 10 µM and 30 µM. Between concentration changes, 3 minutes incubation was executed. After the FOC measurement, a carbachol washout step followed. Rinsing twice for 5 minutes with Tyrode solution enriched with 0.8 Mm calcium concentration allowed for further measurement. In the second part of the measurement, isopropanol was added. Initially, at a calcium concentration of 0.8 mM, the tissue is incubated with 1 µM ISO for 3 minutes. Then the first concentration of previously used carbachol - 10 µM - is added to the solution. After 3 minutes, the concentration is increased to 30 µM.

3.2.7.2. EHT analysis

After the experiment was completed, the raw data were modified for analysis in LabChart 8 software. Each measurement was adjusted in three versions:

- Force of contraction (FOC) – raw data, the difference between the maximum and minimum value of the force;
- Beats per minute (BPM) – raw data preparation: normalize 5s, noise 0.1 mN, peak height 0.5 SD, detection two-sided height, peak search window 30s. Long, around 1 min selection was marked for each step;
- Speed of contraction – raw data preparation: 1st derivative, window width 5 points, scale 10/s. Total duration time, contraction and relaxation time.

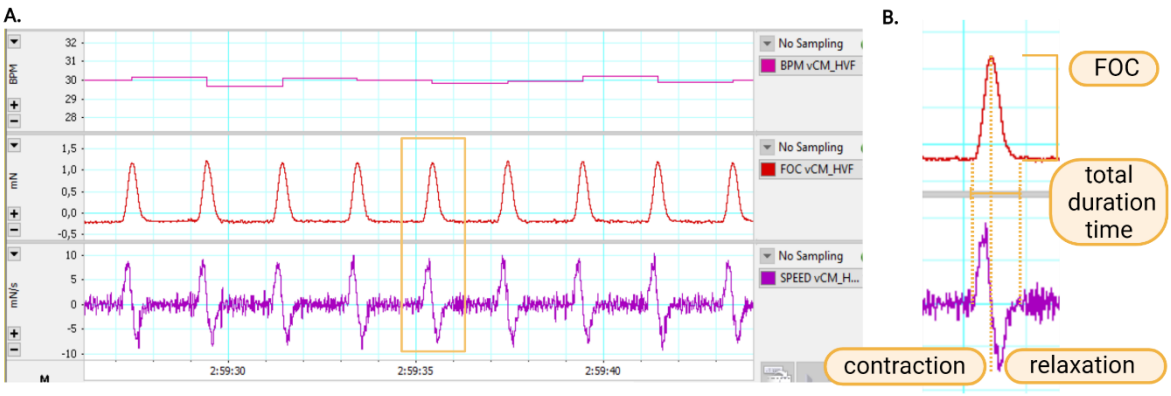

Figure 12 Modification of raw data. A) Three main modifications for FOC, BMP and speed of contraction analysis. B) Detailed description. Measurements presets vCM_HVF, in concentration 0.8 mM Ca^{2+}. Created with BioRender.com.

For each point on the curve, 10 measurements were collected during the last minute before changing the stretch or the concentration of the stimulating agent.

3.2.8. RNA isolation

To investigate the expression of cardiac-related genes, between 0.5 - 1mln cells were collected for RNA isolation. To obtain RNA from cardiomyocytes or EHT, following procedures have to be performed: homogenization, phenol-chloroform extraction method, RNA isolation using a silica membrane technology and RNA purification.

After the EHT measurements, the tissue was washed twice in DPBS to remove any residual substances. Both - EHT or cells collected from 2D culture condition, were resuspended in 1ml TRI reagent (Sigma) and transferred to a previously cooled zirconium bead tube, provided by the Bead-Beat Total RNA Mini Kit (A&A Biotechnology).

Homogenization was executed in 3 cycles consisting of 11s homogenization at a speed of 7 m/s and 10s break. When the tissue disintegrated, 200 µl of chloroform (Sigma) was added to the lysates, and the samples were gently mixed by inverting the tubes several times. The samples were left for 3 minutes at room temperature and then centrifuged for 10 minutes at 10 000 RPM. The upper fractions, approximately 450 µl of supernatant, were carefully collected into new 1.5 ml test tubes and, 500 µl of isopropanol (POCH) was added. After 10 min incubation on ice, the mixture was then applied to the spin

column, provided by RNeasy Mini Kit (Quigen), and centrifuged for 15 s at ≥8000g. The supernatant was removed, and 700 µl of RW1 was added to the spin columns, centrifuged for 15 s at ≥8000g, and flow-through was discarded. The next step was washing with 500 µl of RPE. The step was performed twice, first centrifuged for 15 s at ≥8000g, and secondly - 2 min at ≥8000g. Each time, the flow-through was removed. After the final centrifugation at a full speed for 1min, the columns were placed in new RNA-free 1.5 ml elution tubes. To elute the purified RNA, 30 µl of RNA-free water was added to the spin columns and left for 3 minutes at room temperature. The columns were then centrifuged for 1 min at ≥8000g.

To purity of the extracted RNA and remove any remaining genomic DNA (gDNA), a digestion step was carried out using the TURBO DNAse Kit (Thermo Fisher Scientific). This kit effectively degrades gDNA without affecting the integrity of RNA. 0.1 volume of 10X TURBO DNase™ Buffer was added to the RNA and gently mixed, then - 1 µL of TURBO DNase™ Enzyme. The samples were incubated at 37°C for 25 min. After the incubation, 3 µL of the DNase Inactivation Reagent was added and incubated for another 5 minutes at RT. Following this, the samples were centrifuged at 10000g for 1.5 min and the supernatant, which contained the RNA, was carefully transferred to a fresh tube without disturbing the pellet of DNase Inactivation Reagent.

The concentration of obtained RNA was determined using a Nanodrop and the purified RNA was stored at - 80°C for further use.

3.2.9. Reverse - transcription

1 µg of the purified RNA was required to reverse transcription using the SuperScript™ IV kit (Thermo Fisher Scientific). First, 1 µg of RNA was mixed with Random Primers and DNTP mix (Table 18). Then the mixture was heated to 65°C. After 5 min incubation, the samples were placed on ice for at least 3 min. During this time, another mix was prepared (Table 18) and then added to the sample. The reverse transcription was performed with the program: 23°C for 10min/50°C for 10min/80°C for 10min/ 4°C. The obtained cDNA was diluted to a working concentration of 5ng/µl cDNA and stored at -20°C.

Table 18 The reverse transcription reaction composition.

Reagent	µl per sample
Random primers	1
dNTP mix (10 mM each)	2
Template RNA (1000 ng)	10
5x SSIV Buffer 4,0	4
DTT (100 Mm)	1
RNaseOUT RNase Inhibitor (40 U/µl)	1
SuperScript® IV Reverse Transcriptase (200U/µl)	1
total volume	**20**
cDNA concentration	**20 ng/µl**

3.2.10. Real-time PCR

The mRNA expression levels were measured by performing quantitative real-time PCR (qRT-PCR) with the PowerUp SYBR Green Master Mix (Thermo Fisher Scientific). The reaction was performed in volume 10µl, as presented in Table 19. The cDNA used in the qRT-PCR was a 5x diluted product of reverse transcription to obtain final concentration of 10 ng/µl.

Table 8 contains the list of primers that were used for iPSCs and CMs characteristics. To normalize the data for an accurate comparison, the control gene (housekeeping gene) was always included in the analysis. *GAPDH* was chosen as a reference genes for this purpose.

Table 19 The single qRT-PCR reaction composition

Reagent	µl per sample
PowerUp SYBR green Master Mix	5.0

primers (20 µM)	F 0.15 R 0.15
cDNA(10ng/µL)	2
H_2O	2.7

The qRT-PCR reaction was performed with the program presented in Table 20, using the CFX96 Touch Real-Time PCR Detection System. The results were analyzed with CFX Maestro™ Software, applying the comparative ΔΔCt method for relative quantification of gene expression, by comparing the target gene expression to a reference gene (*GAPDH*) and a control group.

Table 20 The standard condition of qRT-PCR reaction.

Temperature	Time	Cycle
50°C	2 min	x1
95°C	2 min	
95°C	15 sec	x40
60°C	15 sec	
72°C	1 min	
55 - 95°C	2-5 sec	x1
0. 5°C	2-5 sec	
4°C	∞	x1

3.2.11. Immunofluorescence staining

The immunofluorescence staining was performed after specimen preparation. Depending on the material, the seeding and preparation process were different:

- iPSCs: cells were seeded on pre-coated with 16mg/ml Geltrex cover glasses at a density of approximately 50 000 cells per cover glass and incubated until cells reached the desired colony morphology. Every day the E8 Medium was changed.

Before the immunofluorescence staining, cells were washed 3 times with 500µl DPBS for 5 min.

- EBs: after transfer EBs from AggreWell to Geltrex coated cover glasses were cultured in E6 medium supplemented with 20% HyClone Fetal Bovine Serum for a period of 12 days, with medium changes every 48 hours. Before the immunofluorescence staining, cells were washed 3 times with 500µl DPBS for 5 min.
- CMs: cells were seeded on pre-coated with Geltrex cover glasses at a density of approximately 30 000 cells per cover glass and incubated for 24 hours in Cardiac Digestion Medium (7.3. Cardiomyocytes digestion). Within the next 24h medium was changed for Cardiac Culture Medium. After 2 days, the cells were ready for immunofluorescence staining. Before the procedure, CMs were washed once with 500µl DPBS for 5 min, and once with 500µl relaxation buffer (containing DPBS with magnesium and calcium ions, $MgCl_2$ (Sigma) and EGTA (Sigma)). Then, were incubated in a relaxation buffer for 5 min at 37°C.

After washing, all the cells followed the same steps of the immunofluorescence staining protocol. Fixation was performed by incubation with 4% buffered paraformaldehyde (Sigma) for 20min at 4°C. Following fixation, the cells were washed again, three times with 500µl DPBS for 5 min and stored in a 1% solution of bovine serum albumin (BSA, Sigma) in DPBS until further analysis, for a maximum of two weeks at 4°C.

Every staining procedure took 2 days. On day 1, cells were washed three times with 500µl PBS and then permeabilized with 0.5% Triton-X-100 (Sigma) in PBS for 15 minutes. The next step was 1-hour incubation at 4°C, in 10% goat or donkey serum (Sigma) diluted in PBS containing 0.1% Triton-X-100 to block nonspecific epitopes. After blocking, a solution of primary antibodies (Table 11) with goat/donkey serum was added and incubated overnight at 4°C in 1% BSA in PBS + 0.5% Triton X-100. On day 2, cells were first washed three times with 500µl PBS, and a solution of secondary antibodies (1:500) conjugated with fluorochromes (Table 11) with goat/donkey serum was added for an hour incubation at 4°C. Three washes with 500µl PBS were performed before the visualization of the cell nuclei, by adding one drop of Fluoroshield DAPI (Sigma) on the cover glass. The prepared specimen was attached to the glass slides. To detect the

presence and localization of specific proteins cells, were observed under a Leica DMi8 confocal microscope.

3.2.12. Flow cytometry

Cells were washed three times with 500µl PBS before fixation. The cell pellet was resuspended in 5 ml of 4% paraformaldehyde (PFA) and incubated for 10 minutes at RT. Following fixation, cells were centrifuged at 300g for 5 minutes at RT and the fixative was aspirated. The cell pellet was resuspended in PBS and stored at 4°C for a maximum of one month.

On Day 1, the cells were centrifuged at 300g for 5 minutes at 4°C, and the fixative was aspirated. The cell pellet was then resuspended in 300 µl of blocking buffer (filtered through a 70 µm strainer) and transferred to 1.5 ml tubes for permeabilization at 4°C for 5 minutes. After another centrifugation at 300g for 5 minutes at 4°C, the supernatant was removed. The primary antibody (Table 11) was prepared in blocking buffer and added at a volume of 150 µl per tube, followed by overnight incubation at 4°C. On Day 2, 500 µl of PBS at 4°C was added, and the cells were centrifuged again at 300g for 5 minutes at 4°C, with the supernatant aspirated. The cells were washed with 500 µl of blocking buffer, centrifuged, and the supernatant was removed. The secondary antibody (Table 11), was prepared in blocking buffer and added to each tube at 150 µl per tube for a 1-hour incubation at 4°C. After another washing step with PBS and blocking buffer, the cells were resuspended in 500 µl to 1 ml of PBS and transferred to CytoFLEX Flow Cytometer for analysis.

3.2.12. RNA sequencing analysis

The RNA material isolated from one million cells per sample was transported on ice for external analysis.

RNA sequencing was performed by Eurofins Genomics Europe Sequencing GmbH, Germany applying the INVIEW Transcriptome (NGS Built for You (eurofinsgenomics. eu)) product. This included purification of mRNA, fragmentation, strand-specific cDNA

synthesis, end-repair, ligation of sequencing adapters, amplification and purification. The prepared libraries were then quality-checked, pooled and sequenced on an Illumina platform with the following sequencing parameters: at least 40M reads/sample, read configuration 2x 150bp (Illumina NovaSeq6000, PE150 model). RNA libraries were fr-firststrand - the right-most end of the fragment (in transcript coordinates) is the only sequenced for single-end readsRaw data were preprocessed to generate clean data for downstream analysis. Then, High-quality sequence reads were aligned to the reference genome using STAR (Spliced Transcripts Alignment). Gene quantification was achieved by inspecting transcriptome alignments using featureCounts. All the data were presented to emphasize variation as a Principal component analysis (PCA) technique. The abundance counts of each gene were then used to perform differential gene expression (DGE).

Further data analysis and visualization were performed in collaboration with an external bioinformatics service provider (Data2biology, Poznan, Poland).

3.2.13. Secretome analysis

The medium from 2 mln cardiomyocytes and 1 mln fibroblasts was collected for each sample, centrifuged at 300g for 5 minutes at RT, and transferred for external analysis.

The service was performed by Institute of Biochemistry and Biophysics of the Polish Academy of Sciences in Warsaw. Performance of the service of quantitative and qualitative measurement of proteins in the culture medium by mass spectrometry and bioinformatic analysis of the protein secretome carried out on the basis of the following procedure: FASP purification; FAIMS fractionation; quantitative measurement of proteins using the label-free method on the LC-MS system consisting of the Evosep One chromatograph and the Orbitrap Exploris 480 spectrometer. The results were divided into two groups, according to qualitative and quantitative. Qualitative results included 2868 proteins, which had to be identified based on at least 2 unique peptides in at least 2 samples. Quantitative results indicated 445 proteins, which obtained $p<0.02$ in at least 1 comparison and were identified in at least 5 samples, in at least 2 groups and based on at least 2 unique peptides). In total, 446 secreted proteins were detected in the samples.

3.2.14. Statistical analysis

To improve results reliability, each experiment was conducted with multiple biological (N) and technical (n) repetitions, as indicated in the figure.

All statistical analyses were performed in GraphPad Prism 9. Student's t-test was applied to determine the statistical significance of results from RT-qPCR, contraction analysis in 2D culture, and EHT physiological measurements. Correlations between atrial and ventricular cardiomyocytes in 2D/3D systems, before and after pharmacological stimulation, were determined using a one-way ANOVA test, Bonferroni correction. Results were considered statistically significant when $p<0.05$ (ns), and represented as *, **, *** or **** when $p<0.05$, $p<0.01$, $p<0.001$ and $p<0.0001$, respectively.

4. RESULTS

To fulfill the determined aim of studies, the results are divided into three parts:

1. Formation and characterization of full chEHT, consist of atrial cardiomyocytes and atrial fibroblasts, and respectively - ventricular cardiomyocytes and ventricular cardiac fibroblasts.

2. Application of chEHT in atrial-specific drug development;

3. Instead of full chamber-specificity, the study focused on the chamber development process. Investigation of cardiac fibroblasts influence on ventricular cardiomyocytes phenotype on a physiological and transcriptomic level was the key to understand the process. For the sake of clarity, Figure 7 is recited, illustrating the determined setups.

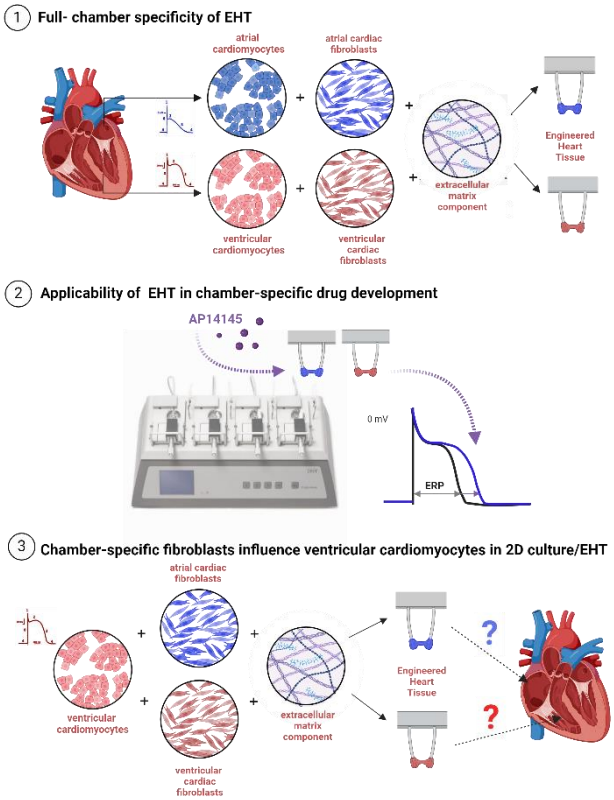

Figure 7 Experimental approach scheme.

NOTE: Throughout all the sections of the results, the blue color on graphs indicates atrial heart components (cardiomyocytes, EHT, fibroblasts) and respectively the ventricular components - red color.

4.1. Establishment of full chEHT, using iPSCs-derived chamber specific cardiomyocyte, cardiac fibroblast and extracellular matrix component

To present full chEngineered Heart Tissue, **atrial cardiomyocytes** and **atrial fibroblasts**, and respectively - ventricular **cardiomyocytes** and ventricular **fibroblasts** were mixed together with extracellular matrix component (collagen I). EHT phenotype characteristics was performed.

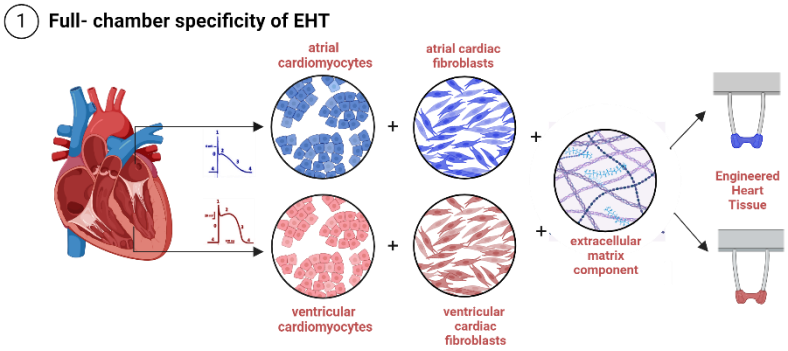

Figure 7.1. Full chamber-specificity of EHT. Created with BioRender.com.

To achieve that followed tasks were accomplished:

- iPSCs characteristics,
- iPSCs differentiation into cardiomyocytes,
- Characterization of chamber-specific cardiomyocytes,
- Optimization of atrial cardiomyocyte differentiation,
- Characterization of chEHT.

In the first section of the dissertation, the characteristics of the cells that enabled the creation of EHT were described. In the later sections, cells that meet the same quality standards were used.

4.1.1. iPSCs characteristic

To confirm that the iPSCs cell lines - iPSC_1 and iPSC_2 possessed stem cell characteristics, three distinct types of experiments were conducted to provide evidence of the pluripotency of the cells.

4.1.1.1 Molecular evaluation of pluripotency markers

Four genes were selected for analysis: *KLF4*, *NANOG*, *OCT4*, and *SOX2*, due to their significant roles in pluripotency and cellular reprogramming. To ensure accurate comparisons, a control gene (housekeeping gene) was included in the analysis. *GAPDH* was chosen as the reference gene for this purpose. Both cell lines, iPSC_1 and iPSC_2, exhibited higher gene expression of the four selected genes compared to the HVF line.

The gene expression level of *KLF4* was higher in iPSC_1 than in iPSC_2, while the expression levels of *NANOG*, *OCT4*, and *SOX2* were lower in iPSC_1 compared to those in iPSC_2, however observed differences were not statistically significant. For all of the genes *KLF4*, *NANOG*, *OCT4*, *SOX2* the expression was 10-30 times higher in the two iPSCs lines compared to the HVF ($p<0.01$). The expression results for these genes in the both cell lines - iPSC_1 and iPSC_2 are presented in Figure 13.

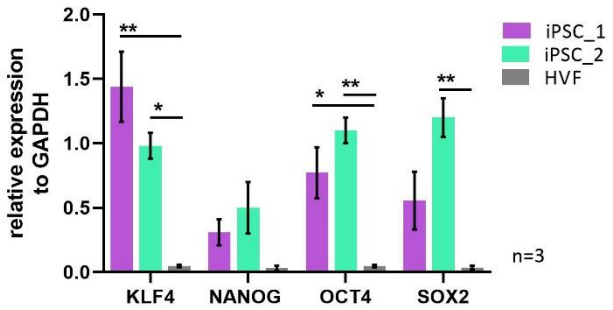

Figure 13 Pluripotency gene expression levels in cells from the iPSC_1 and iPSC_2 lineage. All values are expressed as mean ± SEM. *$p<0.05$, **$p<0.01$. Where statistical significance was not observed, it has not been indicated on the graph.

4.1.1.2 Pluripotency markers analysis on protein level

To visualize specific protein markers associated with pluripotency, the immunofluorescence was performed.

Four proteins associated with cell pluripotency were studied: NANOG, OCT3/4, SSEA4, and SOX2 (Figure 14,Figure 15**Błąd! Nie można odnaleźć źródła odwołania.**). The panels demonstrate staining with efficiency above 98 ± 1.59% for iPSC_1 line and above 91 ± 0.79% for iPSC_2 of pluripotency markers, with NANOG, OCT3/4, and SOX2 exhibiting nuclear localization, and SSEA4 present on the cell membrane.

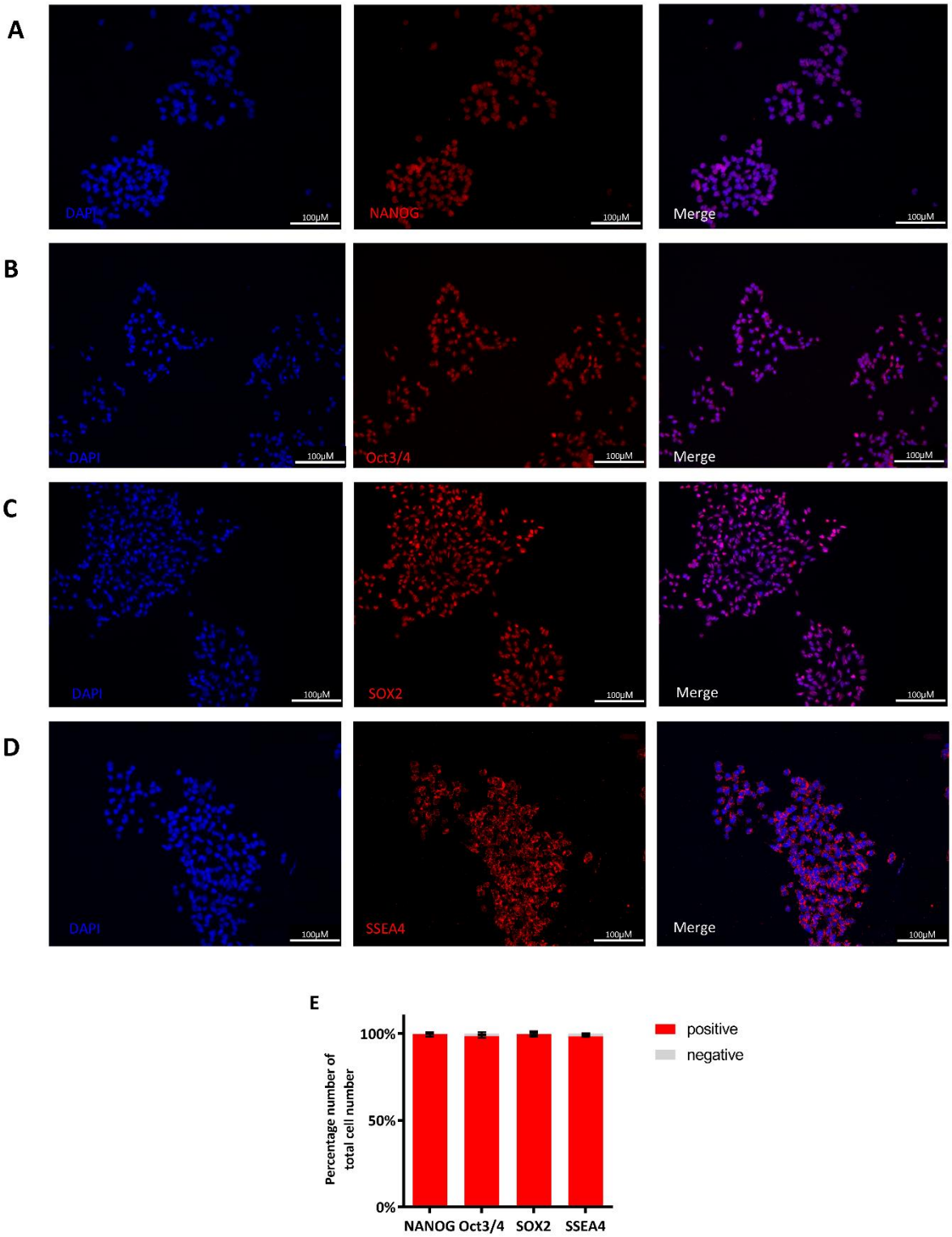

Figure 14 Immunofluorescence staining of iPSC_1 line for proteins associated with cell pluripotency. The left image shows the nuclear staining (DAPI), the middle image represents the staining of a specific marker, and the right image is a merged view combining the DAPI and marker signals. A) NANOG (red) localized in the nucleus of the cells, B) OCT3/4 (red) localized in the nucleus of the cells, C) SOX2 (red) localized in the nucleus of the cells, D) SSEA4 cell surface antigen (red). E) Percentage of total cell number based on immunostaining results. Scale bars = 100 µm.

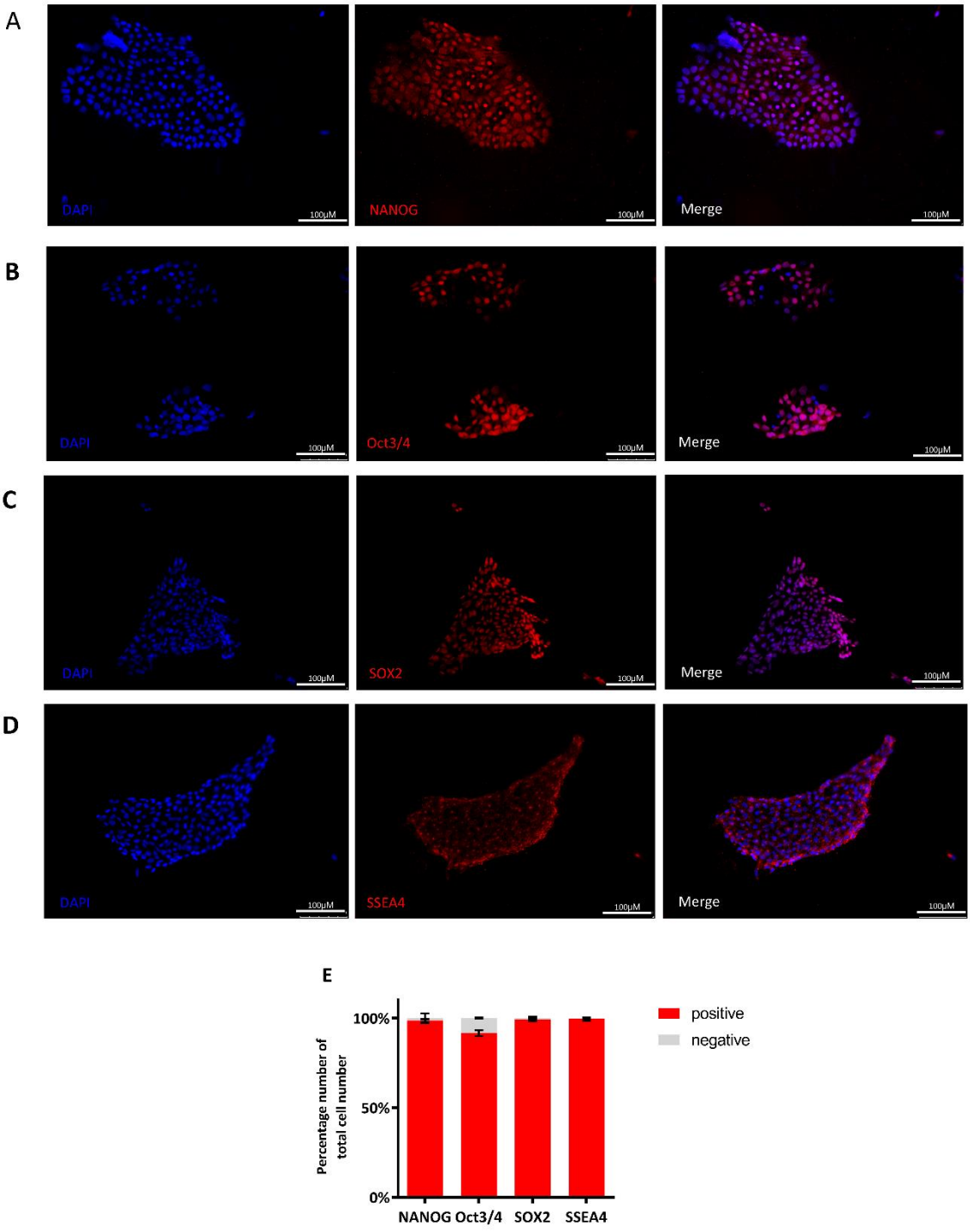

Figure 15 Immunofluorescence staining of iPSC_2 line for proteins associated with cell pluripotency. The left image shows the nuclear staining (DAPI), the middle image represents the staining of a specific marker, and the right image is a merged view combining the DAPI and marker signals. A) NANOG (red) localized in the nucleus of the cells, B) OCT3/4 (red) localized in the nucleus of the cells, C) SOX2 (red) localized in the nucleus of the cells, D) SSEA4 cell surface antigen (red). E) Percentage of total cell number based on immunostaining results. Scale bars = 100 µm.

4.1.1.3 iPSCs differentiation potential analysis

Embryoid bodies are three-dimensional cell aggregates that mimic the early stages of embryonic development. EBs were formed from both cell lines: the iPSC_1 and iPSC_2 cell lines.

The EBs immunofluorescence staining was performed with the use of antibodies directed against markers associated with the three germ layers: SOX17 (endoderm), SMA (mesoderm), and TUJ1 (ectoderm).

The intensity and pattern of immunostaining in both iPSCs lines - iPSC_1 and iPSC_2 (Figure 16, Figure 17) present:

1) for SOX17, the strong nuclear immunostaining with efficiency above 67.62 ± 10.63% for iPSC_1 line and above 62.62 ± 3.46% for iPSC_2, along with the absence of staining in other cellular regions, indicates endodermal differentiation.
2) The TUJ1 immunostaining with efficiency above 42.81 ± 4.01% for iPSC_1 line and above 40.76 ± 10.02% for iPSC_2, highlights the neurite networks typical of neuronal cells, suggesting ectoderm differentiation into neuronal lineages.
3) The SMA immunostaining shows a red cytoplasmic staining with efficiency above 39.93 ± 6.26% for iPSC_1 line and above 35.94 ± 3.21% for iPSC_2, characteristic of the filamentous structure of smooth muscle cells which suggests an effective mesodermal differentiation.

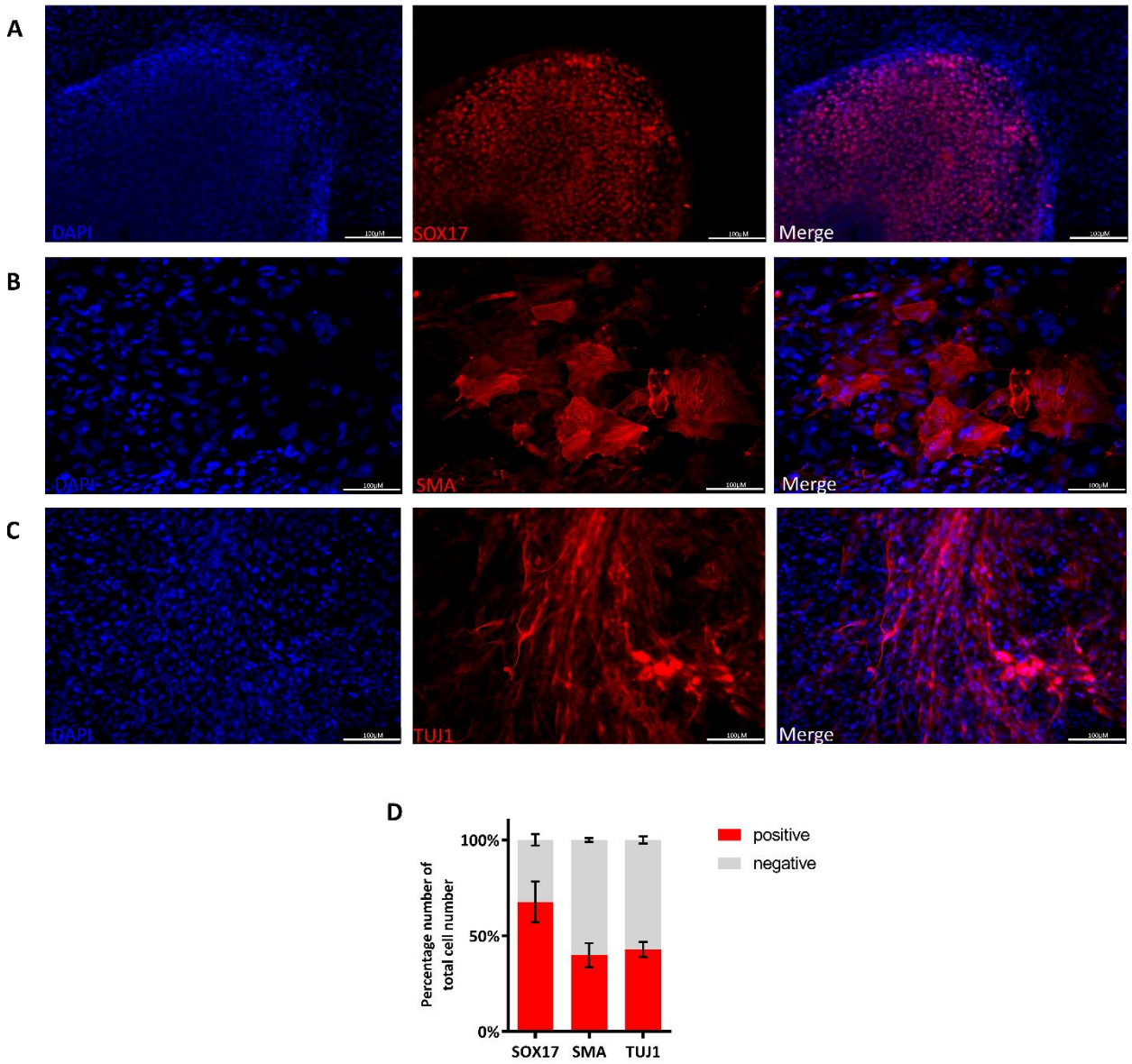

Figure 16 Immunofluorescence staining of EBs was obtained from the iPSC_1 line for the three germ layers. The left image shows the nuclear staining (DAPI), the middle image represents the staining of a specific marker, and the right image is a merged view combining the DAPI and marker signals. A) SOX17 (red) localized in the nucleus of the cells and associated with the endoderm germ layer, B) SMA (red) localized in the cytoplasm of the cell and associated with the mesoderm germ layer, C) TUJ1 (red)) localized in the cytoplasm and associated with the ectoderm germ layer, D) Percentage of total cell number based on immunostaining results Scale bars = 100 µm.

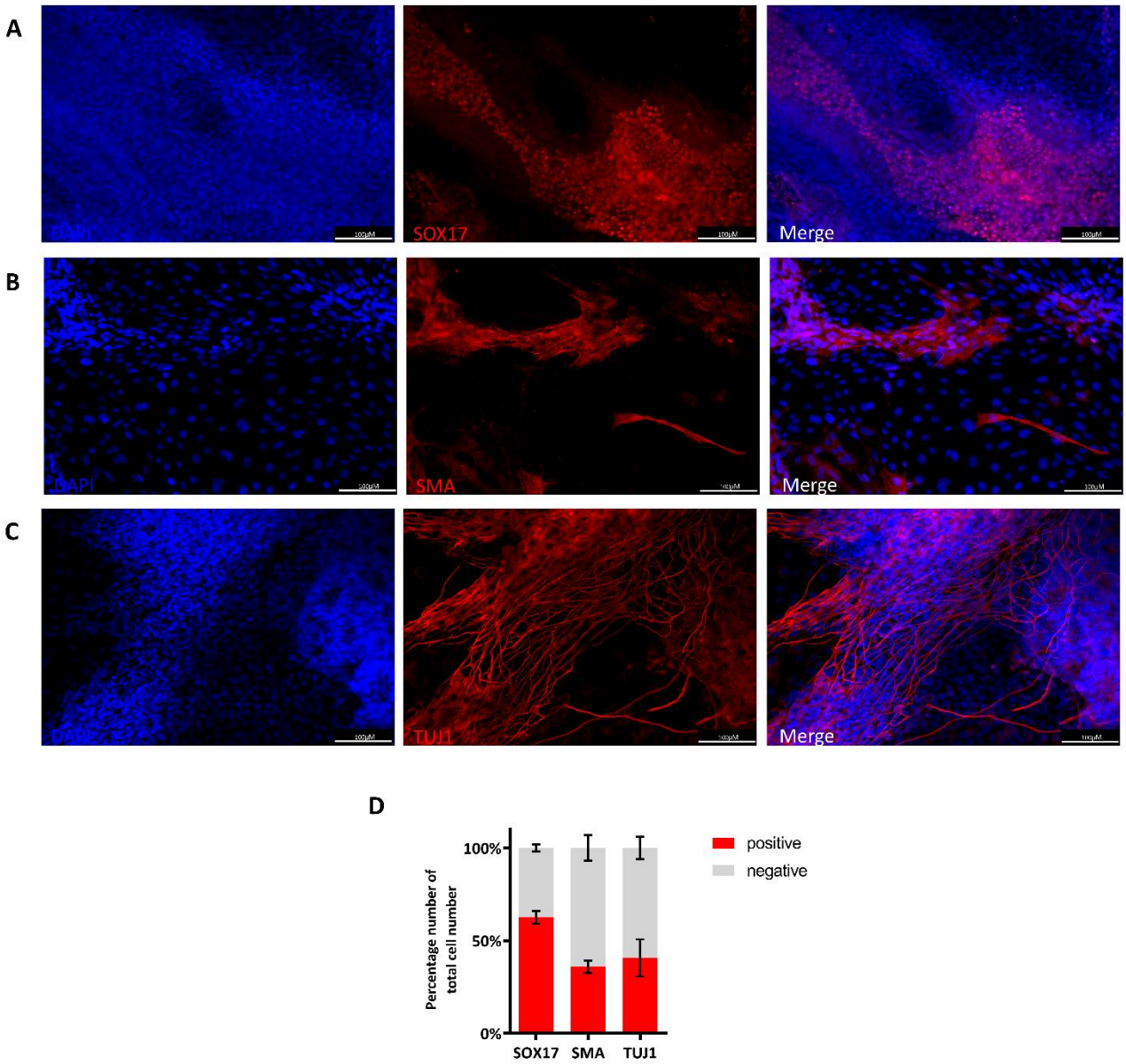

Figure 17 Immunofluorescence staining of EBs was obtained from the iPSC_2 line for the three germ layers. The left image shows the nuclear staining (DAPI), the middle image represents the staining of a specific marker, and the right image is a merged view combining the DAPI and marker signals. A) SOX17 (red) localized in the nucleus of the cells and associated with the endoderm germ layer, B) SMA (red) localized in the cytoplasm of the cell and associated with the mesoderm germ layer, C) TUJ1 (red) localized in the cytoplasm and associated with the ectoderm germ layer. D) Percentage of total cell number based on immunostaining results. Scale bars = 100 µm.

It indicates EBs capacity for tri-lineage differentiation and the robust pluripotent state of iPSC_1 and iPSC_2.

4.1.2. iPSCs - derived cardiomyocytes

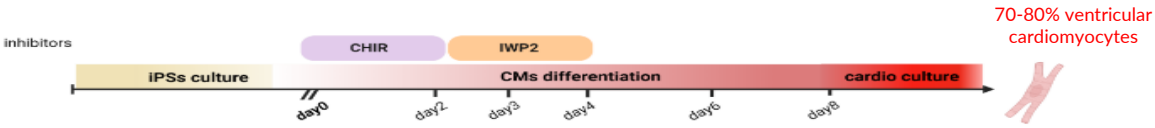

Figure 18 Process of iPSCs differentiation into the ventricular cardiomyocytes. Modified from (Cyganek et al., 2018). Created with BioRender.com.

To obtained ventricular cardiomyocytes, iPSCs (iPSC_1 and iPSC_2) were differentiated into ventricular cardiomyocytes, following the protocol by Lian *et al.* (Lian *et al.*, 2012). By blocking the BMP pathway, iPSCs were differentiated into mesoderm and then, within 8 days into ventricular cardiomyocytes, with an efficiency of approximately 70-80% (Figure 18). Modified from (Cyganek et al., 2018). Created with BioRender.com.

4.1.2.1. Cardiac markers analysis

To confirm cardiac phenotype, immunostaining of contractility apparatus components: α-actin, troponin type T (cTNT), and ventricular-specific myosin light chain 2 (MLC2v) was performed (Figure 19). The efficiency of the immunostaining of α-actinin, cTnT, and MLC2v is presented in Figure 19C. For α-actinin, the graph shows 96.55 ± 5.21% of the cells are positive, for cTnT, it appears that around 61.62 ± 4.72% of the cells are positive and for the expression of MLC2v is observed at 74.12 ± 3.90% of the cell population.

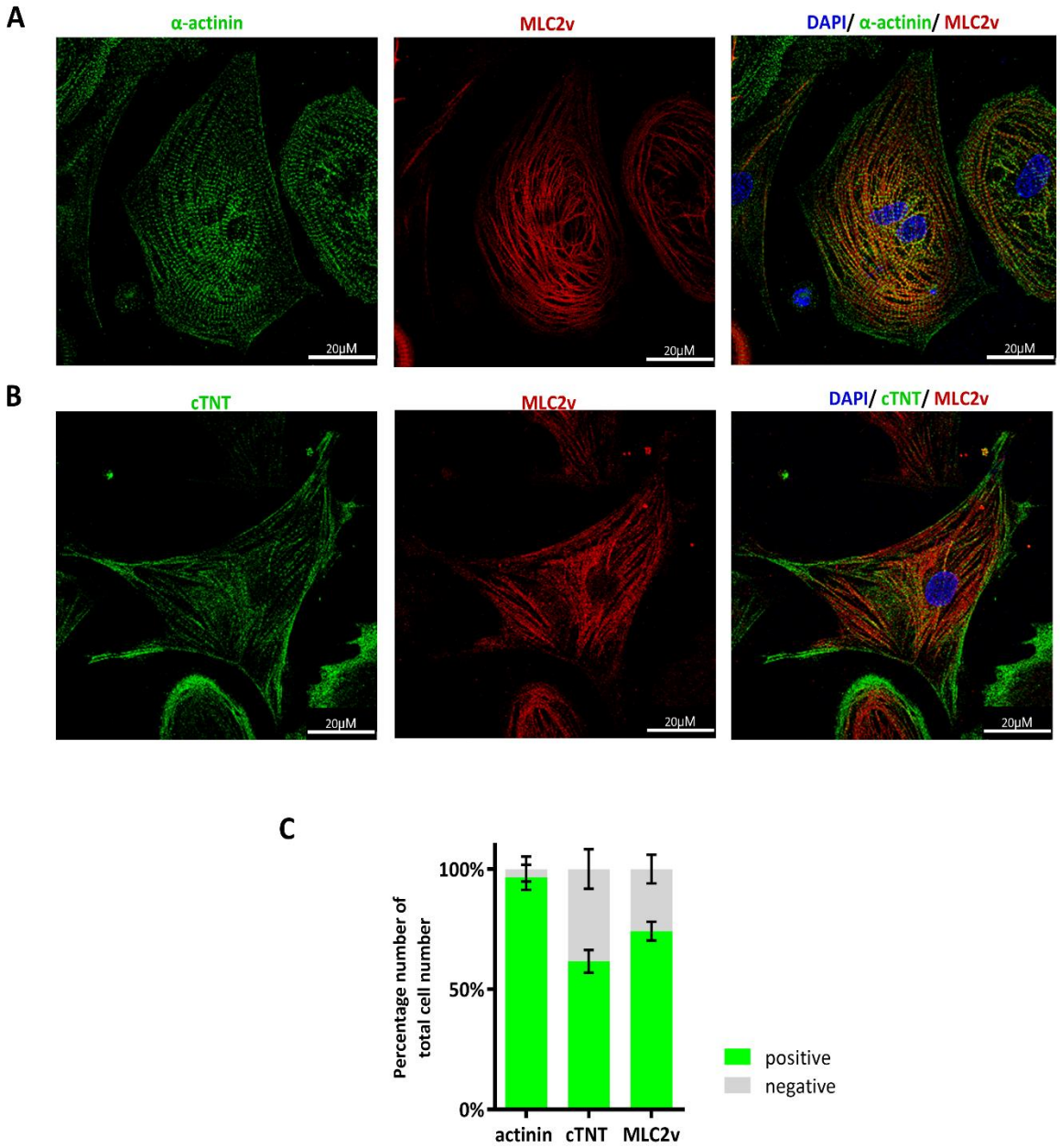

Figure 19 Immunofluorescence staining of ventricular cardiomyocytes phenotype. The left image shows the nuclear staining (DAPI), the middle image represents the staining of a specific marker, and the right image is a merged view combining the DAPI and marker signals. Structural proteins: A) α-actin (green) with ventricular-type myosin light chain 2 (red), B) cardiac troponin T (green) with ventricular-type myosin light chain 2 (red), C) Percentage of total cell number based on immunostaining results. Staining performed in ventricular cardiomyocytes on the 35th day of cell culture. The green bars represent the percentage of cells positive for each marker, while the gray portions denote negative expression. Scale bars = 20 µm.

4.1.3. Atrial-specific cardiomyocytes

To induce atrial cardiomyocytes differentiation, an additional change in protocol was needed. Briefly, the protocol changes required addition of RA (retinoic acid) to the cell culture. CMs during differentiation were incubated with RA between days 3-6 (Figure 20). The efficiency of this process is estimated to be around 50%, and phenotype was characterized by immunofluorescence procedure, flow cytometry and qPCR.

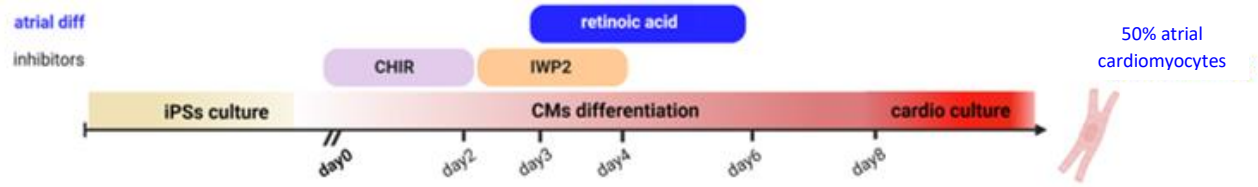

Figure 20 Process of iPSCs differentiation into the atrial cardiomyocytes. Modified from (Cyganek et al., 2018). Created with BioRender.com.

The optimization of atrial cardiomyocyte differentiation was based on the protocol by Cyganek *et al.*, where the incubation with retinoic acid for 3-6 days presents the highest efficiency of the process. However, to prove the correctness of the selected protocol, iPSCs were differentiated into aCMs, following 4 different variants. Based on the literature, the difference concerned retinoic acid's concentration and its incubation time, respectively: 1) 3-6 days incubation of 1mM RA, 2) 2-8 days incubation of 1mM RA, 3) 2-20 days incubation of 0.5mM RA, 4) 2-20 days incubation of 1mM RA. The differentiated cells were collected, and gene expression analysis was performed for key chamber-specific markers (*MYL7* and *MYL2*). The differentiation variant characterized by the highest proportion of cells expressing an

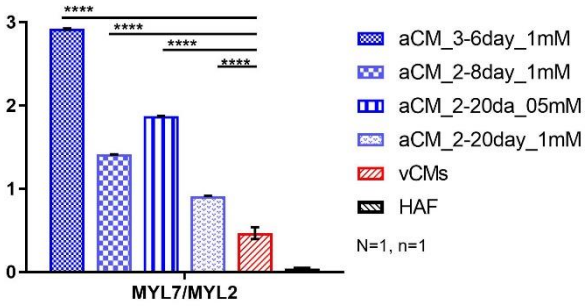

Figure 21 Figure Influence of RA concentration and incubation time on aCMs differentiation. By comparing the ratio of *MYL7* to *MYL2*, the cell population with the highest expression of the atrial-specific marker was presented (3-6 days, 1 mM). All values are expressed as mean ± SEM. ****p<0. 0001. Where statistical significance was not observed, it has not been indicated.

atrial phenotype was determined by analyzing the ratio of *MYL7* to *MYL2*. The highest ratio between *MYL7* and *MYL2* was the highest for the differentiation performed with 1 mM RA incubation. For all atrial differentiation variants, the ratio was significantly higher ($p<0.001$) than in standard ventricular cardiomyocytes protocol without RA incubation (Figure 21).

4.1.3.2. Characterization of atrial-specific cardiomyocytes

4.1.3.2.1. Molecular evaluation of chamber-specific markers

The difference between aCMs and vCMs was investigated on a molecular level, by analyzing gene expression patterns for chamber-specific markers, among others, on structural, transcription, and ion channel levels. The aCMs presented statistically significant higher gene expression of atrial-specific markers: *HEY1* ($p<0.01$), *KCNA5* ($p<0.01$), and *MYH6* ($p<0.0001$). Also, higher expression was shown for *ANP* and *KCNJ3*, however, the statistical significance wasn't presented. In the case of vCMs, statistically significant higher gene expression of ventricular-specific markers: *HEY2* ($p<0.0001$), and *MYH7* ($p<0.0001$) was presented (Figure 22).

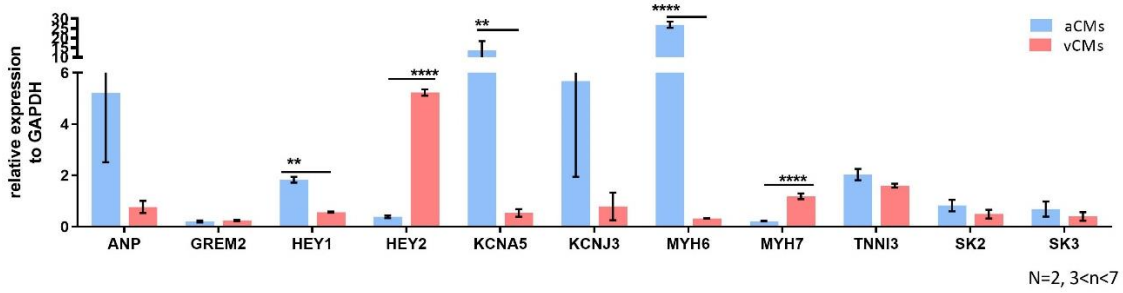

Figure 22 Gene expression analysis of chamber-specific cardiomyocytes. Analysis of gene expression proved differences between chamber-specific cardiomyocytes. Atrial-specific markers (*ANP*, *HEY1*, *MYH6*, *KCNA5*, *KCNJ3*, *SK2, SK3*) expressed higher in aCMs, and ventricular-specific markers (*HEY2*, *MYH7*) in vCMs. *GREM2*, fibroblast marker, which is required in atrial differentiation during embryonic development presented low expression in both CMs subpopulations. Structural marker – troponin I3 (*TNNI3*) was expressed higher in atrial-EHT. All values are expressed as mean ± SEM. *p<0.05, **p<0.01, ***p<0.001, ****p< 0.0001. Where statistical significance was not observed, it has not been indicated.

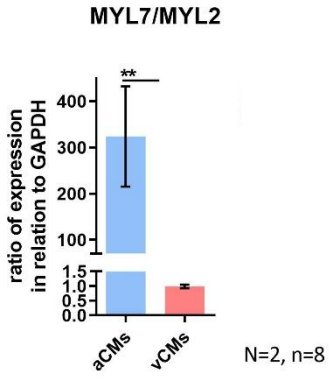

Figure 23 Ratio between *MYL7* vs. *MYL2*. **p<0.01.

Additionally, the ratio between chamber-specific myosin light-chain *MYL7* to *MYL2* was investigated. aCMs showed the statistically significant higher ratio (p<0.01), compared to vCMs (Figure 23). The *MYL7*/*MYL2* ratio is a commonly reported marker in the literature for distinguishing between atrial and ventricular phenotypes (Kolanowski *et al.*, 2020).

4.1.3.2.2. Analysis of atrial-specific cardiomyocytes protein expression

Another method to distinguish chamber-specific CMs is flow cytometry. Each of the histograms illustrates the distribution of cell populations based on the fluorescence intensity of specific markers: cTNT (for CMs identification) and KCNA5 (for aCMs identification) (Figure 24). For cTNT, the blue peaks represent unstained controls, while the red peaks indicate the stained cell population, with 81.26% in the top histogram and 67.36%, demonstrating the efficiency of the cardiomyocyte differentiation process. For KCNA5, the stained cell populations are 33.31% and 6.95% positive, respectively, highlighting the presence of atrial markers in aCMs compared to vCMs.

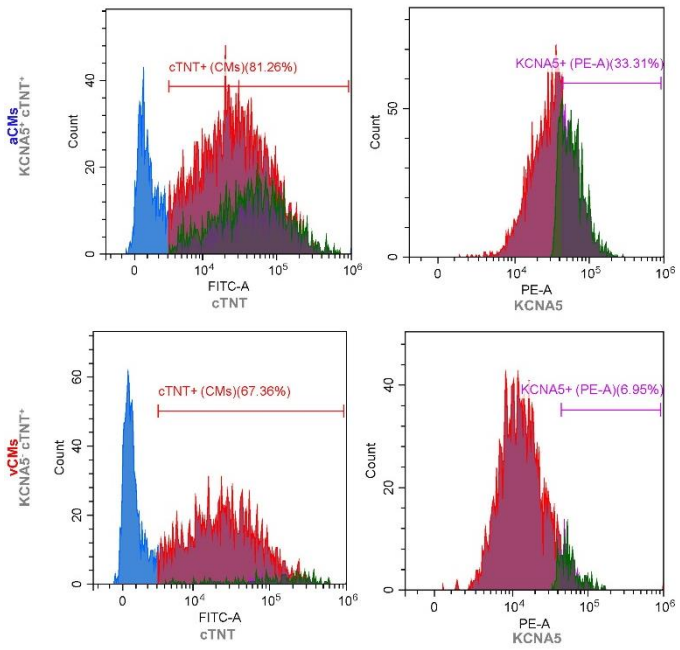

Figure 24 Flow cytometry. Distribution of cell populations based on the cardiac-specific markers: cTNT and KCNA5.

4.1.3.2.3. Chamber-specific markers analysis

To present atrial phenotype, immunofluorescence staining was performed to mark atrial-specific structural protein, myosin light chain 2, atrial type - MLC2a. The set of fluorescence microscopy (Figure 25) demonstrates the immunostaining of chamber-specific myosin-light chain markers in differentiated cell populations (atrial and ventricular cardiomyocytes).

The expression of cardiac markers MLC2a and MLC2v within the cell populations was presented on the graph (Figure 25D). The graph shows that for aCMs, approximately 61.90 ± 2.60% of the cells are positive for MLC2a, suggesting an atrial phenotype. In contrast, 79.84 ± 8.63% of the ventricular cardiomyocytes (vCMs) are positive only for MLC2v, indicative of a ventricular phenotype. The presence of cells co-expressing MLC2a and MLC2v as indicator of immature cardiomyocytes was also noticed in a small fraction of aCMs and vCMs.

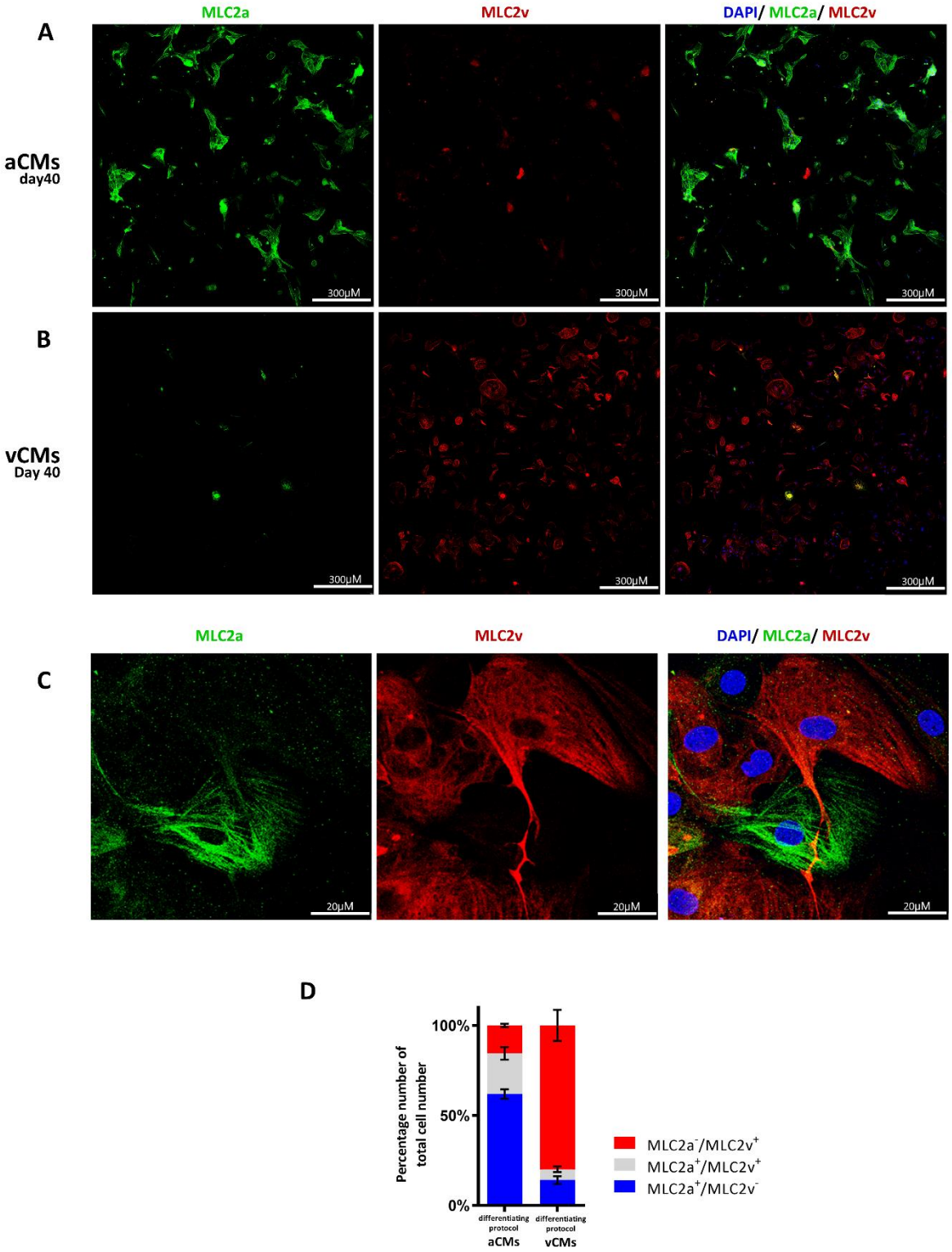

Figure 25 Immunofluorescence staining of cardiomyocytes phenotype. The left and middle image represents the staining of a specific marker, and the right image is a merged view combining both marker signals**.** Atrial-type myosin light chain 2 (green) with ventricular-type myosin light chain 2 (red)**.** A) cardiomyocytes on the 40th day of cell culture obtained through atrial cardiomyocytes differentiation, B) cardiomyocytes on the 40th day of cell culture obtained through ventricular cardiomyocytes differentiation, C) cardiomyocytes on the 35th day of cell culture through atrial cardiomyocytes differentiation, D) Percentage of total cell number based on immunostaining results**.** Scale bars = 20 µm**.**

4.1.4. Chamber-specific Engineered Heart Tissue

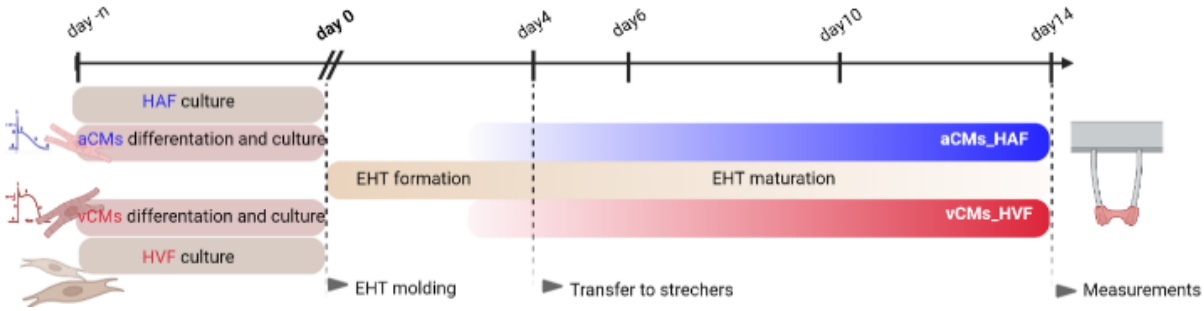

Figure 26 Scheme of chEHT formation. By combining atrial cardiomyocytes with atrial cardiac fibroblasts and ventricular cardiomyocytes with ventricular cardiac fibroblasts, the establishment of chamber-specific tissue is possible. Modified from (Tiburcy *et al*. 2014). Created with BioRender.com.

By being able to differentiate iPSCs into atrial and ventricular cardiomyocytes. chEHT was ready to perform. Modifying the protocol published in 2014 by Tiburcy *et al.* (Tiburcy *et al*, 2014), atrial and ventricular cardiac fibroblasts were implemented in the model, as a novelty factor to increase its specificity. As the result, chamber-specific cell composition was obtained. Atrial cardiomyocytes were mixed with atrial fibroblasts, and ventricular cardiomyocytes with ventricular fibroblasts and transferred to molds (3.2.5. Molding dish and stretcher preparation). After 5 days, when the cell suspension was condensed, created ring (Figure 27) were transferred into the stretcher. After 10 days of isometric exercises, on day 14, tissue measurements were performed (Figure 26).

Figure 27 Engineered Heart Tissue

4.1.5.1. ChEHT chamber-specificity on molecular level

EHT model allows the derivation of chamber-specific tissue types with differences presented on gene expression level. Atrial EHT presented a statistically significant higher

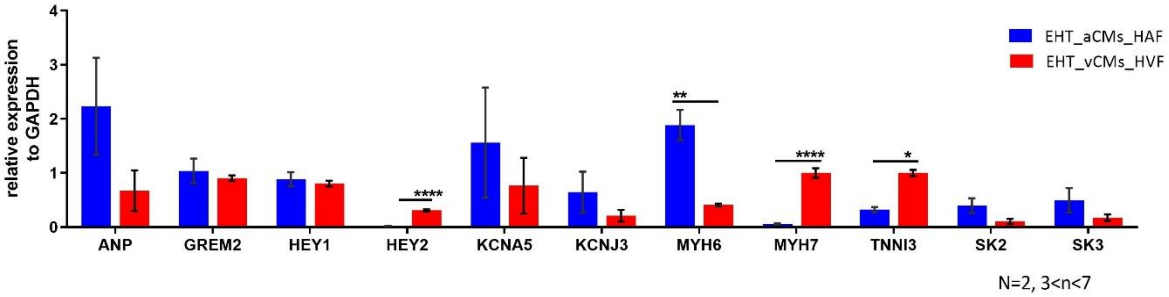

Figure 28 Gene expression analysis of chamber-specific EHT. Analysis of gene expression proved differences between chamber-specific EHTs. Atrial-specific markers (*ANP*, *HEY1*, *MYH6*, *KCNA5*, *KCNJ3*, *SK2, SK3*) expressed higher in atrial-EHT, and ventricular-specific markers (*HEY2*, *MYH7*) in ventricular-EHT. *GREM2*, fibroblast marker, which is required in atrial differentiation during embryonic development presented similar expression level in both CMs subpopulations. Structural marker, *TNNI3* was expressed higher in ventricular-EHT. All values are expressed as mean ± SEM. *p<0.05, **p<0.01, ***p< 0.001, ****p<0. 0001.. Where statistical significance was not observed, it has not been indicated.

expression (p<0.01) of atrial-specific myosin heavy chain (*MYH6*). Also, higher expression of other atrial-specific markers was presented (*ANP*, *HEY1*, *KCNJ3*, *KCNA5*, *SK2*), however, significance wasn't proven. For ventricular EHT, all ventricular-specific markers (*HEY2, MYH7*) presented statistical significance (p<0.0001) (Figure 28).

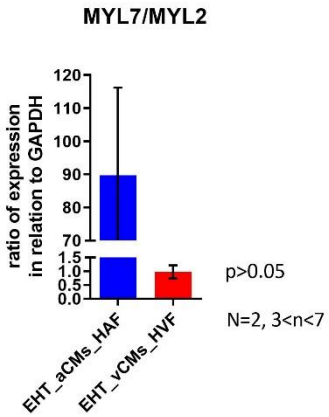

Figure 29 Ratio between *MYL7* vs. *MYL2.* p>0.05.

The ratio between chamber-specific myosin light-chain *MYL7* to *MYL2* was investigated. aCMs showed the 90 times higher ratio compared to vCMs (p>0.05) (Figure 29).

4.1.5.2. ChEHT vs. human heart markers

The comparison of iPSCs-derived CMs and EHT with human ventricular heart tissue was possible to investigate. Six samples were taken to analysis: iPSCs, aCMs, atrial EHT (aCMs_HAF), vCMs, ventricular EHT (vCMs_HVF) and heart ventricular transplantation biopsy (HTX biopsy). Four gene were analyzed: *TNNI3*, *KCNJ3*, *MYL2*, and *MYL7* relative expression of each gene normalized to a housekeeping gene (*GAPDH*) was presented on Figure 30.

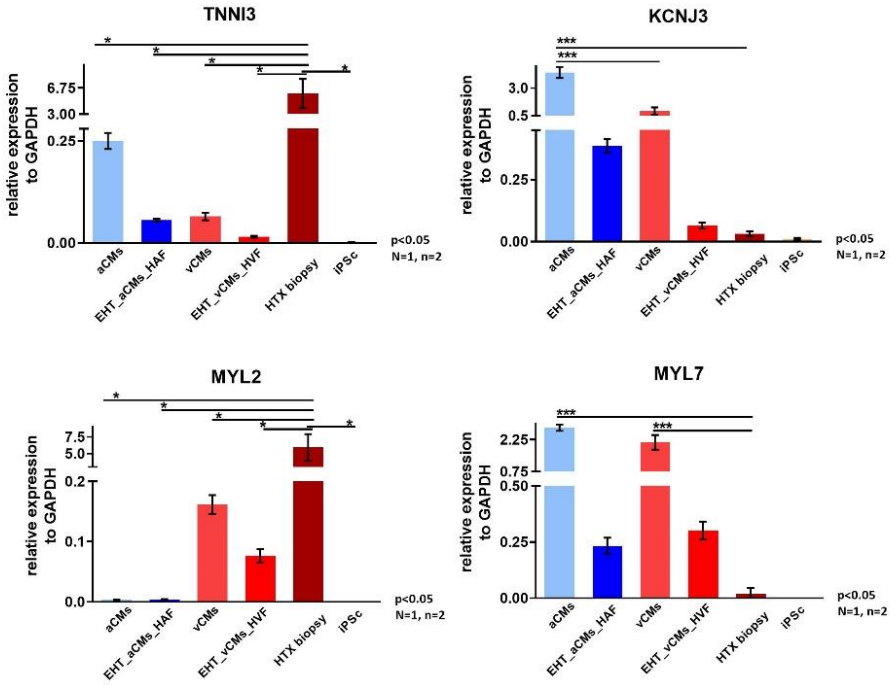

Figure 30 Comparison of HTX biopsy to EHT and its components. By compering gene expression level *of TNNI3, KCNJ3, MYL2, MYL7*, high level of contractility apparatus maturation was proven. All values are expressed as mean ± SEM. *p<0.05, **p<0.01, ***p<0.001, ****p<0.0001. Where statistical significance was not observed, it has not been indicated.

- *TNNI3* - structural marker: between iPSCs-derived CMs in 2D and 3D model, the highest expression was in aCMs. However, an almost 30 times higher expression was in HTX biopsy. iPSCs showed negligible expression.
- *KCNJ3* - atrial-specific ion channel marker: the highest expression was in aCMs. What is more, between the chamber-specific groups in 2D culture system, aCMs vs. vCMs, a statistically significant difference was observed (p<0.001). The atrial

subtype presented higher expression compared to the ventricular equivalent. HTX biopsy and iPSCs showed negligible expression.

- *MYL2* - in ventricular-specific structural marker: there is a significant increase in expression in all vCMs samples from 2D/3D system and *in vivo.* What is more, between culture systems and human ventricular tissue was almost 40 times difference in gene expression. The HTX biopsy showed a statistically higher expression ($p<0.05$). iPSCs didn't express *MYL2*.
- *MYL7* - atrial-specific structural marker: in human ventricular tissue was a minimal expression of *MYL7*, compared to vCMs from 2D/3D systems. Between the chamber-specific groups in different culture systems, aCMs vs. and vCMs (2D culture); aEHT vs. vEHT (3D culture) the statistically significant difference was observed ($p<0.001$). The ventricular subtype presented higher expression compared to atrial equivalent. HTX biopsy showed negligible expression. iPSCs didn't express *MYL7*.

4.1.5.3. Contractility pattern of chEHTs

As a part of the first phase of the thesis, concerned upon development of fully atrial and ventricular EHTs, the impact of cardiac fibroblasts implemented into a 3D model on cardiomyocyte's contractility pattern was investigated. Initially, according to the previously noted data, atrial cardiomyocytes exhibited a higher contraction rate, likely due to the automaticity provided by specialized pacemaker cells. Speciation of these pacemaker cells may explain the observed differences in beating rate between the atria and ventricles, mimicking the natural pacing system of the heart.

In the 2D culture system, atrial cardiomyocytes contacted with an average of 111.25 ± 5.55 BPM, whereas ventricular subtypes with a slower rate, an average of 40.70 ± 5.17 BPM ($p< 0.001$) (Figure 31A).

The addition of cardiac fibroblasts to the 3D culture system not only preserved the distinct contractility patterns between the atrial and ventricular cardiomyocytes but also resulted in a significant reduction of the beat rate for both cell types ($p<0.001$). The atrial CMs showed a decrease to 62.20 ± 6.30 BPM, while the ventricular CMs decreased to around 12.55 ± 1.01 BPM, at the same time, reflecting the physiological differences

observed between chambers in the human heart (Figure 31A). Furthermore, within the same type of cardiomyocytes, the significant decrease in contractility patterns was observed across culture models (p< 0.001).

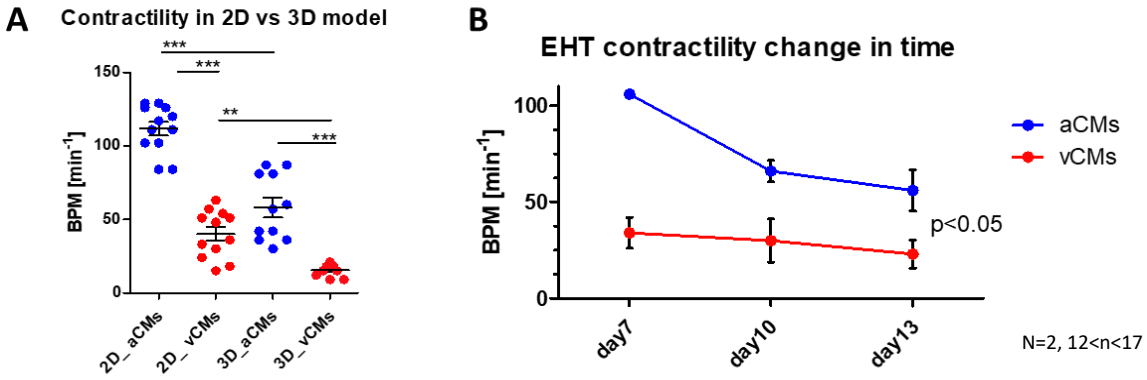

Figure 31 Contractility changes in atrial and ventricular cardiomyocytes in the 2D/3D culture system. All values are expressed as mean ± SEM. *p<.05, **p<0.01, ***p<0.001, **** p< 0.0001.

Additionally, a temporal analysis of contractility changes within the 3D EHT model presented differences during the maturation period (Figure 31B). Initially, on day 7 of tissue maturation, the beat rate did not exhibit noticeable discrepancy from the 2D culture rates. However, by day 10 of tissue development, a marked decrease in BPM was recorded, with atrial CMs and ventricular CMs demonstrating beat rates of 66.45 ± 5.81 BPM and 30.20 ± 11.01 BPM, respectively. By day 14 of tissue maturation, the beat rates for atrial CMs remained at 56 ± 10.86 BPM and for ventricular CMs – 23 ± 7.03 BPM (Figure 31B).

4.1.5.4. Physiological parameters measurements

To perform precise measurements of the major parameters of heart tissue function: force, contraction/relaxation kinetics, and responses to pharmacological stimuli at day 14, the myograph system 840 MD was used. During the measurement, three mains physiological phenomena of the human heart were considered.

4.1.5.4.1. Frank-Starling mechanism

The relation between stretch and force of contraction, which mimics Frank-Starling mechanism *in vivo*, was presented in both - atrial and ventricular EHT. Each waveform from the myograph's records represented the contraction cycles of cardiomyocytes, with peaks indicating contraction events (Figure 32A). FOC exhibited a logarithmic increase in mN with each additional stretch, yet a plateau phase occurred after approximately the fifth elongation (Figure 32B). The Frank-Starling (FS) curve enabled the determination of the active force for subsequent measurements, providing a precise baseline for further analysis.

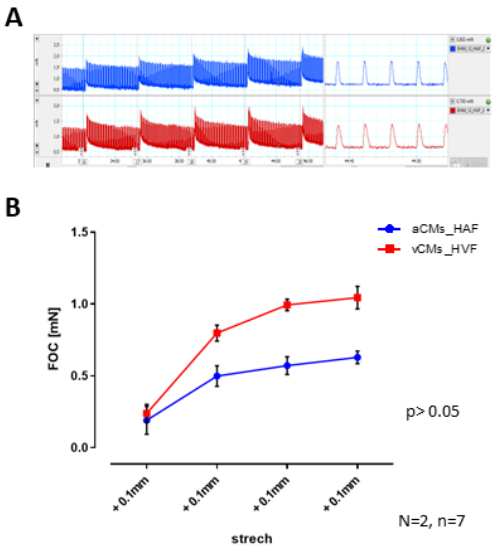

Figure 32 Frank-Starling mechanism in EHT. A) The Frank-Starling mechanism explanation, B) Frank-Starling mechanism in EHT. All values are expressed as mean ± SEM. p>0.05.

4.1.5.4.2. Calcium response

Calcium is crucial for the proper function of the heart and is critical for, among others, contributing to the electrical signal that moves from cell to cell to produce a uniform contraction or the excitation - contraction coupling process.

Contraction force of EHTs was measured just before each increment in calcium concentration (Figure 33). In both types of tissues—atrial and ventricular—the force of

contraction increased in correlation with the rising calcium levels in the solution surrounding the cells. Both subtypes revealed significant difference between each other ($p<0.001$). The logEC50 values for the atrial EHT were 1.529 and 0.754 for ventricular EHT - indicating the potency at which calcium elicits a 50% maximal response.

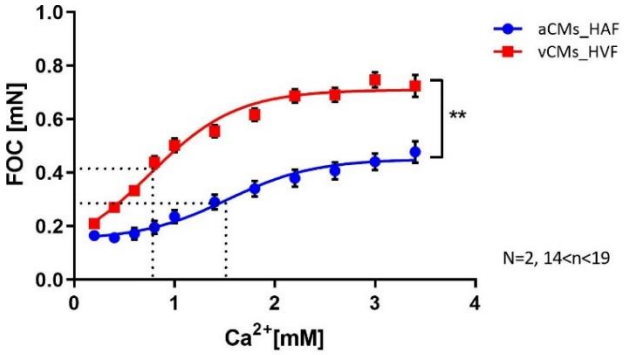

	aCMs_HAF	vCMs_HVF
LogEC50	1.529	0.7543

Figure 33 EHT response for calcium. All values are expressed as mean ± SEM. *p<0.05, **p<0.01, ***p<0.001, ****p<0.0001.

4.1.5.4.3. Reaction for β-adrenergic stimulation

The third characteristic physiological heart phenomenon is the reaction for β- adrenergic stimulation. To stimulate the β-adrenergic receptors EHT, the analog of adrenaline - isoprenaline (ISO) was used.

By using the 1 µM isoprenaline concentration in the Tyrode solution in both atrial and ventricular EHT, the FOC was increased. In atrial EHT, the FOC was significantly 1,15 times higher compared to the basal state ($p<0.01$). Respectively, in ventricular EHT - 1,7 times higher compared to the basal state ($p< 0.001$) (Figure 34).

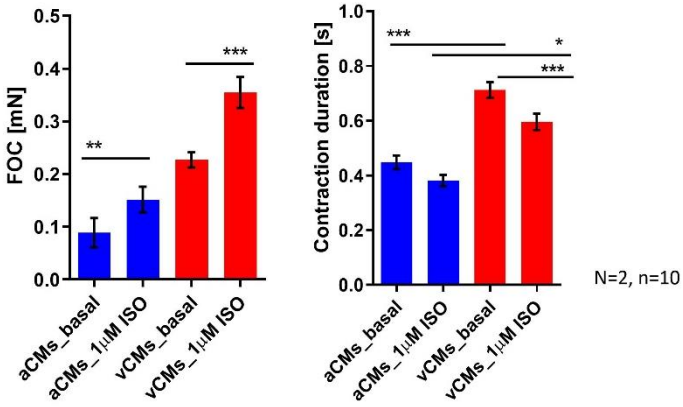

Figure 34 EHT response for 1 µM isoprenaline – force of contraction and contraction duration. All values are expressed as mean ± SEM. *p<0.05, **p<0.01, ***p<0.001, ****p<0.0001. Where statistical significance was not observed, it has not been indicated.

At the same time, 1 µM isoprenaline concentration affected contraction duration. For atrial EHT, contraction duration was shorter. Respectively, in ventricular EHT, 0,75 times shorter concentration duration compared to the basal state was observed ($p<0.001$) (Figure 34).

Full chEHTs were generated.

Sum up 8.3.1. Comprehensive characterization of EHTs at the molecular, structural, and physiological levels revealed significant differences. Notably, atrial-specific EHTs exhibited higher expression of potassium channels (*KCNA5*, *KCNJ3*) and shorter contraction duration than their ventricular subtype.

4.2. Influence of AP14145 inhibitor on small-conductance calcium-activated potassium ($K_{Ca}2$) channel – chEHT for drug testing prove of concept

Small-conductance calcium-activated potassium ($K_{Ca}2$) channels, also known as SK channels, were recently presented in the literature as the target for atrial fibrillation treatment. AP14145, one of the commonly known inhibitors specific for two subtypes of SK channel, became the prove of concept for the chEHT developed previously. An investigation of chamber-specific drug was performed by applying **atrial cardiomyocytes** with **atrial fibroblasts**, respectively – **ventricular cardiomyocytes** with **ventricular fibroblasts**.

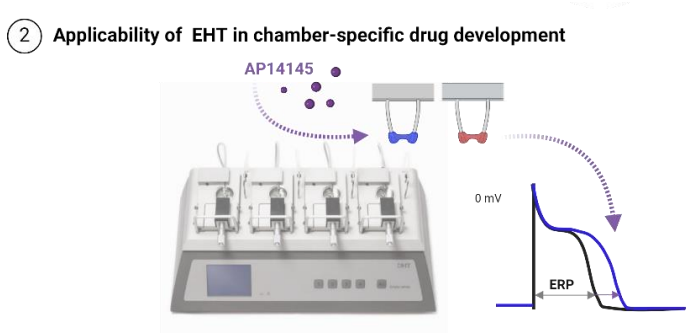

Figure 7.2. Experimental approach scheme. Created with BioRender.com.

4.2.1. SK channel inhibition in 2D culture

First, investigation of SK channel gene expression was necessary. Verifying the expression of *SK2* and *SK3* subtypes was crucial for the further AP14145 investigation in 2D culture.

4.2.1.1. Molecular evaluation of SK channel presence and atrial characteristics in 2D culture

The expression of *SK2* and *SK3* was detected in all samples - aCMs and vCMs. However, in both *SK* subtypes - *SK2* and *SK2*, almost 1,5 times higher gene expression was presented in atrial CMs, and 3D culture (Figure 35).

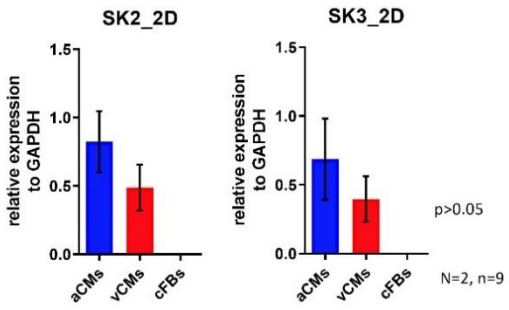

Figure 35 Identification of *SK2* and *SK3* subtype in 2D system. All values are expressed as mean ± SEM. p>0.05. Where statistical significance was not observed, it has not been indicated.

Additionally, due to the application of different differentiation into molding EHTs for this part of the experiments, the atrial phenotype was confirmed. At day 25, gene expression investigation of four atrial-specific markers (*ANP*, *KNCA5*, *KCNJ3*, *MYL7*) and ventricular-specific marker *MYL2*, was performed (Figure 31). The ratio between chamber-specific myosin light-chain *MYL7* to *MYL2* showed almost 250 times higher ratio in aCMs compared to vCMs (p<0.05) (Figure 36).

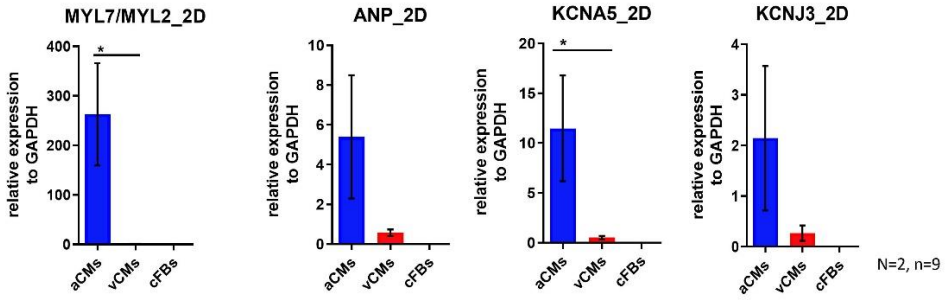

Figure 36 Investigation of atrial-specific markers in aCMs. All values are expressed as mean ± SEM. *p<0.05. Where statistical significance was not observed, it has not been indicated.

4.2.1.2. Video-based analysis of AP14145 influence on contractility patterns in 2D culture

With the confirmation of *SK2* and *SK3* expression in atrial cardiomyocytes, it was possible to investigate the AP14145 inhibitor influence on contractility patterns in 2D culture. By using MotionVector software, the analysis of the CMs contractility patterns in 2D culture is possible. The software gives the opportunity to investigate the grid of

contraction vector in 2D culture video, and as a consequence, provides the parameters values, among others: BPM, total duration time, time and amplitude of contraction/relaxation (Figure 37A).

Atrial/ventricular CMs were incubated with 10 µM AP14145 for 3 minutes in a culture medium simultaneously. Videos were then recorded and analyzed using MotionVector software. In both - atrial and ventricular CMs, after incubation with 10 µM AP14145, no changes in duration time were observed (p>0.05) (Figure 37B).

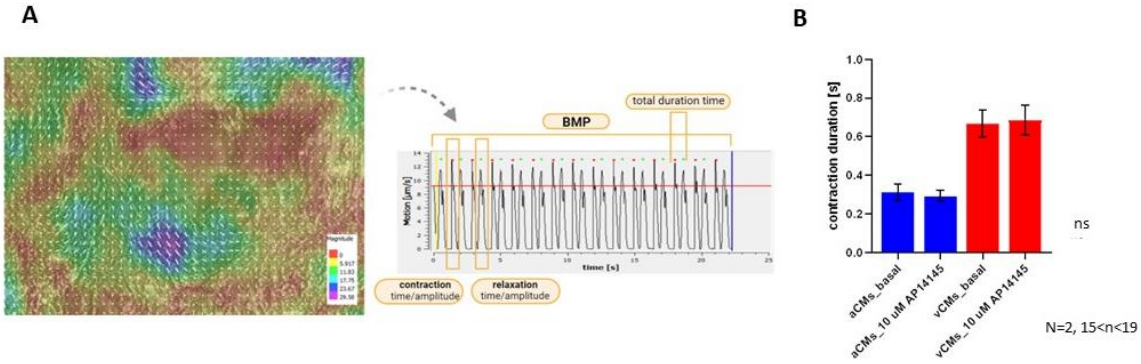

Figure 37 Influence of AP14145 on chamber-specific cardiomyocytes in 2D system. A) An example of processed movie of 2D ventricular CMs culture for contraction analysis in MotionVector software, B) influence of 10 µM AP14145 on atrial/ventricular cardiomyocyte contraction duration in 2D culture. All values are expressed as mean ± SEM. p>0.05.

4.2.2. SK inhibition in 3D culture

After the evaluation of AP14145 in 2D culture, the influence on more mature CMs in EHT model was investigated.

4.2.2.1. Molecular evaluation of SK channel presence and atrial characteristics in 3D culture

As in 2D culture, the starting point for further experiments was the identification of *SK2* and *SK3* gene expression. The expression of *SK2* and *SK3* was detected in all tissues - atrial and ventricular EHT, with significant 4 times higher gene expression in *SK2* (p<0.05) and *SK3* (ns) (Figure 38).

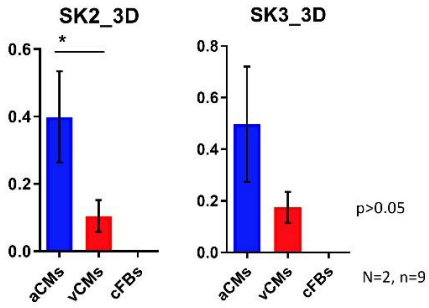

Figure 38 Identification of SK2 and SK3 subtype in 3D system. All values are expressed as mean ± SEM. *p<0.05. Where statistical significance was not observed, it has not been indicated.

Although the atrial phenotype was confirmed at the 2D culture level before modelling, it was also confirmed at day 14 of EHT maturation. Gene expression investigation of four atrial-specific markers (*ANP*, *KNCA5*, *KCNJ3*, *MYL7*) and ventricular-specific marker *MYL2*, was performed (

Figure **39**). The ratio between chamber-specific myosin light-chain *MYL7* to *MYL2* showed almost 100 times higher ratio in aEHT compared to vEHT (p<0.05) (

Figure **39**).

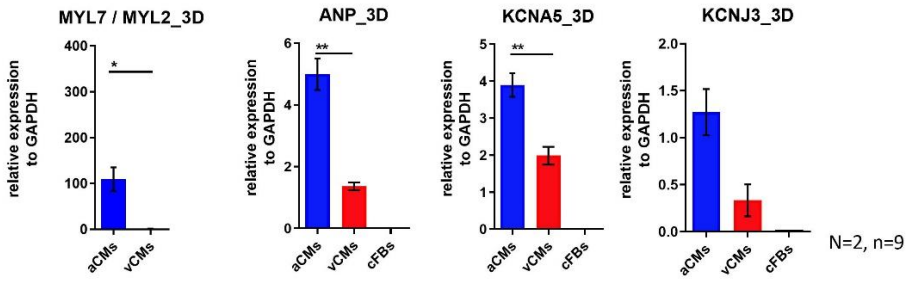

Figure 39 Investigation of atrial-specific markers in atrial EHTs. All values are expressed as mean ± SEM. *p<0.05, **p<0.01, ***p<0.001, ****p< 0.0001. Where statistical significance was not observed, it has not been indicated.

4.2.2.2. AP14145 influence on contractility patterns in 3D culture

The application of logarithmically increasing inhibitor concentration provoked an exponential prolongation of atrial EHT contraction duration (Figure 40). This was in contrast to ventricular EHT, where increasing AP14145 concentration did not affect the

total duration time. The highest concentration of AP14145, 10 µM, was selected for further investigation.

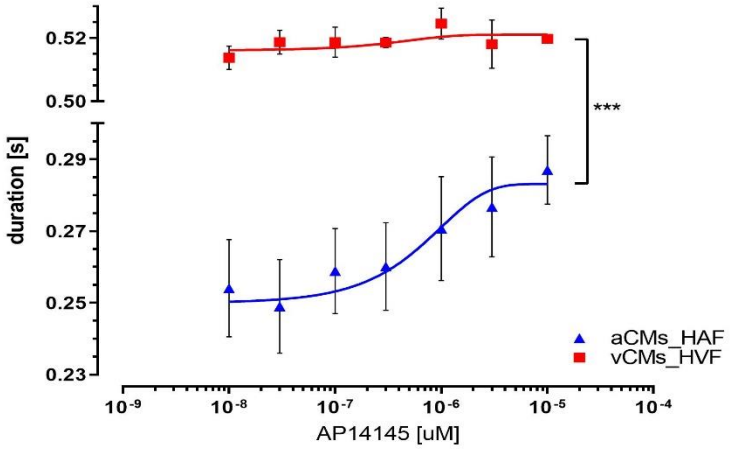

Figure 40 AP14145 response curve for atrial and ventricular EHT. ***p<0.001

EHT incubation with 10 µM AP14145 was performed during physiological measurements to investigate the impact on the tissue's total duration, relaxation and contraction time. In atrial EHT, 10 µM AP14145 significantly prolonged the total duration time from 0.24 s ± 0.005 to 0.28 s ± 0.003 (p<0.001) (Figure 41). In ventricular EHT, the duration time was maintained at the same level, approximately 0.45 s ± 0.003 s.

A more detailed analysis revealed the lack of 10 µM AP14145 influence on contraction time for EHT subtypes. Contraction time for atrial EHT was kept around 0.10 s ± 0.004, and for ventricular EHT – approximately 0.19 s ± 0.004. At the same time, presenting the influence of 10 µM AP14145 on the relaxation time of atrial EHT. Due to the pharmacological incubation, relaxation time was prolonged 1.5 times (p<0.001), then the relaxation time for ventricular EHT was maintained at the same level, approximately 0.26 s ± 0.005 (Figure 41).

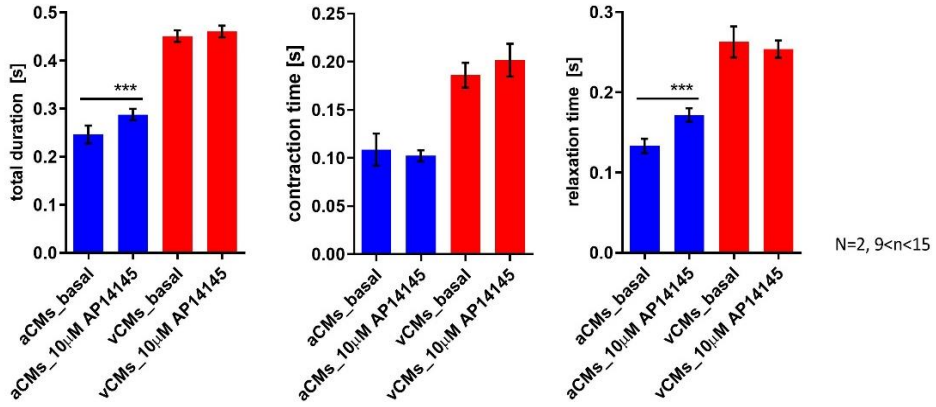

Figure 41 Influence of AP14145 on chamber-specific cardiomyocytes in 3D system. All values are expressed as mean ± SEM. ***p<0.001. Where statistical significance was not observed, it has not been indicated.

Sum up 8.3.2. All performed experiments presented the application of full chEHT in drug development. SK channel inhibitor application AP14145, prolonged the total contraction duration in atrial EHTs, specifically targeting the relaxation phase. There was no effect of atrial-specific drug on ventricular EHTs.

4.3. Cardiac fibroblasts influence on *in vitro* iPSCs-derived cardiomyocytes subtype differentiation

Due to vast elasticity and a number of factors, cardiac fibroblasts seem to be one of the candidates to drive the cardiac subtype differentiation process. To verify if the **chamber-specific cardiac fibroblasts** affect **ventricular cardiomyocytes** fate, one needs to take the way of potential action into account. Several mechanisms have been evaluated: 1) paracrine signaling, 2) cell-to-cell signaling, and mechanical/indirect stimulation in 3D culture conditions and 3) transcriptomic analysis and secretome profiling to investigate the molecular fibroblast-cardiomyocyte interactions.

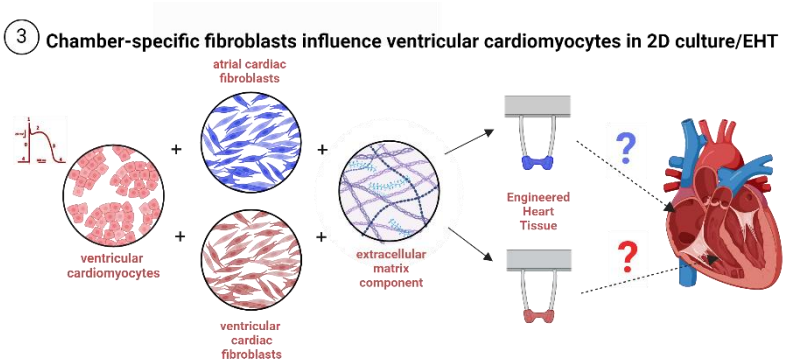

Figure 7.3. Experimental approach scheme. Created with BioRender.com.

4.3.1. Paracrine signaling test in 2D culture

To investigate whether cardiac fibroblasts may have a paracrine influence on cardiomyocytes phenotype, the experiment with conditioned medium was performed. The ventricular cardiomyocytes were incubated with cardiac culture medium or conditioned medium from atrial or ventricular fibroblasts. Every second day cells were collected for immunostaining and gene expression analysis (Figure 42).

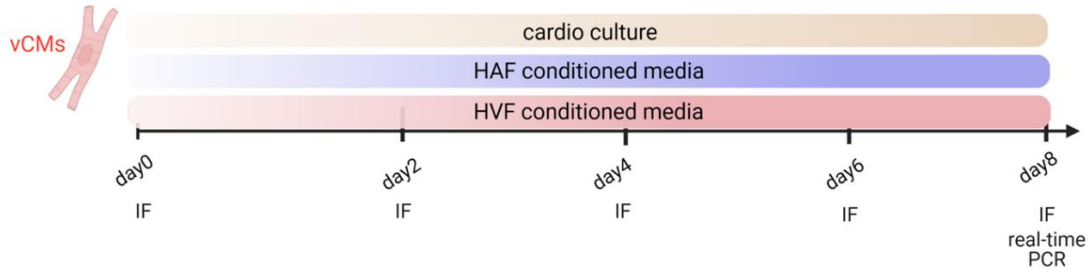

Figure 42 Scheme of experiment with the conditioned medium to investigate cardiac fibroblast paracrine influence on CMs. Created with BioRender.com.

4.3.1.1. Molecular evaluation of cardiac markers

To investigate the influence on molecular level, the gene expression analysis of three groups at day 8 was performed. For analysis atrial-specific markers (*HEY1*, *KCNA5*, *KCNJ3*, *MYL7*, *MYH6*), ventricular-specific (*HEY2*, *MYH7*, *MYL2*) and structural genes (*TNNI3*, *MYH6*, *MYH7*, *MYL2*, *MYL7*) were selected. The fibroblast-condition medium increased the gene expression of *HEY1* and *KCNJ3*. What is more, the expression of atrial-specific *KCNJ3* was 2 times higher in investigated vCMs due to HAF-condition medium application, compared to the control or HVF-condition medium (Figure 43). Additionally, the ratio between chamber-specific myosin light-chain *MYL7* to *MYL2* was investigated. vCMs incubated with HVF-conditioned medium showed 1,5 times higher ratio compared to control vCMs (Figure 43).

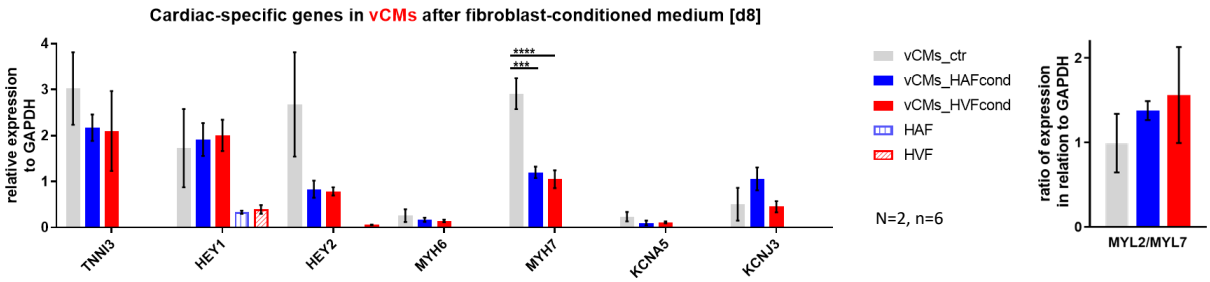

Figure 43 Cardiac-specific gene expression analysis of ventricular cardiomyocytes, after fibroblast-conditioned medium. Atrial-specific markers (*ANP*, *HEY1*, *MYH6*, *KCNA5*, *KCNJ3*, *MYL7*) expressed higher in vCMs with HAF-condition medium, and ventricular-specific markers (*HEY2*, *MYH7*, *MYL2*) in vCMs with HVF-condition medium. *TNNI3* was expressed on similar level in vCMs with HAF- and HVF-condition medium. All values are expressed as mean ± SEM. *p<0.05, **p<0.01, ***p<0.001, ****p<0.0001. Where statistical significance was not observed, it has not been indicated.

4.3.1.2. Cardiac markers analysis

All collected samples were immunostained with atrial-specific myosin (MLC2a) or ventricular-specific myosin light-chain (MLC2v). A double-positive population was indicative of its immature phenotype.

After the application of this conditioned medium, the statistically significant differences weren't noticed, however, in all three groups (control, conditioned medium with HAF

and conditioned medium with HVF), tendencies were observed. The population of immature CMs (MLC2a$^+$, MLC2v$^+$) decreased in all the groups after 8 days: from 45% to 23% in control, from 20% to 11% in HAF-conditioned, from 21% to 12% in HVF-conditioned (Figure 44).

Additionally, incubation with HAF-conditioned medium increased atrial phenotype within 8 days, the % of cell MLC2a$^+$, MLC2v$^-$ increased from 13% to 16%. Respectively, incubation with HVF-conditioned medium increased ventricular phenotype - the % of cells MLC2a$^-$, MLC2v$^+$ increased from 62% to 75% (Figure 44).

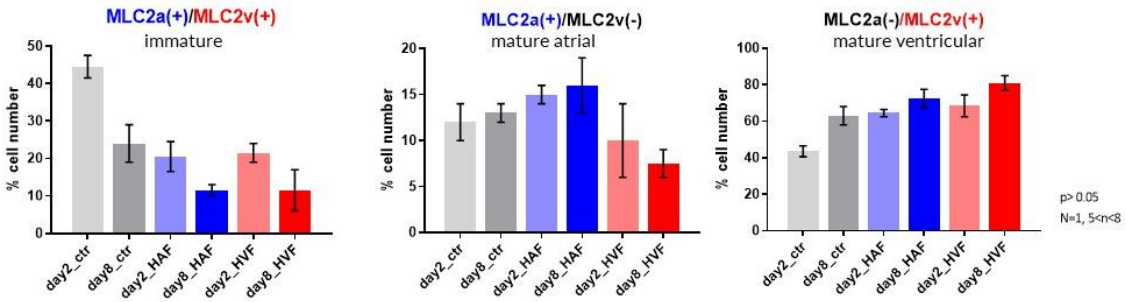

Figure 44 Maturation and chamber-specific changes in vCMs, due to paracrine signaling of cardiac fibroblast influence. All values are expressed as mean ± SEM. p>0.05.

4.3.1.3. Contractility patterns investigation

After applying this conditioned medium, the differences in vCMs contractility patterns were observed. At day 0, the BPM for all three groups of vCMs (control, conditioned with HAF medium and conditioned with HVF) was 26 BPM. On day 4 of the experiment, for both groups with the conditioned medium, a 20% decrease in BPM was observed (Figure 45). The decrease was not observed for vCMs in the control medium. On the last day of the experiment, in all groups, vCMs were beating slower, compared to day0.

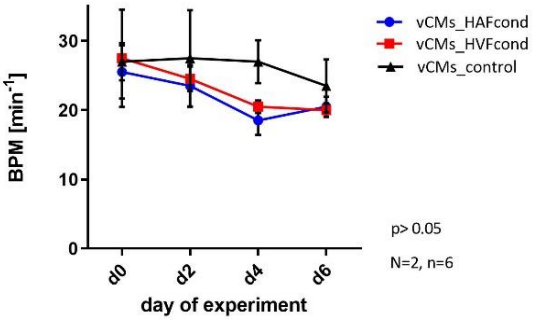

Figure 45 Contractility changes in 2D culture, during the maturation process. All values are expressed as mean ± SEM. p<0.05.

4.3.2. Cell-to-cell signaling, and indirect/ mechanical stimulation in 3D culture

To investigate cell-to-cell signaling and mechanical stimulation influence of cardiomyocytes, ventricular cardiomyocytes with atrial or ventricular fibroblasts were mixed in a 3D culture system. Through the process of formation and maturation, vCM_HAF and vCM_HVF tissues were obtained (Figure 46).

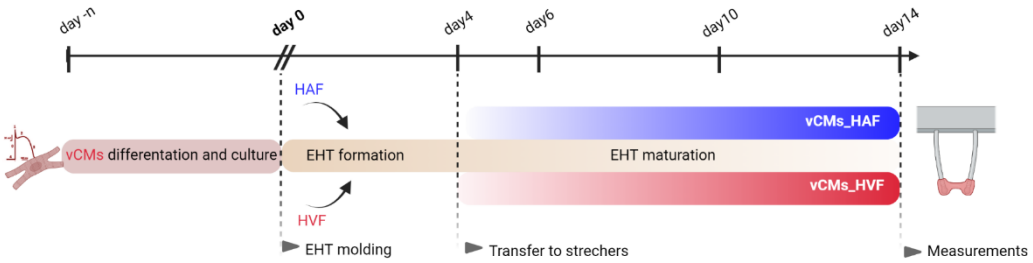

Figure 46 Scheme of EHT formation: vCM_HAF and vCM_HVF. Created with BioRender.com.

4.3.2.1. Molecular evaluation of cardiac markers

First, the application of chamber-specific CFs in EHT model affected gene expressions of chamber-specific cardiomyocyte markers. EHT molded with atrial CFs presented a higher expression of some atrial CMs-specific markers (*HEY1*, *KCNJ3*, *SK3*) (Figure 47).

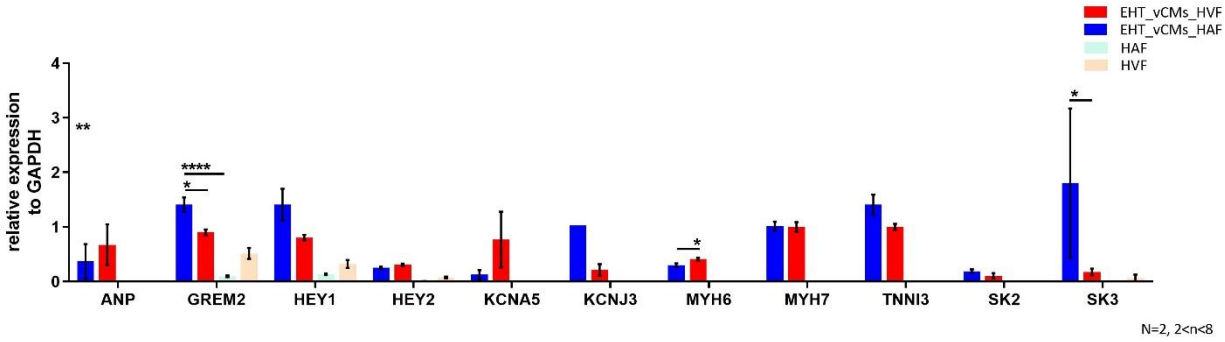

Figure 47 Cardiac-specific gene expression analysis of EHTs. Analysis of gene expression proved differences between chEHTs. Atrial-specific markers (*ANP*, *HEY1*, *MYH6*, *KCNA5*, *KCNJ3*, *SK2*, *SK3*) expressed higher in atrial-EHT, and ventricular-specific markers (*HEY2*, *MYH7*) in ventricular-EHT. *GREM2*, fibroblast marker, which is required in atrial differentiation during embryonic development presented higher expression in atrial-EHT. *TNNI3* was expressed higher in atrial-EHT. All values are expressed as mean ± SEM. *p<0.05, **p<0.01, ***p<0.001, ****p<0.0001. Where statistical significance was not observed, it has not been indicated.

4.3.2.2. Contractility patterns investigation in 3D

Analysis of contractility changes within the 3D EHT model, defined by the type of chamber-specific CFs, presented differences during the maturation period (Figure 48). Initially, on day 7 of tissue maturation, the beat rate did not exhibit a noticeable discrepancy between atrial and ventricular EHT. For EHT molded with atrial CFs was 49.73 ± 11.93 BMP, for EHT with ventricular CFs – 43.04 ± 7.52 BPM. However, by day 14 of tissue development, a marked decrease in BPM in ventricular EHT was recorded, increasing the contrast between EHT subtypes from 7 BMP to 17 BMP. At day 14 of tissue maturation, the beat rates totaled for atrial EHTs – 43.24 ± 4.49 BPM and ventricular CMs – 30.30 ± 6.51 BPM (Figure 48).

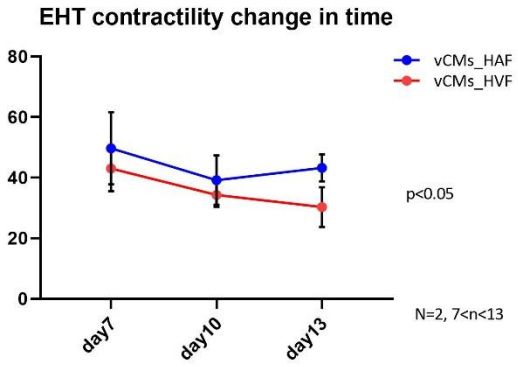

Figure 48 Contractility changes in EHT, during the maturation process. All values are expressed as mean ± SEM. p<0.05, paired *t*-test was used for comparison.

4.3.2.3. Physiological parameters measurements

Following contractility analysis, physiological measurements were conducted at day 14 to assess changes induced by the application of chamber-specific fibroblasts to ventricular cardiomyocytes within EHT.

4.3.2.3.1. Calcium response

For EHT molded with atrial CFs was 0.27 ± 0.07 mN, for ventricular equivalent - 0.52 ± 0.29 mN FOC. In both sub-types, the force of contraction increased in correlation with the rising calcium levels in the solution surrounding the cells (Figure 49). The EC50 values for atrial and ventricular EHT were similar, 0.783 and 0.928, respectively. Despite the force discrepancy of 0.25 mN between the EHT sub-types at the initial concentration of

0.2 mM Ca^{2+}, this discrepancy decreased to 0.05 mM at the last point of the calcium curve - 3.4 mM (p<0.001).

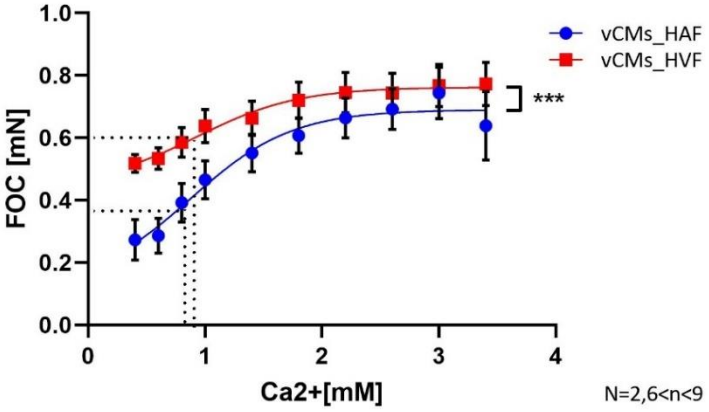

	vCMs_HAF	vCMs_HVF
LogEC50	0.8729	0.9282

Figure 49 EHT response for calcium. All values are expressed as mean ± SEM. *p<0.05, **p<0.01, ***p<0.001, ****p<0.0001.

4.3.2.3.2. Reaction for β-adrenergic stimulation

By using the 1 µM isoprenaline concentration in the Tyrode solution, in both EHT defined by the type of chamber-specific CFs, the FOC increased. In atrial EHT, the FOC changed from 0. 49 ± 0.12 mN to 0.60 ± 0.12 mN, in ventricular: from 0.69 ± 0.18 mN to 0.79 ± 0.16 mN (Figure 50).

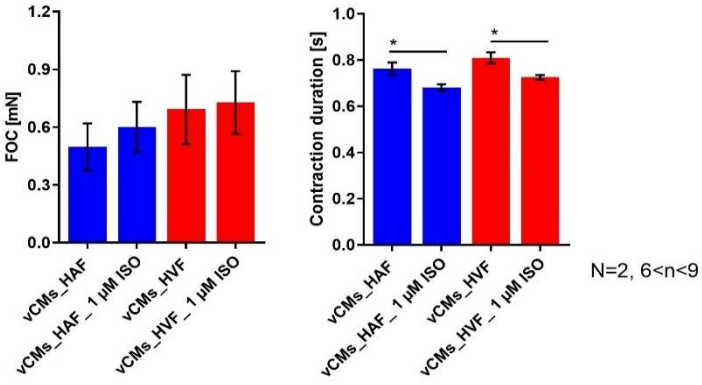

Figure 50 EHT response for 1 µM isoprenaline – force of contraction and contraction duration. All values are expressed as mean ± SEM. *p<0.05, **p<0.01, ***p<0.001, ****p<0.0001. Where statistical significance was not observed, it has not been indicated

At the same time, 1 µM isoprenaline concentration affected contraction duration. For both EHT subtypes, contraction duration was approximately 0.1s faster ($p<0.05$), (Figure 50).

4.3.2.3.3. Muscarinic receptor stimulation

In the last physiological measurement, two pharmaceuticals with opposing actions on the autonomic nervous system were used. Used before - isoprenaline, which increases heart rate and contractility, mimicking the effects of sympathetic nervous system activation and carbachol - cholinergic agonist that primarily stimulates muscarinic acetylcholine receptors, which mimics the effects of parasympathetic nervous system activation.

Depending on the subtype of EHT, tissues respond differently. Treatment with 10 µM and 30 µM carbachol led to a decrease of 20% in FOC in EHT molded with atrial CFs. Opposite to EHT molded with ventricular CFs. In ventricular EHT, the FOC increases by 10% (Figure 51).

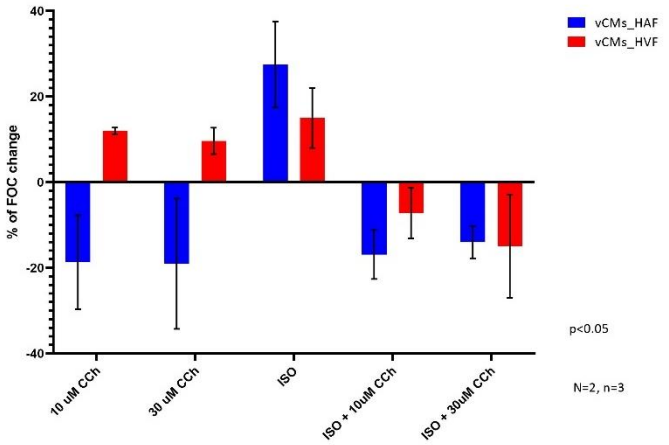

Figure 51 EHT response for 10 µM and 30 µM carbachol l– % of force of contraction change. All values are expressed as mean ± SEM. $p>0.05$.

Treatment with 1 µM isoprenaline alone caused increased in FOC in both atrial and ventricular EHT, however the increase was more significant in atrial EHT and obtained 30%. When for ventricular EHT was 12%. The combination of 1 µM isoprenaline with carbachol further diminishes the isoprenaline-induced increase in FOC in both types of

EHT. For a smaller dose of carbachol, atrial EHT's FOC decreased by 44% and ventricular EHT's - 26% (Figure 51).

4.3.3. Transcriptomic analysis and secretome profiling

To deeply investigate the molecular interactions between chamber-specific fibroblasts and ventricular cardiomyocytes, considering changes over time, transcriptomic analysis using RNA - Seq and secretome profiling was performed.

4.3.3.1. Sample collection for analysis

In main experiment, two main parts were conducted in parallel, to collect necessary samples which would evaluate mechanism of paracrine signaling, cell-to-cell interactions and mechanical/ indirect, necessary for further analysis (Figure 52).

In the first part of the experiment, vCMs were incubated for 14 days in cardio culture, and conditioned medium from HAF and HVF. At three different time points: day 0, day 10, and day 14, medium for secretome evaluation and vCMs for RNA sequencing were collected.

In the second part of the experiment, vCMs from the same differentiation procedure were mixed with atrial or ventricular fibroblasts to mold EHT. Again, the medium and tissues were collected at 3 different time points (day 0, day 10 and day 14) for further investigation.

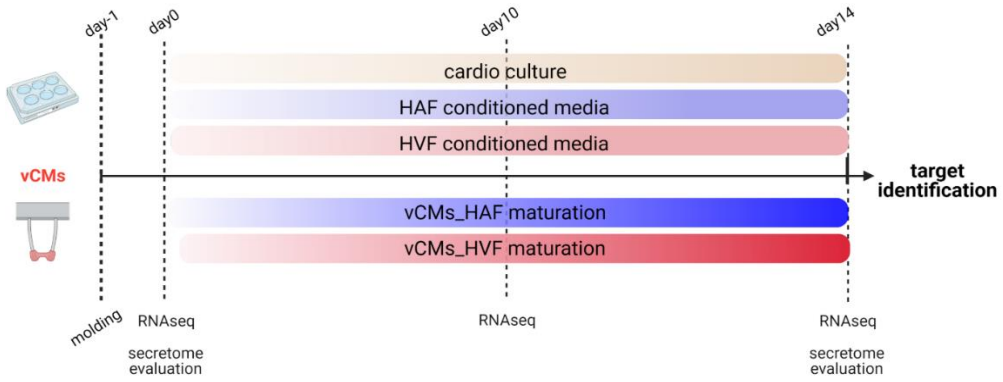

Figure 52 Graphic explanation of the experiment. Created with BioRender.com.

4.3.3.2. RNAseq sample system

For RNA sequencing, 47 samples were collected - 45 samples of ventricular cardiomyocytes and 2 samples of cardiac fibroblasts (HAF, HVF). The analysis was based on three iPSc differentiations into ventricular cardiomyocytes from two different patients (groups: 1_1; 1_2; 2_0). The chamber-specific cardiac fibroblasts were assigned to group 0. Each sample can be characterized by cardiac fibroblast influence, culture system type, patient and collecting day. All sample's characteristic are presented in the Table 21, and distribution based on their similarities was presented on the PCA (principal component analysis) plot in Figure 53.

Table 21 List of samples for RNA seq with general characteristic.

ID	Fibroblast influence	culture system	day of culture	patient lbm76 (1.1, 1.2)/ iwtd2.3 (2)/ fibro (0)
0	-	2D	0	2_0
1	-	2D	0	1_1
2	-	2D	0	1_2
3	-	2D	10	2_0
4	-	2D	10	1_1
5	-	2D	10	1_2
6	-	2D	14	2_0
7	-	2D	14	1_1
8	-	2D	14	1_2
10	HAF	2D	0	2_0
11	HAF	2D	0	1_1
12	HAF	2D	0	1_2
13	HAF	2D	10	2_0
14	HAF	2D	10	1_1
15	HAF	2D	10	1_2
16	HAF	2D	14	2_0
17	HAF	2D	14	1_1
18	HAF	2D	14	1_2
20	HVF	2D	0	2_0
21	HVF	2D	0	1_1
22	HVF	2D	0	1_2
23	HVF	2D	10	2_0
24	HVF	2D	10	1_1
25	HVF	2D	10	1_2
26	HVF	2D	14	2_0
27	HVF	2D	14	1_1
28	HVF	2D	14	1_2
30	HAF	3D	0	2_0
31	HAF	3D	0	1_1
32	HAF	3D	0	1_2
33	HAF	3D	10	2_0
34	HAF	3D	10	1_1
35	HAF	3D	10	1_2
36	HAF	3D	14	2_0
37	HAF	3D	14	1_1
38	HAF	3D	14	1_2
40	HVF	3D	0	2_0
41	HVF	3D	0	1_1
42	HVF	3D	0	1_2
43	HVF	3D	10	2_0
44	HVF	3D	10	1_1
45	HVF	3D	10	1_2
46	HVF	3D	14	2_0
47	HVF	3D	14	1_1
48	HVF	3D	14	1_2
50	HAF	2D	-	0
51	HVF	2D	-	0

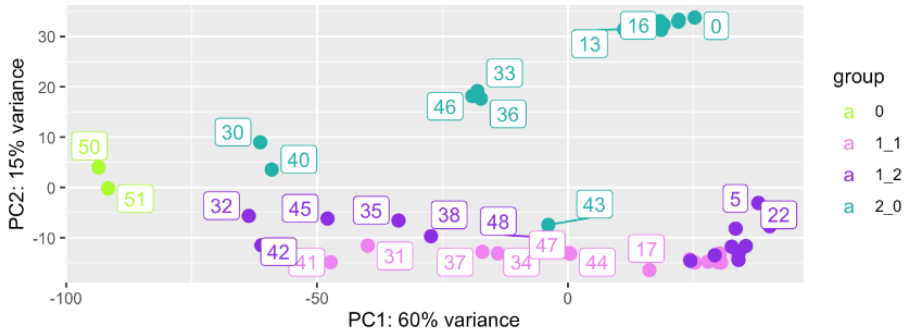

Figure 53 Differences between cell populations presented in PCA analysis.

To easier characterized the vCMs during analysis of RNAseq data, the special numeration system was applied. Each ten and once number in vCM sample's ID, provide detailed information Figure 54.

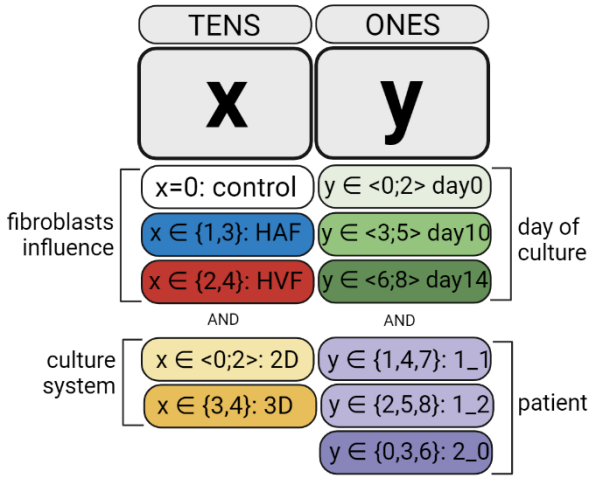

Figure 54 Ventricular cardiomyocyte's numeration system in RNAseq analysis. Created with BioRender.com.

The tens „x" contains the information about the culture system (2D/3D) and chamber-specific cardiac fibroblasts influence (control, HAF, HVF): in 2D culture system - paracrine signaling in 3D culture - cell-to-cell /paracrine signaling. The ones "y" contains the information about the patient (1_1, 1_2, 2_0) and when the sample was collected (day0, day10, day14).

4.3.3.3. Secretome sample system

The same system was applied to code the necessary information in secretome samples ID (Figure 55). The only discrepancies were visible within patients' type (1_1, 1_2, 1_3) and the number of time points when the samples were collected (day0, day14). All samples characteristics are presented in Table 22.

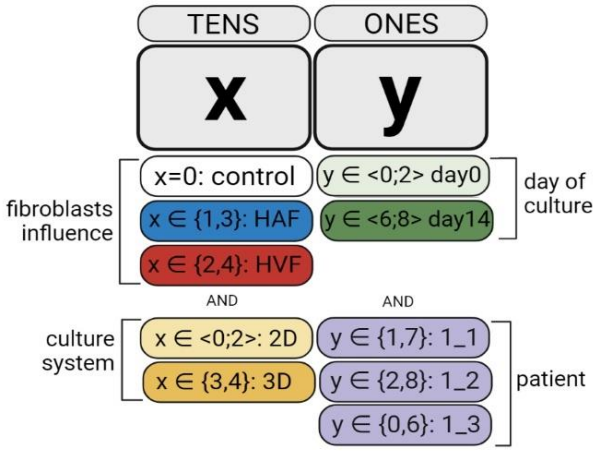

Figure 55 Ventricular cardiomyocyte's numeration system in secretome analysis. Created with BioRender.com.

Table 22 List of samples for secretome analysis with general characteristic.

ID	Fibroblast influence	culture system	day of culture	patient iBM76 (1.1, 1.2, 1.3)
0	-	2D	0	1_3
1	-	2D	0	1_1
2	-	2D	0	1_2
6	-	2D	14	1_3
7	-	2D	14	1_1
8	-	2D	14	1_2
10	HAF	2D	0	1_3
11	HAF	2D	0	1_1
12	HAF	2D	0	1_2
20	HVF	2D	0	1_3
21	HVF	2D	0	1_1
22	HVF	2D	0	1_2
30	HAF	3D	0	1_3
31	HAF	3D	0	1_1
32	HAF	3D	0	1_2
36	HAF	3D	14	1_3
37	HAF	3D	14	1_1
38	HAF	3D	14	1_2
40	HVF	3D	0	1_3
41	HVF	3D	0	1_1
42	HVF	3D	0	1_2
46	HVF	3D	14	1_3
47	HVF	3D	14	1_1
48	HVF	3D	14	1_2
50	HAF	2D	-	0
51	HVF	2D	-	0

4.3.3.4. Principal component analysis

Focusing on differences in ventricular cardiomyocytes according to the culture system (2D/3D), chamber-specific fibroblast influence (HAF/HVF), and day of the experiment (day0/ day10/day14), a distinction between patients was visible (Figure 56). Due to that, the same criteria for each patient were presented separately.

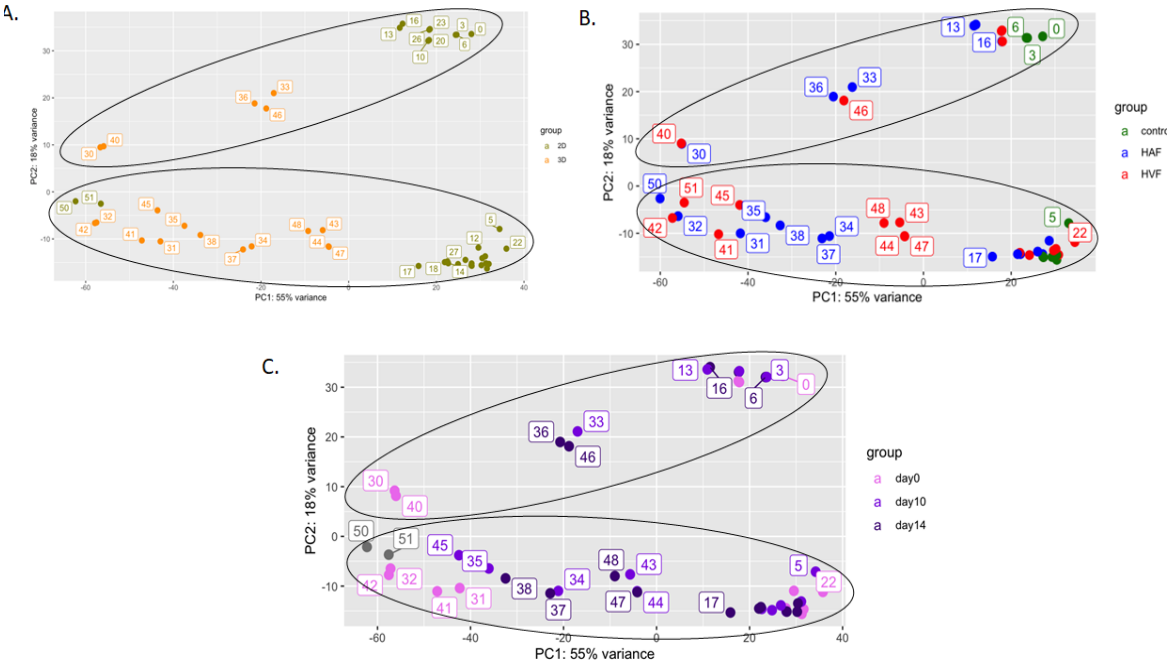

Figure 56 Differences according to the culture system (2D/3D), chamber-specific fibroblast influence (HAF/HVF), and day of the experiment (day0/ day10/day14).

Performing the analysis according to the cell culture system, a clear distinction between 2D and 3D systems in the iPSC_1 cell line can be observed (Figure 57A). Only by applying a 3D culture system, differences between chamber-specific fibroblast subtypes can be visible (cell culture system, a clear distinction between 2D and 3D systems can be observed (Figure 57B). Also, by using an advanced model, the differences between time points are as well observed (cell culture system, a clear distinction between 2D and 3D systems can be observed (Figure 57C). However, analyzing data related to the days of the experiment, differences could only be divided between day 0 and the late stage of EHT maturation (day 10 and day 14).

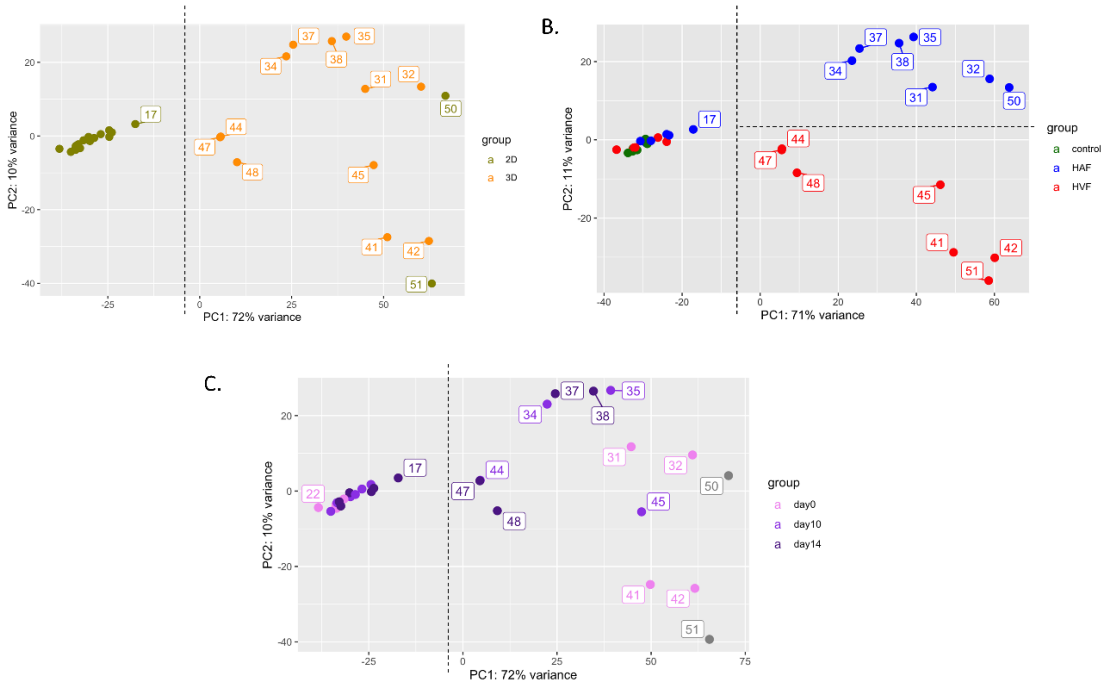

Figure 57 Differences for patient iPSC_1, according to the culture system (2D/3D), chamber-specific fibroblast influence (HAF/HVF), and day of the experiment (day 0/ day 10/day 14).

The same clear division between culture systems 2D vs. 3D was presented for samples from another patient (cell line iPSC_2) (Figure 58A). Also, differences between time points are visible.

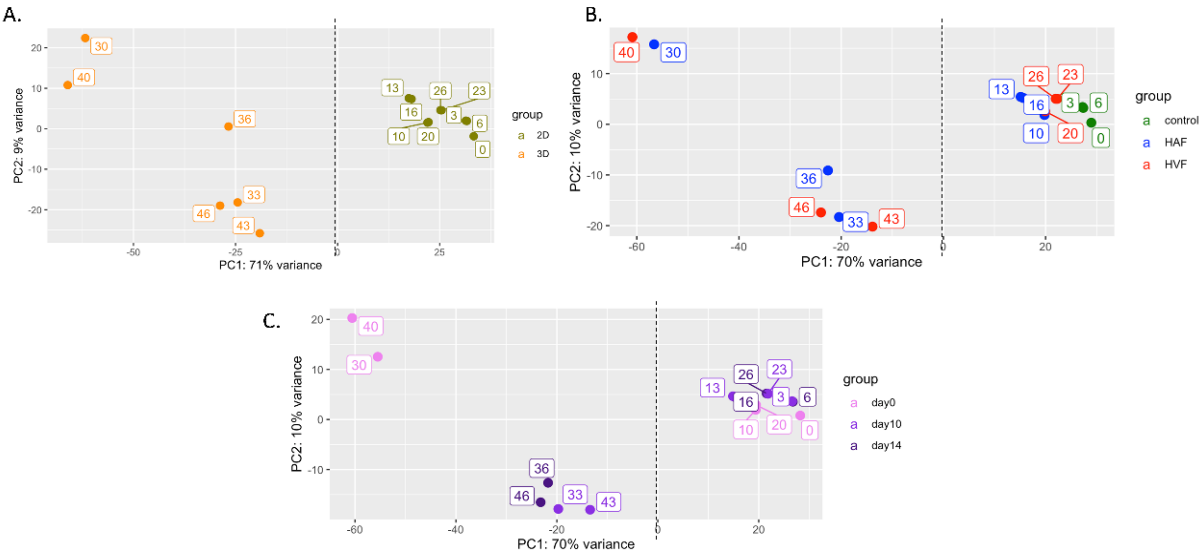

Figure 58 Differences for patient iPSC_2, according to the culture system (2D/3D), chamber-specific fibroblast influence (HAF/HVF), and day of the experiment (day0/ day10/day14).

The same as in the iPSC_1 cell line, samples could be divided into two groups: day 0 and day 10/14 (Figure 58C). However, the distinction between fibroblast subtype influence wasn't observed (Figure 58B).

Based on presented on PCA plots, few assumptions have been made 3D system gave much more possibilities to observe changes of fibroblast's influence on vCMs gene expression patterns, and thus in further analysis focus was on them,

- Due to relatively large biological differences between patients and limitations concerning technical replicates, only patient iPSC_1 was considered for further investigation,
- As results from the late stages of EHT maturation (day 10 and day 14) tended to group together, they were treated as a joined group and challenged against day 0.

4.3.3.5. DEG analysis

Genes obtained as a result of DEG analysis in 3D culture tissue models concerning differences between early and late stages of tissue formation were selected as indicated by the following comparisons:

- vCM_HAF vs. vCM_HVF on day 0
- vCM_HAF vs. vCM_HVF at day 10 and 14
- vCM_HAF day0 vs. vCM_HAF day10/14
- vCM_HVF day0 vs. vCM_HVF day10/14

that were filtered using parameters: adjusted p-value≤0,01 and $\log_{10}$FC ≥2 or ≤-2, and later subdivided into overexpressed and underexpressed list of gene.

4.3.3.5.1. Biological pathway in Reactome

To identify biological pathways connected with filtered overexpressed and underexpressed genes, each of comparison was further analyzed using Reactome, an online database focused on biological pathways (https://reactome.org/) (Milacic *et al.*,

2024). The focus was on identifying statistically significant pathways that might be involved in the embryonic and physiological development of the heart.

On day 0 in vCM_HAF tissues, an increase in the expression of genes linked to cell cycle, DNA repair, and voltage-gated potassium channels were observed. In contrast, for vCM_HVF tissues, in which the sample was an increase in genes associated with extracellular matrix organization, WNT signaling, protein metabolism, and angiogenesis

On days 10 and 14 in vCM_HAF 3D culture, increased expression was noted in pathways related to homeostasis, signal transduction (specifically the RA biosynthesis pathway), while for HVF, there was an increase in extracellular matrix organization and cellular stress response

Moreover, when analyzing changes within the vCM_HAF and vCM_HVF subtypes over time, it was observed that on day 0, HAF showed increased expression in pathways related to cellular response and extracellular matrix organization, whereas at later stages of tissue maturation, pathways related to muscle contraction, homeostasis, and transport of small molecules were evident.

For HVF on day 0, increased expression was seen in pathways related to muscle contraction and extracellular matrix organization, while with tissue maturation, pathways related to developmental biology, cardiogenesis, and transport of small molecules became noticeable.

Collectively, signaling pathways indicative of tissue maturation, such as extracellular matrix organization, muscle contraction, or ion channel transport, were activated in both subtypes: vCM_HAF and vCM_HVF.

Notably, the difference between groups at the last days of maturation, was increased signal transduction pathways – RA biosynthesis pathway and signaling by retinoic acid. Taking into account role of RA in cardiac differentiation and its association with atrial phenotype, while its mechanism of action remains unclear, it brought attention to genes related to the mentioned pathways.

Figure 59 summarizes the pathways with increased activation during the maturation process in both vCM_HAF and vCM_HVF. The Figure 59 presents differences between

activated pathways within groups vCM_HAF vs. vCM_HVF, separately at day 0 and at day10/14. Additionally, the differences between vCM_HAF day 0 vs. vCM_HAF day 10/14 and respectively – vCM_HVF day 0 vs. vCM_HVF day 10/14 are also visualized.

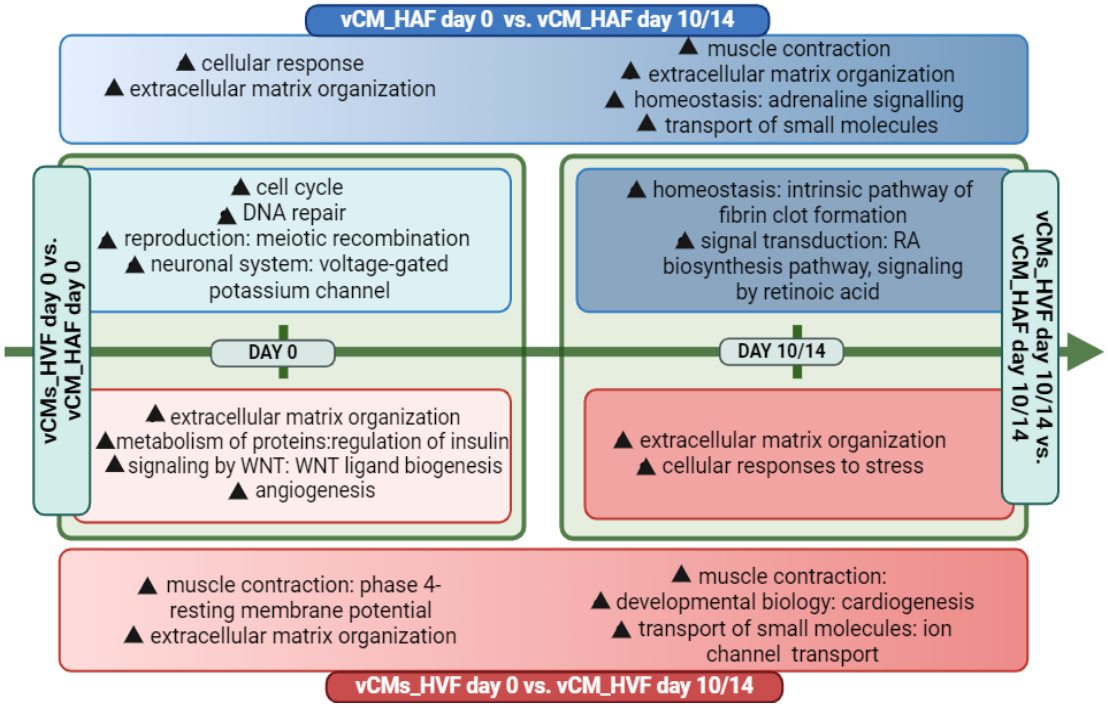

Figure 59 Summary of gene expression upregulation pathways based on DEG analysis for vCM_HAF and vCM_HVF subtypes at two different time points: day 0 and day 10/14. Modified from (Milacic *et al.*, 2024). Created with BioRender.com.

4.3.3.5.2. Gene Ontology and KEGG

All the data obtained from the Reactome analysis was further verified with analysis performed in collaboration with an external bioinformatics service provider (Data2biology). The differences between subtypes (vCM_HAF and vCM_HVF) in two time points (day0 and day10/14) were investigated.

- **vCM_HAF vs. vCM_HVF at day 0**

The results for patient iPSC_1 comparison between vCM_HAF and vCM_HVF at day 0 were presented on Gene Ontology - Molecular Function bubble plot (Figure 60A). The most statistically significant differences between groups were tubulin binding, catalytic

activity on DNA, microtubule binding and ATP hydrolysis activity. Notable differences included extracellular matrix structural constituent, extracellular matrix or collagen binding. This suggests that the largest changes in EHT formation considered editing of the extracellular matrix and intracellular structural components of the cells (Figure 60A).

Furthermore, based on the list of genes (over - and underexpressed) obtained due to the comparison between vCM_HAF and vCM_HVF at day 0, using The Kyoto Encyclopedia of Genes and Genomes (KEGG) pathway database, the most related signaling pathways were presented (Figure 60B). The pathway with the most related genes and the strongest statistical significance was the “cell cycle.” Other visible pathways on the list included DNA replication, cellular senescence, and ECM-receptor interaction (Figure 60B). All together suggested increased cell growth or division and editing of extracellular matrix editing.

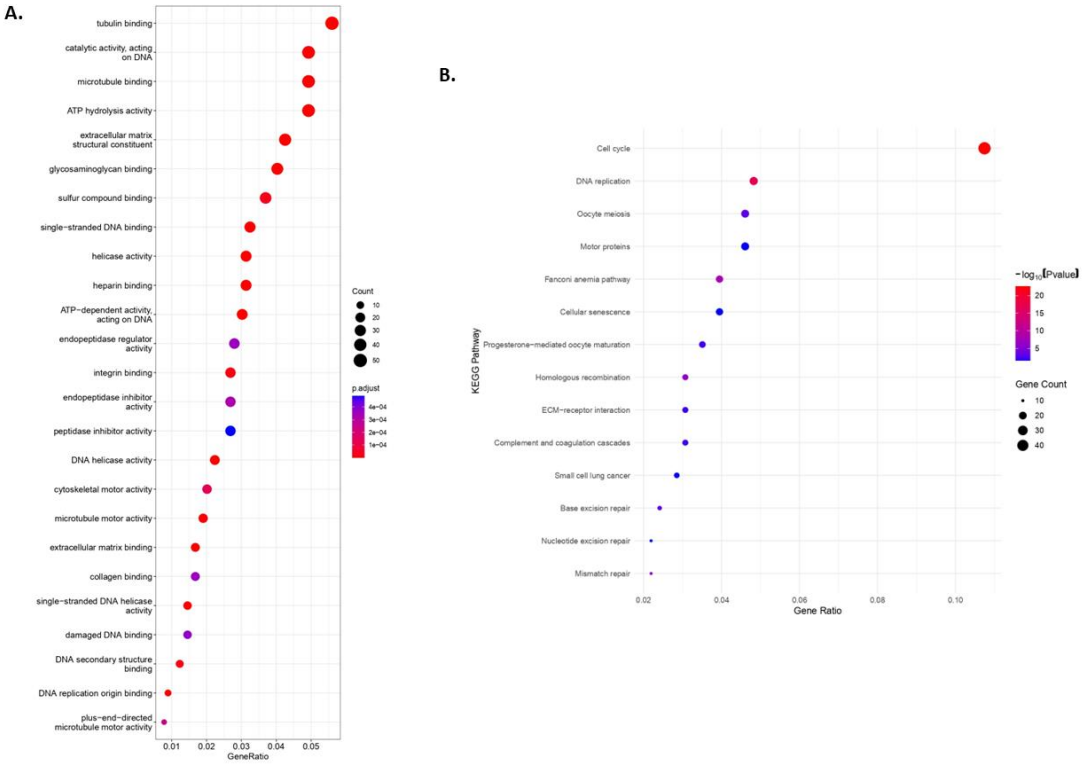

Figure 60 Graphic presentation of results for comparing patient iPSC_1 between vCM_HAF and vCM_HVF EHT at day 0. A. Gene Ontology analysis. The bubble plot illustrates adjusted p-values (color intensity) and gene count (bubble size). B. KEGG pathways. The bubble plot displays -log10 p-values (color intensity) and number of counts.

- **vCM_HAF vs. vCM_HVF at day 10/14**

The same approach was implemented for a comparison between vCM_HAF and vCM_HVF on days 10 and 14. Gene Ontology - Molecular Function analysis presented significant differences in signaling pathways, among others: helicase activity, double-strand RNA binding, RNA helicase activity, and ATP-dependent activity acting on RNA (Figure 61A), suggesting involvement in RNA processing and regulation.

Several significant pathways were identified using the KEGG pathway database (Figure 61B). The top three pathways with the most genes obtained from the comparison of vCM_HAF vs. vCM_HVF and the highest statistical significance, were "coronavirus disease", "influenza A", and "cell adhesion molecules". Additionally, pathways connected with cardiomyopathies were also presented: “dilated cardiomyopathy”, “hypertrophic cardiomyopathy”, and “arrhythmogenic right ventricular cardiomyopathy”, indicating potential dysregulation in cardiac muscle functions between the groups.

The pathway with retinol metabolism was also identified, as it was in DEG’s analysis in Reactome. Although it was ranked lower due to the limited number of associated genes - ***ALDH1A2*** and ***ALDH1A3****,* the retinol metabolism pathway's significance in atrial differentiation made it noteworthy. Especially, due to the fact, that analyzed EHT consisted only of ventricular cardiomyocytes and chamber-specific fibroblasts.

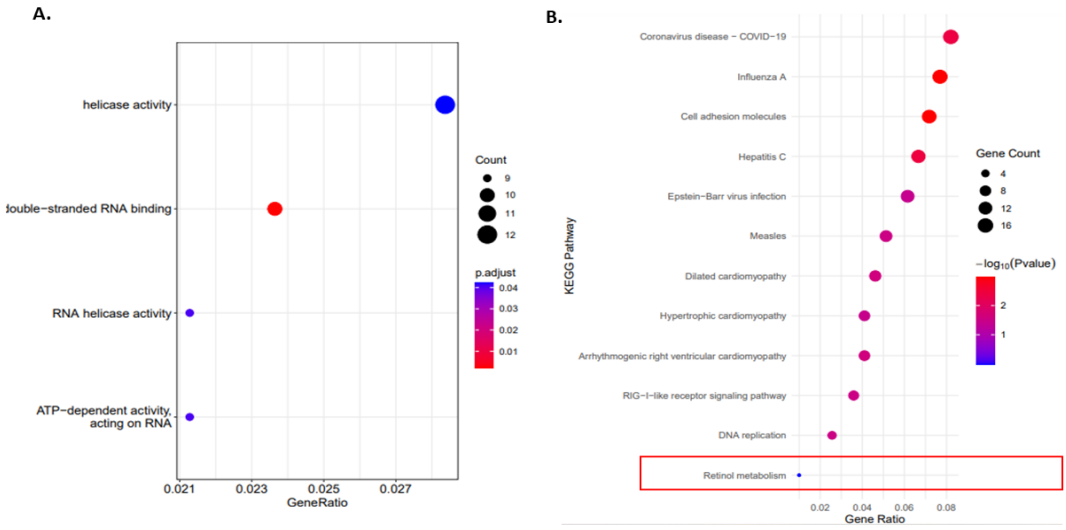

Figure 61 Graphic presentation of results for comparing patient iPSC_1 between vCM_HAF and vCM_HVF EHT at day 10 and 14. A. Gene Ontology analysis. The bubble plot illustrates adjusted p-values (color intensity) and gene count (bubble size). B. KEGG pathways. The bubble plot displays - log10 p-values (color intensity) and number of counts (bubble size).

4.3.3.5.3. Interactions in STRING

In both analyses, performed in the Reactome database and by an external bioinformatics service provider, ***ALDH1A2*** and ***ALDH1A3*** were related to “Signaling by Retinoic Acid” and “Retinol metabolism” pathways.

To investigate additional potential protein-protein interactions, including those involving proteins encoded by exposed genes, the "STRING" database (Search Tool for the Retrieval of Interacting Genes/Proteins, https://string - db.org/, (Szklarczyk *et al.*, 2023)) was used (Figure 62).

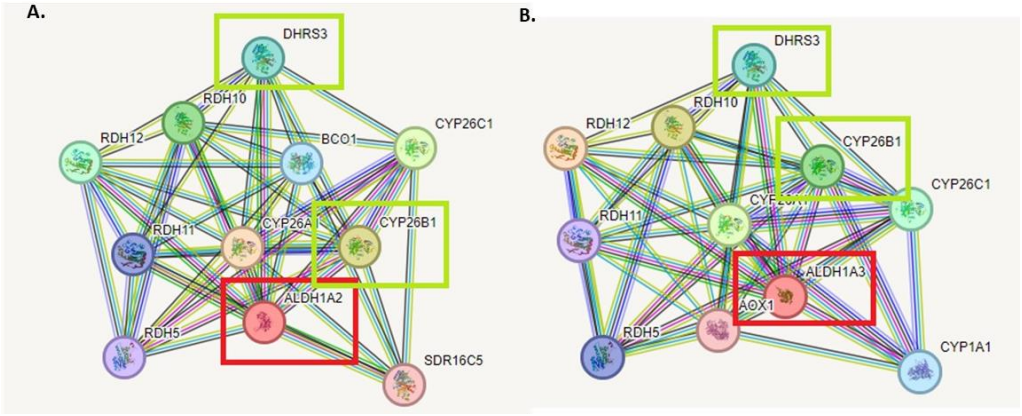

Figure 62 Analysis of protein-protein interactions using the "STRING" database. A. ALDH1A2, B. ALDH1A3. Modified from (Szklarczyk *et al*., 2023).

Every gene encoding a protein that was identified as a potential interaction for **ALDH1A2** and **ALDH1A3** was cross-referenced with the analyzed lists of genes. The lists related to all four comparisons presented at the beginning of chapter:

- vCM_HAF vs. vCM_HVF on day 0
- vCM_HAF vs. vCM_HVF at day 10 and 14
- vCM_HAF day0 vs. vCM_HAF day10/14
- vCM_HVF day0 vs. vCM_HVF day10/14

applying the filters: adjusted p - value ≤0,01 and log10FC≥2 or ≤-2.

Due this action, additional genes from the Retinoic acid signaling pathway were identified: ***CYP26B1*** and ***DHRS3***, which showed statistically significant differences in gene expression between the selected groups.

4.3.3.5.4. Retinoic acid signaling pathway components

Identification of four genes with increased expression – *ALDH1A2*, *ALDH1A3*, *CYP26B1* and *DHRS3* in the Retinoic acid signaling pathway, prompted a detailed analysis of the entire pathway (Figure 63).

All genes connected with the retinoic acid signaling pathway and their differential expression within the analyzed four comparison groups were collected in the table (Table 23). Statistically significant differences ($p<0.05$) were highlighted in green in the table. Genes*: **RDH10**, **DHRS3**, **ALDH1A2**, **ALDH1A3**, **CRBP (RBP1)**, **CYP26B1*** and ***RXRγ*** were confirmed in the Retinoic acid signaling pathway ($p<0.05$).

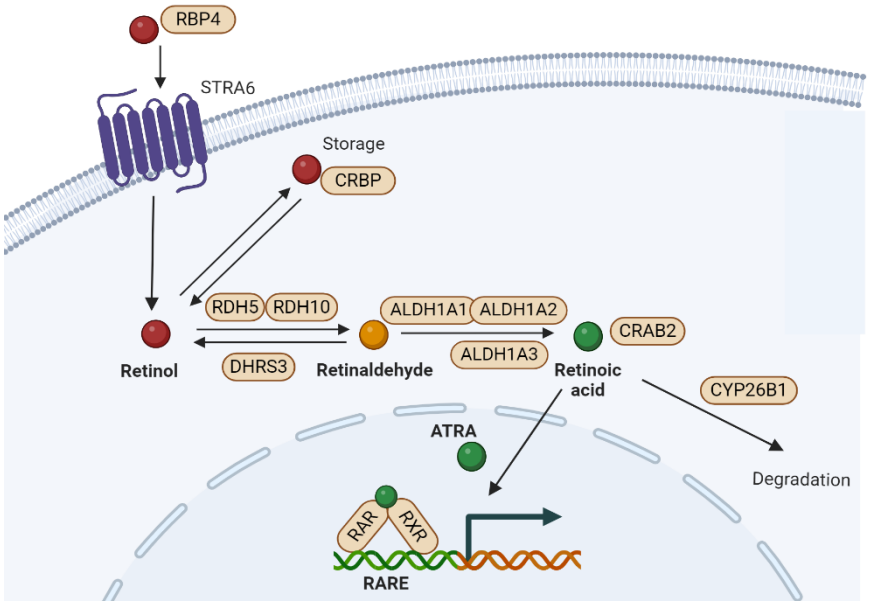

Figure 63 Biosynthesis and metabolism of retinoic acid. Modified from (Thompson *et al*., 2019). Created with BioRender.com.

Table 23 Analysis of genes involved in the "Signaling by Retinoic Acid" pathway.

gene	•▯CM_HAF vs vCM_HVF on day 0				vCM_HAF day0 vs vCM_HAF day10/14				•▯CM_HVF day0 vs vCM_HVF day10/14				vCM_HAF vs vCM_HVF at day 10/14				gene cards
	vCM_HAF		vCM_HVF		vCM_HAF day0		vCM_HAF day10/14		vCM_HVF day0		vCM_HVF day10/14		vCM_HAF		vCM_HVF		
	p.value adj	*logFC*	*p.value adj*	*logFC*	*p.value adj*	*logFC*	*p.value adj*	*logFC*	*p.value adj*	*logFC*	*p.value adj*	*logFC*	*p.value adj*	*logFC*	*p.value adj*	*logFC*	
RBP4			0,98497	-0,47587	0,08900	-1,89861			0,17106	-3,17719			0,89963	0,70660			extracellular
STRA6	NA	NA	NA	NA	NA	NA	NA	NA			0,40197	0,65739	NA	NA	NA	NA	plasma membrane
ADH1A	n/a	0,0394987			NA	-2,34657			NA	-1,01138			n/a	n/a	n/a	n/a	cytosol
ADH1B			n/a	-0,06792			0,07111	2,82297			NA	1,28156	0,32156	1,75597			cytosol
ADH1C	n/a	0,50176					NA	0,74096			NA	0,30778	0,84975	0,97580			nucleus/cytosol
ADH7			n/a	-0,34857	NA	-0,39836					NA	NA	1,49566	n/a			cytosol
RDH5			0,54012	-1,18466			0,44787	0,42376	0,75941	-0,44977					0,85228	-0,35026	endoplasmic reticulum
RDH10			0,01148	-1,36834	0,02763	-0,79750			0,21396	-1,24978					0,40761	-0,95692	endoplasmic reticulum
DHRS3			0,90034	-0,57290	0,10409	-1,55036			0,00692	-2,78488			0,82529	0,63297			cytosol
ALDH1A1			0,99279	-0,51241	0,85542	-0,37187			NA	-2,31722			0,57032	1,47789			cytosol/extracellular
ALDH1A2	0,08210	3,16717			0,86324	-0,13203					0,91199	0,34432	0,00014	2,4360987			cytosol
ALDH1A3			0,79641	-0,75255	0,33775	-0,45956			0,00000	-3,67861			0,00000	2,41029			cytosol
CRBP (RBP1)			0,35119	-0,71585			0,02134	0,81401	0,15287	-1,24828					0,70754	-0,48202	nucleus/cytosol
CRABP (CRABP1)			n/a	-1,30955	NA	-0,09700					NA	0,67178			0,30788	-1,74692	cytosol
CYP26A1			0,37958	-3,17489	NA	-0,55711			NA	-3,49874					0,98253	-0,20952	endoplasmic reticulum
CYP26B1			0,00772	-2,96095			0,96488	0,06599	0,00641	-2,46663						-0,45787	endoplasmic reticulum
CYP26C1			0,93889	-1,51254	0,83678	-0,53086			NA	-4,77472			0,38907	2,71722			endoplasmic reticulum
RARA			0,80251	-0,52275	0,51520	-0,30993			0,50330	-0,41316					0,05474	-0,46076	nucleus/cytosol
RARB			0,94114	-0,46196			0,72602	0,32730	0,63313	-0,63106			0,81430	0,47706			nucleus
RARG			0,99382	-0,13194	0,39714	-0,30842			0,25524	-1,13249			0,58530	0,63576			nucleus
RXRA	0,99005	0,12830					0,20384	0,28161			0,69686	0,27342	0,91462	0,09423			nucleus
RXRB	0,80884	1,65124	0,98857	-0,12315	0,61512	-0,12869			0,88493	-0,11908					0,83738	-0,17631	nucleus
RXRG	0,78144	0,53247					0,00002	3,08748			0,00004	5,25353			0,85734	-0,49902	nucleus
FABP5							0,40446	0,42557			0,21357	0,81435	0,94255	0,10737			cytosol/extracellular
RBP6 (CRABP2)			0,34062	-1,19274	0,79522	-0,28295			0,32079	-0,79947					0,51825	-0,69694	nucleus/cytosol

Gene expression differences were observed depending on EHT subtype and time point. For vCM_HAF, only RDH10 expression was increased on day 0. On day 10/14, however, statistically significant increased expression was observed in *CRBP*, aldehyde dehydrogenase - *ALDH1A2* and *ALDH1A3*, and *RXRγ* (Figure 64).

For vCM_HVF, on the other hand, increased expression was observed in the genes *RDH10*, *DHRS3*, *ALDH1A3*, and *CYP26B1* on day 0. By day 10/14, only *RXR gamma* expression was visible (Figure 64).

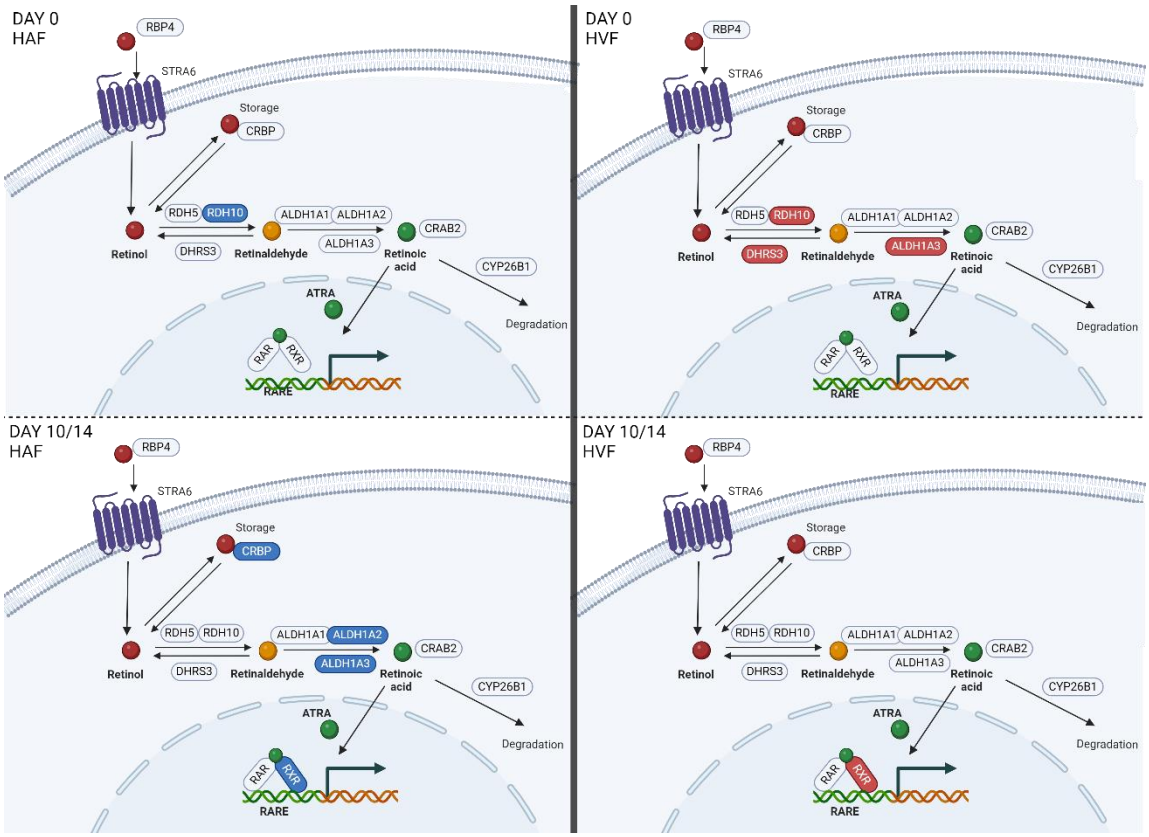

Figure 64 Differences in gene expression level between EHT subtypes and days of culture. Genes with higher expression in HAF 3D were marked in blue color, in HVF 3D – red. Modified from (Thompson *et al*., 2019). Created with BioRender.com.

In both groups, vCM_HAF and vCM_HVF, the retinoic acid signaling pathway was activated, albeit at distinct time points. Retinoic acid signaling is essential for various stages of heart development, including establishing anteroposterior polarity and forming inflow and outflow tract progenitors (Nakajima, 2019). The balance of retinoic acid is primarily regulated by DHR3, which acts as a negative regulator of RA synthesis

by converting retinaldehyde (a precursor of RA) back into retinol (a less active form of vitamin A) (Adams *et al.*, 2014).

Data analysis revealed DHR3 activity exclusively in the vCM_HVF group. It suggested that due to the absence of DHR3-mediated regulation in the vCM_HAF group likely led to an accumulation of RA. DHRS3 was identified as a key differentiating factor between vCM_HAF and vCM_HVF in the analysis.

To further understand its function, identifying the regulatory elements of DHRS3 was necessary. Analysis of the databases providing information on biological interactions: Reactome, IntAct, and available literature confronted with lists of genes for four comparisons, revealed potential interactions between *DHRS3* and *C5AR2*. ***C5AR2*** gene overexpression was observed only on day 0 for vCM_HVF.

C5AR2 (Complement component 5a receptor 2), a component of the immune system involved in inflammation, cell migration, and tissue repair, has been identified in heart tissue (www.proteinatlas.org)**.**

4.3.3.6. The role of fibroblasts

Focusing on the selected receptor, the subsequent step involved choosing a ligand or inhibitor that could modulate receptor activity. With the aim of demonstrating the influence of fibroblasts on cardiomyocytes, attention was paid to the data obtained from RNAseq and mass spectrometry for a fibroblast's comparison: HAF vs. HVF.

4.3.3.6.1. DEG analysis

First, the investigation of differences between cardiac fibroblast subtypes were performed to identified pathways with the highest number of related genes. The results for comparison between HAF and HVF were presented on Gene Ontology - Molecular Function bubble plot. Most of the genes were related to extracellular matrix binding and BMP receptor binding, which corresponds to the difference between chamber-specific fibroblasts in the produced matrix (Figure 65A). Additionally, using the KEGG pathway database, the most significant differences were associated with signaling pathways, representing cell line characteristics. (Figure 65B).

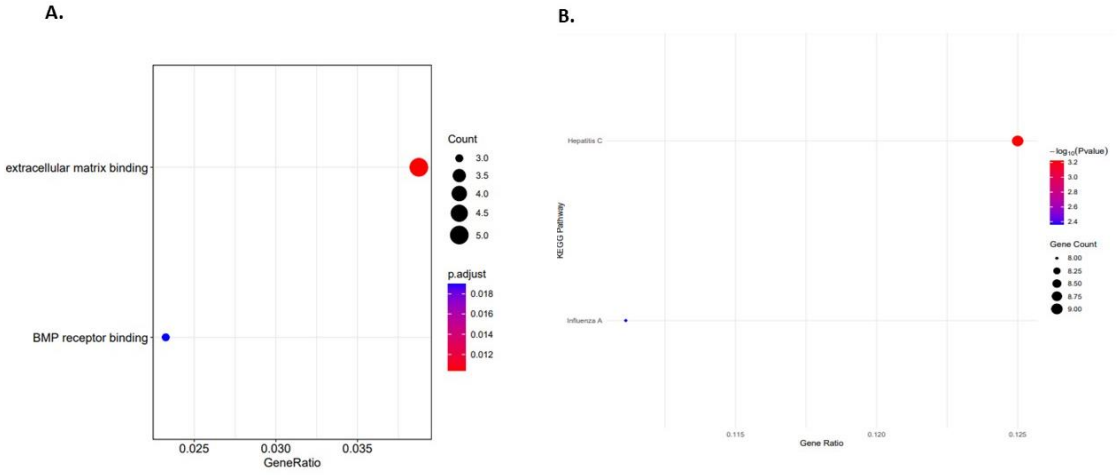

Figure 65 Graphic presentation of results for comparing HAF and HVF. A. Gene Ontology analysis. B. KEGG pathways. A. Gene Ontology analysis. The bubble plot illustrates adjusted p-values (color intensity) and gene count (bubble size). B. KEGG pathways. The bubble plot displays -log10 p-values (color intensity) and number of counts.

4.3.3.6.2. Secretome analysis

Secondly, the investigation of differences between cardiac fibroblast subtypes was investigated on protein level.

The results for comparing HAF and HVF protein levels were presented on Gene Ontology - Molecular Function and Biological Process plots, with PANTHER - Protein ANalysis THrough Evolutionary Relationships (www.pantherdb.org) (Thomas & Mushayahama, 2022).

The highest number of genes were associated with molecular functions: binding (above 240 genes) and catalytic activity (180 genes). In the Biological process, the significant

majority related to the cellular process (almost 320 genes), metabolic process (approximately 200 genes), and biological regulation (140 genes) pathways (Figure 66).

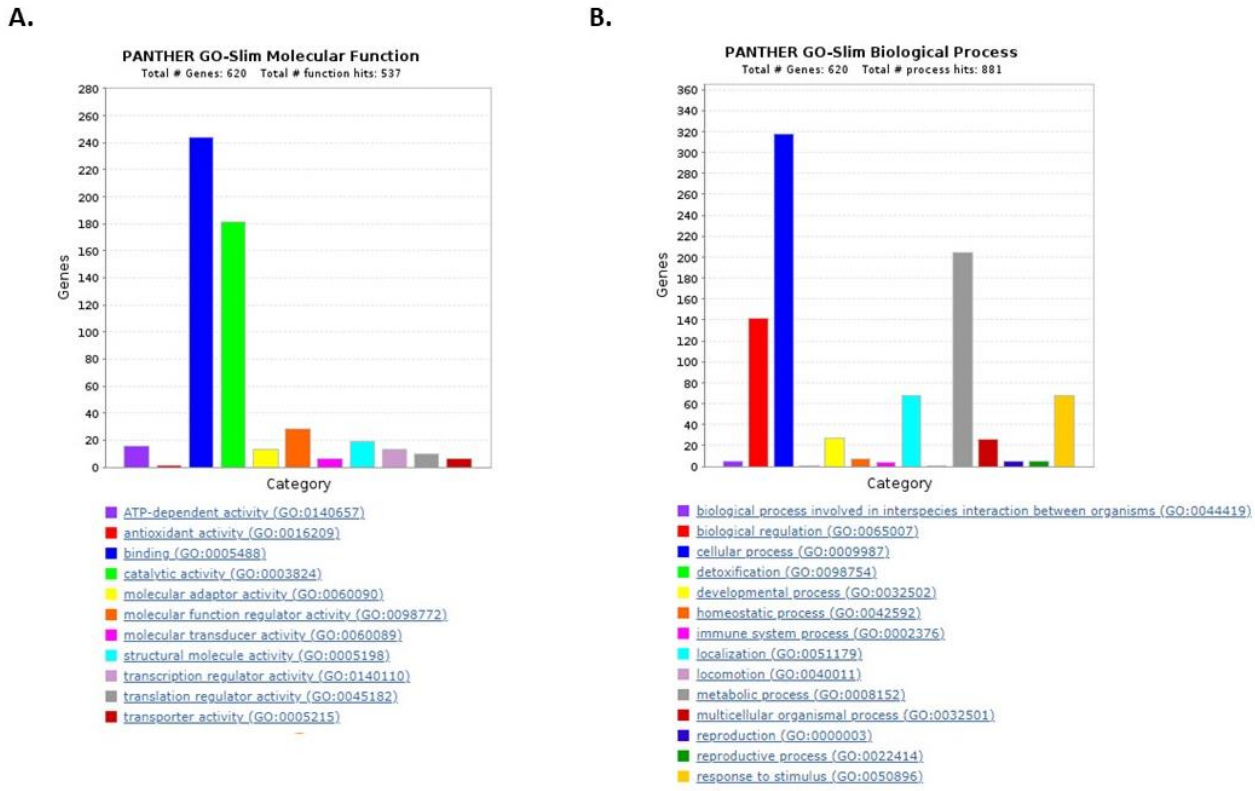

Figure 66 Graphic presentation of proteins results for comparing HAF and HVF with PANTHER. A. Gene Ontology - Molecular Function. B. Gene Ontology - Biological Processes. Modified from **(Thomas & Mushayahama, 2022).**

Since the results had to be a ligand or an inhibitor for C5AR2, the proteins which were only produced by one type of fibroblasts (HAF or HVF) were listed. Due to the activity of DHRS3 only in vCM_HVF, the C5AR2 receptor should be either activated to positively influence DHRS3 in vCM_HVF or inhibited to block DHRS3 activity in vCM_HAF.

Selected proteins were confronted with the databases providing information on biological interactions with C5AR2: Reactome, IntAct, and available literature. Among the list of proteins, ADP Ribosylation Factor Like GTPase 6 Interacting Protein 5 (**ARL6IP5**) was found. The protein was detected in the HAF sample secretome only and, according to databases, interacts with C5AR2.

Sum up 8.3.3. Despite the lack of significant paracrine fibroblasts effect on cardiomyocytes in 2D culture, their influence in 3D culture has been proven. The use of

atrial fibroblasts in EHT with ventricular cardiomyocytes resulted in increased contractile pattern, decreased FOC and decreased FOC after muscarinic stimulation. Moreover, RNAseq and secretome data analysis allowed us to propose a mechanism of HAF action on the differentiation of vCMs towards the atrial phenotype via the retinoic acid signaling pathway.

5. DISCUSSION

The human heart is one of the most specialized organs in the human body. It works continuously to circulate blood and deliver needed nutrients and oxygen throughout the body. Unlike other muscles in our body that can regenerate, the heart muscle, which consist of cardiomyocytes, does not have that ability (Zebrowski *et al.*, 2016). Such specialized muscle cells impart to the heart the ability to rhythmic and coordinated contractions, making the heart pump blood efficiently through the body. Cardiomyocytes, however, are unable to divide. This characteristic makes it unfortunate for the heart to be so easily vulnerable to damage (Bergmann *et al.*, 2015).

However, there is another major cell type in heart tissue, called fibroblasts, which are the second largest population in the human heart (Fan *et al.*, 2012). Unlike cardiomyocytes, fibroblasts do not contract. Instead, they play a key role in the production of signaling molecules and proteins, among others, collagen, which is responsible for the structural integrity and elasticity of cardiac tissue (Kular *et al.*, 2014).

Recent studies have also revealed additional functions of fibroblasts that go beyond their traditional role in maintaining tissue architecture, including active participation in immune responses and regulation of inflammation. By modulating the immune environment through the secretion of various cytokines and chemokines, among others, TGF-β or IL-6 (Ma *et al.*, 2012) cardiac fibroblasts recruit and activate immune cells. Moreover, cardiac fibroblasts can secrete signaling molecules - SDF-1 or CCL-2 that attract immune cells to the site of injury (Shao *et al.*, 2015; Shen *et al.*, 2014). What is more, cardiac fibroblasts respond to mechanical forces by modulating the extracellular matrix. Mechanical stretch directly influences the secretion of matrix proteases and matricellular proteins, independently of biochemical signaling, and also indirectly affects biochemical signaling (Pesce *et al.*, 2022; Rogers *et al.*, 2021). As with cardiomyocytes, in the heart, we can distinguish ventricular and atrial fibroblasts, which exhibiting differences in morphology, electrical properties, and protein expression(Burstein *et al.*, 2008).

The investigation of interactions between cardiomyocytes and fibroblasts constitutes a crucial aspect of this work, essential for achieving the stated aims:

1. Establishment of full chamber-specific EHT (chEHT), using IPSCs-derived chamber specific cardiomyocyte, cardiac fibroblast and extracellular matrix component with adequate gene expression pattern and contraction features

2. Evaluation of chEHT model through pharmacological-grade studies of atrial-specific AP14145 inhibitor of small-conductance calcium-activated potassium channel

3. Investigation of the role of cardiac fibroblasts in the terminal cardiomyocyte differentiation process

Ad. 1. To establish 3D model, iPSCs were necessary. iPSCs have become a valuable model for investigating developmental processes, predicting drug effects, and gaining insights into diseases. Their ability to differentiate into any cell type in the body, combined with their self-renewal properties, provides unlimited number of cells. Consequently, the first phase was focused on the comprehensive characterization of implemented cell lines, which were used in all further studies in the dissertation. Molecular evaluation of key pluripotency genes of iPSC_1 and iPSC_2, while immunofluorescence staining and embryoid body formation confirmed a stem cell characteristic and validated the quality of these cell lines as a foundation for further experiments (**4.1.1. iPSCs characteristic**).

Differentiation of iPSCs to cardiomyocytes requires manipulating in signaling pathways, crucial for *in vivo* embryonic development (Batalov & Feinberg, 2015). As a result of the standard differentiation procedure, ventricular cardiomyocytes are obtained with the efficiency of approximately 70-80%. In order to obtain atrial cardiomyocytes, incubation with retinoic acid is necessary and contributes to the creation of 40-60% of the aCMs population. Optimization of the timing and concentration of retinoic acid impacts atrial differentiation efficiency (**4.1.4. aCMs differentiation optimization**), which highlights the importance of a vitamin A derivative in the process, although the mechanisms of the process remain unknown.

When analyzing results, the purity of the chamber-specific CMs populations applied in experiments must be considered. While the differentiation protocol aims to enhance one type of lineage, the process is not entirely selective. Differentiation protocols

produce heterogeneous population of cardiomyocytes and non-cardiomyocytes, with majority of intended cells (Jiang et al., 2022). The application of selection stage with lactic acid during regular cardiomyocytes culture (Tohyama et al., 2013) allowed to narrowed down the population to cardiomyocytes, however, this selected population still contained a mix of pacemaker, atrial, and ventricular cardiomyocytes, what can influence the observation.

The presence of atrial and ventricular cardiomyocytes with their different functional properties offers a better understanding of cardiac physiology and enables 3D heart model improvement (among others: Engineered Heart Tissue). EHT which combines chamber-specific human induced pluripotent stem cell-derived cardiomyocytes and chamber-specific cardiac fibroblasts, gave the unique opportunity to create an accurate 3D model - atrial and ventricular

The contractility differences between atrial and ventricular EHT mimic *in vivo* heart tissue, presenting increased atrial EHT contraction frequency than ventricle EHT, while showing a similar contraction value to the physiological values It demonstrates superiority over 2D cultures, where both chamber-specific cardiomyocytes tend to be characterized by increased contraction frequency (**4.1.5.3. Contractility pattern**). EHT exhibit specific physiological properties of the heart, like pharmacological stimulation response or tissue elasticity. Compared to other 3D heart models, the EHT provides a more physiologically relevant environment, where cardiomyocytes and fibroblasts can interact between each other and physical properties of the heart: the Frank-Starling mechanism, the response to changes in calcium concentration or the reaction to β-adrenergic stimulation can be observed.

In the human heart, Frank-Starling mechanism is a concept used to describe the relationship between the amount of blood that enters the heart (end - diastolic volume) and the force with which the heart contracts (stroke volume) (Kumar *et al.*, 2019). When the heart receives more blood - the walls of the heart chambers stretch, and it leads to an increase in the force of contraction (FOC). The length of the sarcomere plays a crucial role. When the heart chambers are filled with blood, the sarcomeres are stretched. This stretching leads to an optimal overlap between the myosin and actin filaments within the sarcomere, allowing for more efficient contraction (Solaro, 2007). The same physiological response was presented in EHT, indicates the maturity of EHT's

contractility apparatus maturation. In both, atrial and ventricular EHT, by increasing, the EHT's stretch, the force of contraction was changed until the plateau was reached (

4.1.5.4.1. Frank-Starling mechanism). Also, the differences between FOC in chEHT was mimicking the physiological heart condition – FOC in atrial EHT, was lower compared to the ventricle EHT, as in the heart, when in the atria, the pressure needed to move blood into the ventricles is relatively low, in compared to ventricles with higher FOC, which have to deliver blood to the entire body.

Another physiological parameter is response to calcium - dose change. When the concentration of calcium ions increases within the cytoplasm, calcium binds to troponin and changes its conformation. Due to that, it shifts the position of tropomyosin and enables myosin-actin binding - the sliding filament mechanism of muscle contraction signaling (Kuo & Ehrlich, 2008). Consequently, an increased concentration of calcium ions generally leads to a stronger force of contraction in cardiac muscle cells. The same physiological relationship was presented in EHT. As the concentration of calcium in the Tyrode solution increased, the force of the contraction changed, proving the maturation of contractility apparatus and ion channels. The relationship was evident in atrial and ventricular EHTs (**4.1.5.4.2. Calcium response**).

The third characteristic physiological heart phenomenon is the β-adrenergic stimulation. As a result of the action of adrenaline, the heart rate is increased, and it enhances the force of contraction. To validate the reaction to stress in EHT, an analog of adrenaline - isoprenaline was used, which is also a non-selective β1-adrenergic receptor agonist, increasing heart rate and contractility. By binding to the β-adrenergic receptors in cardiac muscle cells, it enhances calcium influx and increases calcium release from the sarcoplasmic reticulum(Yoo *et al.*, 2009). Consequently, the higher concentration of calcium within the cell leads to stronger and more frequent heartbeats. Due to β-adrenergic stimulation, in both EHT subtypes, was noticed the increase of FOC and shortening the contraction time, an effect that would be expected *in vivo*. In our hands, EHT showed sensitivity to β-adrenergic stimulation (by Isoprenaline), which is similar to adult heart tissue levels (EC_{50}heart≈2nM ≈ EC_{50}EHT=3-10nM << EC_{50}iPSCs-CM=200-400nM) (Figure 34). Such sensitivity could only be achieved in a model characterized by

high maturity of ion channels and sarcomeres, and is one of the best results achieved with this 3D model (Dobson *et al.*, 2008; Mathur *et al.*, 2015).

All the collected results demonstrated how the advanced chEHT model effectively mimics physiological phenomena occurring in the human heart. However, our model is still limited as it comprises of a combination of two cell types only - cardiomyocytes and cardiac fibroblasts. Other cell types, such as endothelial cells, smooth muscle cells or adipocytes, which contribute to the overall tissue architecture, vascularization, energy homeostasis and paracrine signaling within the heart are still to be implemented in the model (Krüger-genge et al., 2019; Lin et al., 2019; Tang et al., 2023). Application of additional cell types could enhance the physiological relevance of the model by promoting tissue maturation, however it would be associated with increased costs and complexity of the model.

Ad. 2. The EHT remains a promising and innovative approach in pharmacological studies. The established atrial EHT model has shown great potential in the therapeutic targets for atrial fibrillation patients.

By using chamber-specific iPSCs-derived cardiomyocytes and fibroblasts, the EHT could be tailored to mimic the atrial tissue, providing a relevant platform to study the influence of inhibitor AP14145 on SK channels - a recent atrial fibrillation's therapeutic target (Gu *et al.*, 2018).

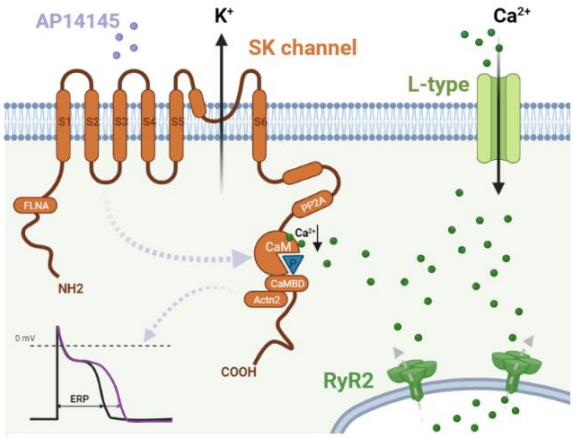

Figure 67 Inhibition of SK channels. Created with BioRender.com.

Small conductance calcium-activated potassium ($K_{Ca}2$) channels are characteristic of atrial action potential and activated by an increase in the concentration of intracellular calcium. And inhibition of SK channels prolongs atrial effective refractory period (AERP), what would be a solution for

irregular and shortened action potential in AF patients (Figure 67).

So far, AP14145, which is specific for two subtypes of SK channel - SK2 and SK3, was widely investigated through many *in vivo* models, among others: mouse, rat, guinea pig, and pigs, however in the mouse model its effectiveness has not be confirmed (Diness *et al.*, 2017; Simó-Vicens *et al.*, 2017). Interestingly, in studies on isolated guinea pig and rat hearts, 10 µM AP14145 was the first dose in the dose-response curve to show AERP prolongation (Kirchhoff et al., 2019; Simó-Vicens et al., 2017), and this concentration also had a statistically significant impact on our chEHT models.

By applying chEHT, the statistically significant inhibitor effect SK channels on atrial EHT could be presented (**4.2.2. SK inhibition in 3D culture**). AP14145 implementation caused prolongation of contraction total duration, specifically targeting the relaxation phase in atrial EHT, while no significant influence of A14145 in ventricle EHT was observed. This confirms the results from animal studies.

Additionally, examination of AP14145's influence on chamber-specific CMs in 2D culture didn't present any effect, even though SK2 and SK3 were identified in atrial CMs on a molecular level (**4.2.1. SK channel inhibition in 2D culture**). This contrasts with the literature, where AP14145 effect was observed with an IC_{50}=1.1 µM in patch-clamp experiments using CHO-K1 isolated cell line model with overexpression of $K_{Ca}1.1$, $K_{Ca}2.1$, $K_{Ca}2.2$, or $K_{Ca}2.3$ (Simó-Vicens et al., 2017). The lack of an effect in 2D culture might result from differences in gene expression levels, which may have been influenced by a heterogeneous cardiomyocyte population or the presence of less mature vCMs compared to the EHT model.

By investigating the influence of atrial-specific inhibitor on SK channels, we could prove the chEHT model sensitivity. ChEHT was presented as an effective tool for investigating the physiological properties of human atria and ventricles. These findings align with the recent FDA initiative - FDA's New Alternative Methods Program - which encourages the application of alternative models that can replace, reduce, and refine animal testing (Strauss et al., 2022).

Ad. 3. Last, but not least, by providing a three-dimensional microenvironment that mimics the native heart tissue, the EHT allows for evaluation of cell types interactions during tissue development process. EHT presents as a valuable tool for investigating the role of cardiac fibroblasts in the terminal differentiation process of cardiomyocytes.

Fibroblasts also play significant role during the development of the embryo - a period during which the initially thin and multilayered heart tube transforms into a more robust, complex structure. The process is commonly known as heart compaction. This phase of dramatic remodeling, improving mechanical function and reshaping involves the development of an atrium and ventricle (Misra & Garg, 2013; Plikus *et al.*, 2021). Recent studies have highlighted the contributions of fibroblasts in cardiac compaction through their ability to undergo a process epithelial-to-mesenchymal transition (EMT). Fibroblasts invade the developing myocardium and contribute to extracellular matrix deposition, which gives structural integrity to the developing heart (Chen *et al.*, 2017).

Apart from heart compaction, the EMT processes driven by fibroblasts can take part in tissue repair and remodeling during postnatal life. Fibroblasts become activated upon injury or due to stress and then undergo EMT, which contributes to the development of fibrosis and scar formation in the heart (Stone *et al.*, 2016). Cardiac fibroblasts influence cardiomyocytes by cell-to-cell interaction, by modifying the ECM, and by modulating the electrophysiological properties (Calderon *et al.*, 2023). The role that fibroblasts play in modulating cardiomyocyte function and fate has increasingly come into focus.

With a view to investigate cardiomyocytes – fibroblasts influence, it has been observed that there is a difference in the outcomes obtained by 2D and 3D culture systems by combining only ventricular cardiomyocytes with atrial or ventricle fibroblasts. In the 2D culture system, the paracrine effect of fibroblasts on the structural maturation process of ventricular cardiomyocytes was not demonstrated (**4.3.1. Paracrine signaling test in 2D culture**). The molecular investigation, immunostaining and contractility pattern, did not provide significant evidence of chamber-specific fibroblasts influence on ventricular cardiomyocytes. These results present paracrine signaling as less prominent in the communication between the two major cardiac populations.

The application of the 3D model allowed for the assessment of direct fibroblast effects on cardiomyocytes and introduced indirect signaling through mechanical influences on both cell populations. Using either atrial or ventricular fibroblasts in tissues with ventricular cardiomyocytes led to results consistent with those obtained in the first part of the dissertation, where EHT were molded with atrial fibroblasts paired with atrial cardiomyocytes (vCM_HAF), and ventricular fibroblasts with ventricular cardiomyocytes (vCM_HVF).

The presence of different fibroblast populations only, allowed to observe the initial discrepancy in the contraction frequencies between EHTs at last days of maturation, which reflects the physiological difference between atria and ventricles (**4.3.2.2. Contractility patterns investigation in 3D**).

Chamber-specific differences between vCM_HAF and vCM_HVF tissues were also proven during physiological measurement. Not only vCM_HAF were characterized by lower FOC, compared to vCM_HVF, but also the contraction duration of vCM_HAF was faster than vCM_HVF (**4.3.2.3. Physiological parameters measurements**).

To further validate these findings, a pharmacological test using carbachol was conducted. There are five subclasses of muscarinic receptors, among which the M2 receptor is expressed on cardiomyocytes and smooth muscle (Dhein, 2001). This G protein-coupled receptor stimulates a Gα protein, inhibiting adenylyl cyclase and increasing K^+ conductance. Consequently, M2 action leads to a decrease in beating rate and force of contraction.

Due to the varying distribution of M2 muscarinic receptors (Kitazawa *et al.*, 2016), the carbachol-induced FOC differs between the atria and ventricles. Additionally, atrial cardiomyocytes possess more potassium channels, rendering the increase in K^+ conductance more influential compared to ventricular cardiomyocytes. As a result, carbachol induces a more pronounced decrease in FOC in atrial CMs. In ventricular cardiomyocytes, this effect is less evident due to a lower abundance of M2 receptors and physiological properties (including reduced K^+ currents). Additionally, ventricles express both M1 and M2 receptors, potentially leading to more complex outcomes (Maria *et al.*, 1993; Sharma *et al.*, 1995). While M1 activation has been shown to induce

positive inotropic effects, potentially through increased L-type Ca^{2+} currents (Maria *et al.*, 1993) or enhanced Ca^{2+} release (Sharma *et al.*, 1995), the combined influence of M1's stimulatory and M2's inhibitory actions on contraction remains complex.

Additionally, by applying isoprenaline, which increases FOC, the potency of carbachol to antagonize isoprenaline can be assessed. This refers to carbachol's ability to counteract or reduce the effects of isoprenaline (Eschenhagen *et al.*, 1996).

Similar to cardiac tissue, EHTs exhibited distinct muscarinic receptor distributions and responses to carbachol, between atrial and ventricular EHTs (**4.3.2.3.3. Muscarinic receptor stimulation**). Additionally, the antagonistic effects of carbachol on isoprenaline-induced increases in FOC were also observed. What is most interesting, distinct physiological responses were observed between EHTs composed of ventricular cardiomyocytes and atrial or ventricular fibroblasts. EHT composed of ventricular cardiomyocytes and atrial fibroblast showed decreased FOC as a consequence of carbachol stimulation when ventricular cardiomyocytes and ventricular fibroblast presented an increase in FOC. This difference was not visible after stimulation of the receptors with isoprenaline and then carbachol implementation. This experiment not only proved the maturation level of EHT, but also focused attention on the potential role of cardiac fibroblasts on cardiomyocyte phenotype. All physiological measurements confirmed the atrial tissue phenotype, which suggests that cell-to-cell and indirect/mechanical signaling are likely the primary determinants of cardiac subtype differentiation.

The observed differences have clear manifestation in the RNA sequencing results, which also proved that by only applying different chamber-specific fibroblasts, a distinction between atrial and ventricular tissues in the gene expression profile was visible. This contrasts with control 2D condition medium studies, where the difference was not obtained.

Further analysis of the difference in gene expression highlighted the "Retinoic Acid signaling" pathway. Retinoic acid plays many important roles throughout development, cell specialization (differentiation), and maintaining healthy function (homeostasis). It Is an active derivative of vitamin A (retinol), which is bound by plasma retinol-binding

protein (RBP) and transferred into the cell through cell-surface receptor STRA6 (Kawaguchi *et al.*, 2013). Then retinol is processed by short-chain dehydrogenase/reductase RDH10, to be converted into retinaldehyde (Sandell *et al.*, 2007). The process is reversed, and retinaldehyde might me converted back to retinol for storage due to DHRS3 activity. The full catalytic activity of DHRS3 depends on the presence of RDH10 activity (Adams *et al.*, 2014). Next, enzymes known as retinaldehyde dehydrogenases (ALDH1A1 - 3) convert retinaldehyde into the active form of vitamin A, retinoic acid (RA) (Duester, 2009). Once produced, RA is taken up by cells using CRABP proteins. These proteins then deliver RA either to the nucleus, where it controls gene activity, or to CYP26 enzymes (CYP26A1, CYP26B1 and CYP26C1) for degradation (Kedishvili, 2017).

RA has a critical role in many stages of heart development. It guides the formation of various heart muscle cells and is involved in the development of the epicardium (outer layer of the heart), the outflow tract (where the aorta and pulmonary artery leave the heart),the muscular wall of the ventricles (lower chambers), and the coronary arteries supplying the heart with blood (Wiesinger *et al.*, 2021). In line with *in vivo* studies, the role of RA has also been investigated - 10 nM RA accelerates cardiac differentiation (Wobus *et al.*, 1997), but the higher concentration of RA (1 mM) at day3 of differentiation, directs differentiation toward atrial fate (Devalla *et al.*, 2015) (**4**.1.4. aCMs differentiation optimization).

The analysis of RNA sequencing data confirmed changes in gene expression within the retinoic acid pathway (**4.3.3.5.4. Retinoic acid signaling pathway components** . At day 0 for vCM_HAF, there are no visible gene expression changes except for RDH10, compared to vCM_HVF, where the entire retinoic acid signaling pathway is activated. The process begins with retinol conversion into retinaldehyde, involving increased activity of RDH10, followed by further retinoic acid transition to retinoic acid, with increased activity of ALDH1A3, and concluding with RA degradation involving CYP26B1.

The results revealed a lack of activity in the retinoic acid signaling pathway in vCM_HAF at day 0, suggesting that the pathway was inhibited at the beginning of the process. Due to the continued activity of RDH10, the target for inhibition turned out to be DHRS3, which is necessary for maintaining the balance between retinol and retinaldehyde in the

cell. DHRS3 inhibition in vCM_HAF, consequently, led to the accumulation of retinaldehyde and, subsequently, increased expression of ALDH1A1-3. The higher expression of enzymes (ALDH1A2 and ALDH1A3) is responsible for significant RA synthesis entering the nucleus. In comparison, the DHRS3 activity is kept in vCM_HAF, conducive to maintaining balance and, consequently, supplying only the necessary amount of retinoic acid to the cell.

Further analysis of the literature showed DHRS3 interacts with receptor C5AR2 (Huttlin *et al.*, 2017), which was overexpressed in vCM_HVF only at the beginning of EHT maturation process, but there was no activity registered in vCM_HAF samples. It turns out that C5AR2 interacts with a protein ARL6IP5, protein which exhibited negative regulation properties in L-glutamate import across the plasma membrane (Siddique *et al.*, 2023). ARL6IP5 protein was found in the secretome of atrial fibroblasts only. Altogether, HAF can affect the retinoic acid signaling pathway and are responsible for gaining the atrial phenotype.

First, molecular confirmation of retinoic acid signaling pathway targets by qPCR analysis is necessary. Next, the C5AR2 role in CMs phenotype feedback has to be investigated. By inhibiting the receptor C5AR2, the influence could be examined, however despite the advances in developing drugs against C5AR2 complement receptor - C5AR1, there has been great difficulty in producing selective C5AR2 antagonists (Ricklin *et al.*, 2013). Inhibiting gene transcription or translation of the receptor protein is needed.

It is important to note that the proposed mechanism was based on the interaction between iPSC-derived ventricular cardiomyocytes and fully developed fibroblast from adult donor. To truly demonstrate the impact of fibroblasts on cardiomyocyte phenotype during heart development, we must also consider the developmental stage of the fibroblasts themselves.

Literature points three main distinct origin of fibroblasts - epicardium, endocardium, or neural crest (Moore-Morris et al., 2014), which are contributing to regional differences in the cardiac microenvironment of the developed heart. The newest RNAseq studies present a comprehensive examination of cardiac fibroblast heterogeneity, revealing distinct subpopulations, characterized by expression of lineage-specific genes. However,

tracing the development of chamber-specific fibroblast subtypes is still difficult to elucidate (Deng et al., 2023).

During embryogenesis, fibroblasts migrate and invade the myocardium, contributing to the structural and functional maturation of the heart. This invasion process involves complex signaling pathways, including paracrine and mechanical cues, which might guide cardiomyocyte maturation and differentiation (Kovacic et al., 2019). The characteristics of fibroblasts at this stage could significantly influence our understanding of their role in cardiac development.

To gain a deeper understanding of fibroblast, it would be ideal to study immature fibroblasts from embryonic sources. However, obtaining these cells raises ethical issues. As a result, most current studies rely on adult fibroblast, which do not fully capture the complex environment present during early heart development.

Additionally, this complex environment is not only composed of two cell populations. The invasion of fibroblasts presents them as a potential driving force in the differentiation of terminal cardiomyocytes, however, fibroblasts are not the only cell types presented during heart development. This limitation is a weakness of the EHT model, which primarily focuses on a narrow range of cellular interactions. Implementing alternative methods, which incorporate a broader variety of cells, like organ-on-chip (Kolanowski et al., 2020) or cardiovascular 3D bioprinting (Sun et al., 2023), would be beneficial. This change could improve mimicking of the cardiac environment and allow for more advanced analysis of cellular interactions, among others – mechanosensing (Pesce et al., 2022).

During heart morphogenesis, the heart undergoes significant changes in shape and size, which generates mechanical forces that influence cellular behavior. Cardiomyocytes and fibroblasts are equipped with mechanosensors that allow them to track changes in the ECM stiffness or shear stress from blood flow (Pesce et al., 2022). The mechanical signals could activate pathways, leading to tissue remodeling and possibly increasing the influence of cardiac fibroblasts on cardiomyocyte specification

We are just starting to understand the important role of cardiac fibroblasts in heart development. Our preliminary research findings in the coming years may change how we approach cardiac tissue development and treatment for various heart diseases. If we want to explain the mechanisms behind heart diseases like non-compaction cardiomyopathy, studying the biology of cardiac fibroblasts and their impact on heart tissue could provide valuable insights, and an advance 3D model - EHT constitutes a valuable tool.

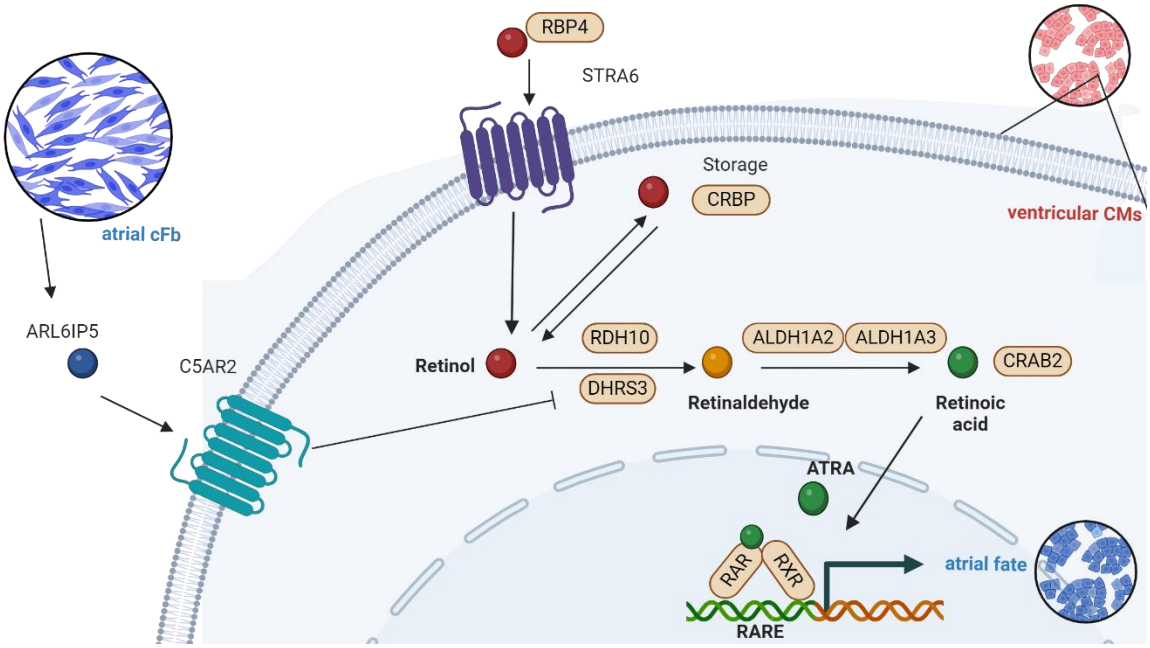

Figure 68 Potential mechanism by which atrial fibroblasts (cFb) induce atrial-like characteristics in ventricular Cardiomyocytes (CMs). Created with BioRender.com.

CONCLUSIONS

1. Chamber-specific Engineered Heart Tissue (chEHT) was successfully established using iPSC-derived chamber-specific cardiomyocytes, cardiac fibroblasts subtypes and extracellular matrix components. EHT model was characterized by differences in gene expression, ion channel activity, and physiological responses, successfully mimicking key human heart tissue parameters, such as the Frank-Starling mechanism, calcium response, and stress response.

2. The chEHT model was proven to be an effective drug functionality assessment tool in pharmacological studies. By investigating the atrial-specific inhibitory effect of the AP14145 on small-conductance calcium-activated potassium channels chEHTs proved their physiological relevancy and drug effectiveness prediction feasibility .

3. An influence on atrial fibroblasts on the terminal differentiation of iPSC-derived vCMs into atrial cardiomyocytes has been proved in EHT tissue model and confirmed through physiological evaluation and molecular profiling.

4. A retinoic acid signaling pathway was proposed to explain the influence of atrial fibroblasts on the fate of cardiomyocytes, however this mechanism requires further investigation.

FIGURES

TABLES

REFERENCES

Adams, M. K., Belyaeva, O. V, Wu, L., & Kedishvili, N. Y. (2014). *The Retinaldehyde Reductase Activity of DHRS3 Is Reciprocally Activated by Retinol Dehydrogenase 10 to Control Retinoid Homeostasis * □*. *289*(21), 14868–14880. https://doi.org/10.1074/jbc.M114.552257

Ahmed, R. E., Anzai, T., Chanthra, N., & Uosaki, H. (2020). A Brief Review of Current Maturation Methods for Human Induced Pluripotent Stem Cells-Derived Cardiomyocytes. *Frontiers in Cell and Developmental Biology*, *8*(March), 1–9. https://doi.org/10.3389/fcell.2020.00178

Aigha, I., & Raynaud, C. (2016). Maturation of pluripotent stem cell derived cardiomyocytes: The new challenge. *Global Cardiology Science and Practice*, *2016*(1). https://doi.org/10.21542/gcsp.2016.6

Anfinson, M., Fitts, R. H., Lough, J. W., James, J. M., Simpson, P. M., Handler, S. S., Mitchell, M. E., & Tomita-Mitchell, A. (2022). Significance of α-Myosin Heavy Chain (MYH6) Variants in Hypoplastic Left Heart Syndrome and Related Cardiovascular Diseases. *Journal of Cardiovascular Development and Disease*, *9*(5). https://doi.org/10.3390/jcdd9050144

Asnes, C. F., Marquez, J. P., Elson, E. L., & Wakatsuki, T. (2006). Reconstitution of the Frank-Starling mechanism in engineered heart tissues. *Biophysical Journal*, *91*(5), 1800–1810. https://doi.org/10.1529/biophysj.105.065961

Augustine, R., Dan, P., Hasan, A., Khalaf, I. M., Prasad, P., Ghosal, K., Gentile, C., McClements, L., & Maureira, P. (2021). Stem cell-based approaches in cardiac tissue engineering: controlling the microenvironment for autologous cells. *Biomedicine and Pharmacotherapy*, *138*. https://doi.org/10.1016/j.biopha.2021.111425

Banerjee, I., Fuseler, J. W., Price, R. L., Borg, T. K., & Baudino, T. A. (2007). Determination of cell types and numbers during cardiac development in the neonatal and adult rat and mouse. *American Journal of Physiology - Heart and Circulatory Physiology*, *293*(3), 1883–1891. https://doi.org/10.1152/ajpheart.00514.2007

Barrick, S. K., & Greenberg, M. J. (2021). Cardiac myosin contraction and mechanotransduction in health and disease. *Journal of Biological Chemistry*, *297*(5), 101297. https://doi.org/10.1016/j.jbc.2021.101297

Baruscotti, M., Barbuti, A., & Bucchi, A. (2010). The cardiac pacemaker current. *Journal of Molecular and Cellular Cardiology*, *48*(1), 55–64.

https://doi.org/10.1016/j.yjmcc.2009.06.019

Batalov, I., & Feinberg, A. W. (2015). Differentiation of cardiomyocytes from human pluripotent stem cells using monolayer culture. *Biomarker Insights*, *10*, 71–76. https://doi.org/10.4137/BMI.S20050

Bergmann, O., Zdunek, S., Felker, A., Salehpour, M., Alkass, K., Bernard, S., Sjostrom, S. L., Szewczykowska, M., Jackowska, T., Dos Remedios, C., Malm, T., Andrä, M., Jashari, R., Nyengaard, J. R., Possnert, G., Jovinge, S., Druid, H., & Frisén, J. (2015). Dynamics of Cell Generation and Turnover in the Human Heart. *Cell*, *161*(7), 1566–1575. https://doi.org/10.1016/j.cell.2015.05.026

Bizy, A., Guerrero-Serna, G., Hu, B., Ponce-Balbuena, D., Willis, B. C., Zarzoso, M., Ramirez, R. J., Sener, M. F., Mundada, L. V., Klos, M., Devaney, E. J., Vikstrom, K. L., Herron, T. J., & Jalife, J. (2013). Myosin light chain 2-based selection of human iPSC-derived early ventricular cardiac myocytes. *Stem Cell Research*, *11*(3), 1335–1347. https://doi.org/10.1016/j.scr.2013.09.003

Buckberg, G. D., Nanda, N. C., Nguyen, C., & Kocica, M. J. (2018). *What Is the Heart ? Anatomy , Function , Pathophysiology , and Misconceptions*. *Figure 1*. https://doi.org/10.3390/jcdd5020033

Burstein, B., Libby, E., Calderone, A., & Nattel, S. (2008). Differential behaviors of atrial versus ventricular fibroblasts: A potential role for platelet-derived growth factor in atrial-ventricular remodeling differences. *Circulation*, *117*(13), 1630–1641. https://doi.org/10.1161/CIRCULATIONAHA.107.748053

Camelliti, P., Borg, T. K., & Kohl, P. (2005). Structural and functional characterisation of cardiac fibroblasts. *Cardiovascular Research*, *65*(1), 40–51. https://doi.org/10.1016/j.cardiores.2004.08.020

Chen, T., You, Y., Jiang, H., & Wang, Z. Z. (2017). Epithelial–mesenchymal transition (EMT): A biological process in the development, stem cell differentiation, and tumorigenesis. *Journal of Cellular Physiology*, *232*(12), 3261–3272. https://doi.org/10.1002/jcp.25797

Crocini, C. (2021). *Cardiac sarcomere mechanics in health and disease*. 637–652.

Cyganek, L., Tiburcy, M., Sekeres, K., Gerstenberg, K., Bohnenberger, H., Lenz, C., Henze, S., Stauske, M., Salinas, G., Zimmermann, W. H., Hasenfuss, G., & Guan, K. (2018). Deep phenotyping of human induced pluripotent stem cell-derived atrial and ventricular cardiomyocytes. *JCI Insight*, *3*(12), 1–17. https://doi.org/10.1172/jci.insight.99941

Deng, Y., He, Y., Xu, J., He, H., & Li, G. (2023). Heterogeneity and Functional Analysis of Cardiac Fibroblasts in Heart Development. *BioRxiv*. https://doi.org/10.1101/2023.07.30.551164

Devalla, H. D., Schwach, V., Ford, J. W., Milnes, J. T., El-haou, S., Jackson, C., Gkatzis, K., Elliott, D. A., Chuva, S. M., Lopes, D. S., Mummery, C. L., Verkerk, A. O., & Passier, R. (2015). *Atrial-like cardiomyocytes from human pluripotent stem cells are a robust preclinical model for assessing atrial-selective pharmacology*. *7*(4), 394–410.

Dhein, S. (2001). *MUSCARINIC RECEPTORS IN THE MAMMALIAN HEART*. *44*(3). https://doi.org/10.1006/phrs.2001.0835

Diness, J. G., Abildgaard, L., Bomholtz, S. H., Skarsfeldt, M. A., Edvardsson, N., Sørensen, U. S., Grunnet, M., & Bentzen, B. H. (2020). Inhibition of KCa2 Channels Decreased the Risk of Ventricular Arrhythmia in the Guinea Pig Heart During Induced Hypokalemia. *Frontiers in Pharmacology*, *11*(May), 1–10. https://doi.org/10.3389/fphar.2020.00749

Diness, J. G., Skibsbye, L., Simó-Vicens, R., Santos, J. L., Lundegaard, P., Citerni, C., Sauter, D. R. P., Bomholtz, S. H., Svendsen, J. H., Olesen, S. P., Sørensen, U. S., Jespersen, T., Grunnet, M., & Bentzen, B. H. (2017). Termination of vernakalant-resistant atrial fibrillation by inhibition of small-conductance Ca2+-Activated K+ channels in Pigs. *Circulation: Arrhythmia and Electrophysiology*, *10*(10), 1–13. https://doi.org/10.1161/CIRCEP.117.005125

Dobson, J. G., Shea, L. G., & Fenton, R. A. (2008). Adenosine A2A and β-adrenergic calcium transient and contractile responses in rat ventricular myocytes. *American Journal of Physiology - Heart and Circulatory Physiology*, *295*(6), 2364–2372. https://doi.org/10.1152/ajpheart.00927.2008

Dolnikov, K., Shilkrut, M., Zeevi-Levin, N., Gerecht-Nir, S., Amit, M., Danon, A., Itskovitz-Eldor, J., & Binah, O. (2006). Functional Properties of Human Embryonic Stem Cell–Derived Cardiomyocytes: Intracellular Ca2+ Handling and the Role of Sarcoplasmic Reticulum in the Contraction. *Stem Cells*, *24*(2), 236–245. https://doi.org/10.1634/stemcells.2005-0036

Doppler, S. A., Carvalho, C., Lahm, H., Deutsch, M. A., Dreßen, M., Puluca, N., Lange, R., & Krane, M. (2017). Cardiac fibroblasts: More than mechanical support. *Journal of Thoracic Disease*, *9*(Suppl 1), S36–S51. https://doi.org/10.21037/jtd.2017.03.122

Dueñas, A., Aranega, A. E., & Franco, D. (2017). More than just a simple cardiac envelope; cellular contributions of the epicardium. *Frontiers in Cell and Developmental Biology*, *5*(MAY), 1–11. https://doi.org/10.3389/fcell.2017.00044

Duester, G. (2009). Retinoic Acid Synthesis and Signaling during Early Organogenesis. *Cell*, *134*(6), 921–931. https://doi.org/10.1016/j.cell.2008.09.002.Retinoic

Egido, J., Zaragoza, C., Gomez-Guerrero, C., Martin-Ventura, J. L., Blanco-Colio, L., Lavin, B., Mallavia, B., Tarin, C., Mas, S., & Ortiz, A. (2011). Animal models of cardiovascular diseases. *Journal of Biomedicine and Biotechnology*, *2011*. https://doi.org/10.1155/2011/497841

Ehra, A. G., Aphrs, J. M. K., Solaece, L. A., Akar, J., Cabrera, J. A., Chen, S. A., Chugh, S. S., Corradi, D., Avila, A. D., Helm, R., Hindricks, G., Ho, S. Y., Hoit, B., Jalife, J., Kim, Y., Lip, G. Y. H., Ma, C., Marcus, G. M., Murray, K., … Denmark, S. (2016). *EHRA / HRS / APHRS / SOLAECE expert consensus on atrial cardiomyopathies : definition , characterization , and clinical implication*. *May*, 1455–1490. https://doi.org/10.1093/europace/euw161

England, J., & Loughna, S. (2013). Heavy and light roles: Myosin in the morphogenesis of the heart. *Cellular and Molecular Life Sciences*, *70*(7), 1221–1239. https://doi.org/10.1007/s00018-012-1131-1

Eschenhagen, T., Mende, U., Diederich, M., Hertle, B., Pohl, A., Schmitz, W., Scholz, H., Steinfath, M., Michel, M. C., Brodde, O., & Raap, A. (1996). *Chronic Treatment With Carbachol Sensitizes the Myocardium to cAMP-Induced Arrhythmia*. *93*(4), 763–771.

Fan, D., Takawale, A., Lee, J., & Kassiri, Z. (2012). Cardiac fibroblasts, fibrosis and extracellular matrix remodeling in heart disease. *Fibrogenesis and Tissue Repair*, *5*(1), 1. https://doi.org/10.1186/1755-1536-5-15

Fink, C., Ergün, S., Kralisch, D., Remmers, U., Weil, J., & Eschenhagen, T. (2000). Chronic stretch of engineered heart tissue induces hypertrophy and functional improvement. *The FASEB Journal*, *14*(5), 669–679. https://doi.org/10.1096/fasebj.14.5.669

Forte, E., Furtado, M. B., & Rosenthal, N. (2018). The interstitium in cardiac repair: role of the immune–stromal cell interplay. *Nature Reviews Cardiology*, *15*(10), 601–616. https://doi.org/10.1038/s41569-018-0077-x

Gabriel, G. C., Devine, W., Redel, B. K., Whitworth, K. M., Samuel, M., Spate, L. D., Cecil, R. F., Prather, R. S., Wu, Y., Wells, K. D., & Lo, C. W. (2021). Cardiovascular development and congenital heart disease modeling in the pig. *Journal of the American Heart Association*, *10*(14). https://doi.org/10.1161/JAHA.121.021631

Goldfracht, I., Efraim, Y., Shinnawi, R., Kovalev, E., Huber, I., Gepstein, A., Arbel, G., Shaheen, N., Tiburcy, M., Zimmermann, W. H., Machluf, M., & Gepstein, L. (2019). Engineered heart tissue models from hiPSC-derived cardiomyocytes and cardiac ECM for disease modeling

and drug testing applications. *Acta Biomaterialia*, *92*, 145–159. https://doi.org/10.1016/j.actbio.2019.05.016

Goversen, B., van der Heyden, M. A. G., van Veen, T. A. B., & de Boer, T. P. (2018). The immature electrophysiological phenotype of iPSC-CMs still hampers in vitro drug screening: Special focus on IK1. *Pharmacology and Therapeutics*, *183*(October 2017), 127–136. https://doi.org/10.1016/j.pharmthera.2017.10.001

Gu, M., Zhu, Y., Yin, X., & Zhang, D. M. (2018). Small-conductance Ca2+-activated K+ channels: insights into their roles in cardiovascular disease. *Experimental and Molecular Medicine*, *50*(4). https://doi.org/10.1038/s12276-018-0043-z

Guo, Y., & Pu, W. T. (2020). Cardiomyocyte maturation: New phase in development. *Circulation Research*, 1086–1106. https://doi.org/10.1161/CIRCRESAHA.119.315862

Hall, C., Gehmlich, K., & Denning, C. (2021). *Complex Relationship Between Cardiac Fibroblasts and Cardiomyocytes in Health and Diseas*. 1–15. https://doi.org/10.1161/JAHA.120.019338

Hall, C., Gehmlich, K., Denning, C., & Pavlovic, D. (2021). Complex relationship between cardiac fibroblasts and cardiomyocytes in health and disease. *Journal of the American Heart Association*, *10*(5), 1–15. https://doi.org/10.1161/JAHA.120.019338

Harvey, R. D., & Hell, J. W. (2013). CaV1.2 signaling complexes in the heart. *Journal of Molecular and Cellular Cardiology*, *58*(1), 143–152. https://doi.org/10.1016/j.yjmcc.2012.12.006

Herum, K. M., Lunde, I. G., Mcculloch, A. D., & Christensen, G. (n.d.). *The Soft- and Hard-Heartedness of Cardiac Fibroblasts : Mechanotransduction Signaling Pathways in Fibrosis of the Heart*. https://doi.org/10.3390/jcm6050053

Huttlin, E. L., Bruckner, R. J., Paulo, J. A., Cannon, J. R., Ting, L., Baltier, K., Colby, G., Gebreab, F., Parzen, H., Szpyt, J., Tam, S., Zarraga, G., Pontano-vaites, L., Swarup, S., White, A. E., Schweppe, D. K., Rad, R., Erickson, B. K., Obar, R. A., … Steven, P. (2017). Architecture of the human interactome defines protein communities and disease networks. *Nature Publishing Group*, *545*(7655), 505–509. https://doi.org/10.1038/nature22366

Iaizzo, P. A. (2005). Chapter 5 Anatomy of the Human Heart. *Handbook of Cardiac Anatomy, Physiology, and Devices: Second Edition*, 1–659.

Id, J. M. D., Saunders, V., Kelly, I. O., & Id, D. I. W. (2022). *Defining cardiac cell populations and relative cellular composition of the early fetal human heart*. 1–17. https://doi.org/10.1371/journal.pone.0259477

Ihara, D., Watanabe, Y., Seya, D., Arai, Y., Isomoto, Y., Nakano, A., Kubo, A., Ogura, T., Kawamura, T., & Nakagawa, O. (2020). Expression of Hey2 transcription factor in the early embryonic ventricles is controlled through a distal enhancer by Tbx20 and Gata transcription factors. *Developmental Biology*, *461*(2), 124–131. https://doi.org/10.1016/j.ydbio.2020.02.001

Jiang, C. L., Goyal, Y., Jain, N., Wang, Q., Truitt, R. E., & Coté, A. J. (2022). Cell type determination for cardiac differentiation occurs soon after seeding of human - induced pluripotent stem cells. *Genome Biology*, 1–29. https://doi.org/10.1186/s13059-022-02654-6

Joyner, M. J., & Casey, D. P. (2015). Regulation of increased blood flow (Hyperemia) to muscles during exercise: A hierarchy of competing physiological needs. *Physiological Reviews*, *95*(2), 549–601. https://doi.org/10.1152/physrev.00035.2013

Kałużna, E., Nadel, A., Zimna, A., Rozwadowska, N., & Kolanowski, T. (2022). Modeling the human heart ex vivo—current possibilities and strive for future applications. *Journal of Tissue Engineering and Regenerative Medicine*, *November 2021*, 1–22. https://doi.org/10.1002/term.3335

Kamakura, T., Makiyama, T., Sasaki, K., Yoshida, Y., Wuriyanghai, Y., Chen, J., Hattori, T., Ohno, S., Kita, T., Horie, M., Yamanaka, S., & Kimura, T. (2013). Ultrastructural maturation of human-induced pluripotent stem cell-derived cardiomyocytes in a long-term culture. *Circulation Journal*, *77*(5), 1307–1314. https://doi.org/10.1253/circj.CJ-12-0987

Kamkin, A., Kiseleva, I., Isenberg, G., Wagner, K. D., Günther, J., Theres, H., & Scholz, H. (2003). Cardiac fibroblasts and the mechano-electric feedback mechanism in healthy and diseased hearts. *Progress in Biophysics and Molecular Biology*, *82*(1–3), 111–120. https://doi.org/10.1016/S0079-6107(03)00009-9

Kawaguchi, R., Zhong, M., Kassai, M., Ter-Stepanian, M., & Sun, H. (2013). STRA6-Catalyzed Vitamin A Influx, Efflux, and Exchange Riki. *J Membr Biol.*, *245*(11), 731–745. https://doi.org/10.1007/s00232-012-9463-1

Kedishvili, N. Y. (2017). RETINOIC ACID SYNTHESIS AND DEGRADATION. *Subcell Biochem.*, *81*, 127–161. https://doi.org/10.1007/978-94-024-0945-1

Kirchhoff, J. E., Skarsfeldt, M. A., Muthukumarasamy, K. M., Simó-Vicens, R., Bomholtz, S. H., Abildgaard, L., Jespersen, T., Sørensen, U. S., Grunnet, M., Hjorth Bentzen, B., & Goldin Diness, J. (2019). The KCa2 channel inhibitor AP14145, but not dofetilide or ondansetron, provides functional atrial selectivity in Guinea pig hearts. *Frontiers in Pharmacology*, *10*(JUN), 1–13. https://doi.org/10.3389/fphar.2019.00668

Kitazawa, T., Teraoka, H., Harada, N., Ochi, K., Nakamura, T., Asakawa, K., Kanegae, S., Yaosaka, N., Unno, T., Komori, S., & Yamada, M. (n.d.). *Chapter 13 Regulation of Heart Contractility by M 2 and M 3 Muscarinic Receptors : Functional Studies Using Muscarinic Receptor Knockout Mouse*. *107*. https://doi.org/10.1007/978-1-4939-2858-3

Kolanowski, Tomasz J., Antos, C. L., & Guan, K. (2017a). Making human cardiomyocytes up to date: Derivation, maturation state and perspectives. *International Journal of Cardiology*, *241*, 379–386. https://doi.org/10.1016/j.ijcard.2017.03.099

Kolanowski, Tomasz J., Antos, C. L., & Guan, K. (2017b). Making human cardiomyocytes up to date: Derivation, maturation state and perspectives. *International Journal of Cardiology*, *241*, 379–386. https://doi.org/10.1016/j.ijcard.2017.03.099

Kolanowski, Tomasz Jan, Busek, M., Schubert, M., Dmitrieva, A., Binnewerg, B., Pöche, J., Fisher, K., Schmieder, F., Grünzner, S., Hansen, S., Richter, A., El-Armouche, A., Sonntag, F., & Guan, K. (2020a). Enhanced structural maturation of human induced pluripotent stem cell-derived cardiomyocytes under a controlled microenvironment in a microfluidic system. *Acta Biomaterialia*, *102*, 273–286. https://doi.org/10.1016/j.actbio.2019.11.044

Kolanowski, Tomasz Jan, Busek, M., Schubert, M., Dmitrieva, A., Binnewerg, B., Pöche, J., Fisher, K., Schmieder, F., Grünzner, S., Hansen, S., Richter, A., El-Armouche, A., Sonntag, F., & Guan, K. (2020b). Enhanced structural maturation of human induced pluripotent stem cell-derived cardiomyocytes under a controlled microenvironment in a microfluidic system. *Acta Biomaterialia*, *102*, 273–286. https://doi.org/10.1016/j.actbio.2019.11.044

Kovacic, J. C., Dimmeler, S., Harvey, R. P., Finkel, T., Aikawa, E., Krenning, G., & Baker, A. H. (2019). Endothelial to Mesenchymal Transition in Cardiovascular Disease: JACC State-of-the-Art Review. *Journal of the American College of Cardiology*, *73*(2), 190–209. https://doi.org/10.1016/j.jacc.2018.09.089

Krüger-genge, A., Blocki, A., Franke, R., & Jung, F. (2019). *Vascular Endothelial Cell Biology : An Update*.

Kular, J. K., Basu, S., & Sharma, R. I. (2014). The extracellular matrix: Structure, composition, age-related differences, tools for analysis and applications for tissue engineering. *Journal of Tissue Engineering*, *5*. https://doi.org/10.1177/2041731414557112

Kumar, K. R., Kirsch, R. E., & Hornik, C. P. (2019). 13 - Cardiovascular Physiology for Intensivists. In *Critical Heart Disease in Infants and Children (Third Edition* (Issue in cm). https://doi.org/10.1016/B978-1-4557-0760-7.00013-9

Künzel, S. R., Rausch, J. S. E., Schäffer, C., Hoffmann, M., Künzel, K., Klapproth, E., Kant, T., Herzog, N., Küpper, J. H., Lorenz, K., Dudek, S., Emig, R., Ravens, U., Rog-Zielinska, E. A., Peyronnet, R., & El-Armouche, A. (2020). Modeling atrial fibrosis in vitro—Generation and characterization of a novel human atrial fibroblast cell line. *FEBS Open Bio*, *10*(7), 1210–1218. https://doi.org/10.1002/2211-5463.12896

Kuo, I. Y., & Ehrlich, B. E. (2008). Muscle sliding filaments. *Cold Spring Harb Perspect Biol*, *19*(DeceMbeR), 2008.

Lajiness, J. D., & Conway, S. J. (2014). Origin, development, and differentiation of cardiac fibroblasts. *Journal of Molecular and Cellular Cardiology*, *70*(317), 2–8. https://doi.org/10.1016/j.yjmcc.2013.11.003

Lian, X., Zhang, J., Azarin, S. M., Zhu, K., Hazeltine, L. B., Bao, X., Hsiao, C., Kamp, T. J., & Palecek, S. P. (2013). Directed cardiomyocyte differentiation from human pluripotent stem cells by modulating Wnt/β-catenin signaling under fully defined conditions. *Nature Protocols*, *8*(1), 162–175. https://doi.org/10.1038/nprot.2012.150

Lin, C. D., Lin, C. D., Tona, F., & Osto, E. (2019). *The crosstalk between the cardiovascular and the immune system*. *8*, 83–88.

Litviňuková, M., Talavera-López, C., Maatz, H., Reichart, D., Worth, C. L., Lindberg, E. L., Kanda, M., Polanski, K., Heinig, M., Lee, M., Nadelmann, E. R., Roberts, K., Tuck, L., Fasouli, E. S., DeLaughter, D. M., McDonough, B., Wakimoto, H., Gorham, J. M., Samari, S., … Teichmann, S. A. (2020). Cells of the adult human heart. *Nature*, *588*(7838), 466–472. https://doi.org/10.1038/s41586-020-2797-4

Lopaschuk, G. D., & Jaswal, J. S. (2010). Energy metabolic phenotype of the cardiomyocyte during development, differentiation, and postnatal maturation. *Journal of Cardiovascular Pharmacology*, *56*(2), 130–140. https://doi.org/10.1097/FJC.0b013e3181e74a14

Lundy, S. D., Zhu, W. Z., Regnier, M., & Laflamme, M. A. (2013). Structural and functional maturation of cardiomyocytes derived from human pluripotent stem cells. *Stem Cells and Development*, *22*(14), 1991–2002. https://doi.org/10.1089/scd.2012.0490

Ma, F., Li, Y., Jia, L., Han, Y., Cheng, J., Li, H., Qi, Y., & Du, J. (2012). Macrophage-stimulated cardiac fibroblast production of IL-6 is essential for TGF β/Smad activation and cardiac fibrosis induced by angiotensin II. *PLoS ONE*, *7*(5), 1–9. https://doi.org/10.1371/journal.pone.0035144

Maass, K., Shekhar, A., Lu, J., Kang, G., See, F., Kim, E. E., Delgado, C., Shen, S., Cohen, L., &

Fishman, G. I. (2015). Isolation and characterization of embryonic stem cell-derived cardiac purkinje cells. *Stem Cells*, *33*(4), 1102–1112. https://doi.org/10.1002/stem.1921

Manabe, I., Shindo, T., & Nagai, R. (2002). Gene expression in fibroblasts and fibrosis involvement in cardiac hypertrophy. *Circulation Research*, *91*(12), 1103–1113. https://doi.org/10.1161/01.RES.0000046452.67724.B8

Marczenke, M., Piccini, I., Mengarelli, I., Fell, J., Röpke, A., Seebohm, G., Verkerk, A. O., & Greber, B. (2017). Cardiac subtype-specific modeling of Kv1.5 ion channel deficiency using human pluripotent stem cells. *Frontiers in Physiology*, *8*(JUL), 1–11. https://doi.org/10.3389/fphys.2017.00469

Maria, B. Y., Gallo, P. I. A., Alloatti, G., Eva, C., Oberto, A., & Levi, R. C. (1993). *Biologia Farmacologia*. 41–60.

Martin, S. S., Aday, A. W., Almarzooq, Z. I., Anderson, C. A. M., Arora, P., Avery, C. L., Baker-smith, C. M., Gibbs, B. B., Beaton, A. Z., Boehme, A. K., Commodore-mensah, Y., Currie, M. E., Elkind, M. S. V, Evenson, K. R., Generoso, G., & Heard, D. G. (2024). *2024 Heart Disease and Stroke Statistics : A Report of US and Global Data From the American Heart Association*. https://doi.org/10.1161/CIR.0000000000001209

Mathur, A., Loskill, P., Shao, K., Huebsch, N., Hong, S. G., Marcus, S. G., Marks, N., Mandegar, M., Conklin, B. R., Lee, L. P., & Healy, K. E. (2015). Human iPSC-based cardiac microphysiological system for drug screening applications. *Scientific Reports*, *5*, 1–7. https://doi.org/10.1038/srep08883

Milacic, M., Bea, D., Gong, C., Gillespie, M., Griss, J., Haw, R., Jassal, B., Matthews, L., May, B., Petryszak, R., Ragueneau, E., Rothf, K., Shamovsky, V., Stephan, R., Weiser, J., W, A., Guanming, W., Stein, L., Hermjakob, H., & Eustachio, P. D. (2024). *The Reactome Pathway Knowledgebase 2024*. *November 2023*, 672–678.

Misra, C., & Garg, V. (2013). Compacting the heart with Notch. *Nature Medicine*, *19*(2), 133–134. https://doi.org/10.1038/nm.3071

Moore-Morris, T., Guimarães-Camboa, N., Banerjee, I., Zambon, A. C., Kisseleva, T., Velayoudon, A., Stallcup, W. B., Gu, Y., Dalton, N. D., Cedenilla, M., Gomez-Amaro, R., Zhou, B., Brenner, D. A., Peterson, K. L., Chen, J., & Evans, S. M. (2014). Resident fibroblast lineages mediate pressure overload-induced cardiac fibrosis. *Journal of Clinical Investigation*, *124*(7), 2921–2934. https://doi.org/10.1172/JCI74783

Moore-Morris, T., Guimarães-Camboa, N., Yutzey, K. E., Pucéat, M., & Evans, S. M. (2015).

Cardiac fibroblasts: from development to heart failure. *Journal of Molecular Medicine*, *93*(8), 823–830. https://doi.org/10.1007/s00109-015-1314-y

Morrison, J. L., Botting, K. J., Darby, J. R. T., David, A. L., Dyson, R. M., Gatford, K. L., Gray, C., Herrera, E. A., Hirst, J. J., Kim, B., Kind, K. L., Krause, B. J., Matthews, S. G., Palliser, H. K., Regnault, T. R. H., Richardson, B. S., Sasaki, A., Thompson, L. P., & Berry, M. J. (2018). Guinea pig models for translation of the developmental origins of health and disease hypothesis into the clinic. *Journal of Physiology*, *596*(23), 5535–5569. https://doi.org/10.1113/JP274948

Mukherjee, P., Roy, S., Ghosh, D., & Nandi, S. K. (2022). Role of animal models in biomedical research: a review. *Laboratory Animal Research*, *38*(1), 1–17. https://doi.org/10.1186/s42826-022-00128-1

Munshi, N. V. (2012). Gene regulatory networks in cardiac conduction system development. *Circulation Research*, *110*(11), 1525–1537. https://doi.org/10.1161/CIRCRESAHA.111.260026

Nakajima, Y. (2019). *Retinoic acid signaling in heart development*. *December 2018*, 1–17. https://doi.org/10.1002/dvg.23300

Nakano, S., Muramatsu, T., Nishimura, S., & Senbonmatsu, T. (2012). Cardiomyocyte and Heart Failure. *Current Basic and Pathological Approaches to the Function of Muscle Cells and Tissues - From Molecules to Humans*, *i*(Fig 1). https://doi.org/10.5772/47772

Nattel, S. (2002). New ideas about atrial fibrillation 50 years on. *Nature*, *415*(6868), 219–226. https://doi.org/10.1038/415219a

O'Donnell, A., & Yutzey, K. E. (2020). To EndoMT or Not to EndoMT: Zebrafish Heart Valve Development. *Circulation Research*, 985–987. https://doi.org/10.1161/CIRCRESAHA.120.316846

Ongstad, E., & Kohl, P. (2016). Fibroblast-myocyte coupling in the heart: Potential relevance for therapeutic interventions. *Journal of Molecular and Cellular Cardiology*, *91*, 238–246. https://doi.org/10.1016/j.yjmcc.2016.01.010

Papke, C. L., & Yanagisawa, H. (2015). Fibulin-4 and Fibulin-5 in elastogenesis and beyond: insights from mouse and human studies. *Matrix Biology*, 142–149. https://doi.org/10.1016/j.matbio.2014.02.004.Fibulin-4

Park, D. S., & Fishman, G. I. (2014). Cell Biology of the Specialized Cardiac Conduction System. In *Cardiac Electrophysiology: From Cell to Bedside: Sixth Edition* (Sixth Edit, Vol. 5). Elsevier

Inc. https://doi.org/10.1016/B978-1-4557-2856-5.00029-7

Pesce, M., Duda, G. N., Forte, G., Girao, H., Raya, A., Roca-Cusachs, P., Sluijter, J. P. G., Tschöpe, C., & Van Linthout, S. (2022). Cardiac fibroblasts and mechanosensation in heart development, health and disease. *Nature Reviews Cardiology*, *November*. https://doi.org/10.1038/s41569-022-00799-2

Pinnell, J., Turner, S., & Howell, S. (2007). Cardiac muscle physiology. *Continuing Education in Anaesthesia, Critical Care and Pain*, *7*(3), 85–88. https://doi.org/10.1093/bjaceaccp/mkm013

Plikus, M. V., Wang, X., Sinha, S., Forte, E., Thompson, S. M., Herzog, E. L., Driskell, R. R., Rosenthal, N., Biernaskie, J., & Horsley, V. (2021). Fibroblasts: Origins, definitions, and functions in health and disease. *Cell*, *184*(15), 3852–3872. https://doi.org/10.1016/j.cell.2021.06.024

Pogwizd, S. M., & Bers, D. M. (2008). Rabbit models of heart disease. *Drug Discovery Today: Disease Models*, *5*(3), 185–193. https://doi.org/10.1016/j.ddmod.2009.02.001

Polak, S., & Fijorek, K. (2012). Inter-individual variability in the pre-clinical drug cardiotoxic safety assessment-analysis of the age-cardiomyocytes electric capacitance dependence. *Journal of Cardiovascular Translational Research*, *5*(3), 321–332. https://doi.org/10.1007/s12265-012-9357-8

Press release. NobelPrize.org. (n.d.). *The Nobel Prize in Physiology or Medicine 2012*. https://www.nobelprize.org/prizes/medicine/2012/press-release/

Querejeta, R., López, B., González, A., Sánchez, E., Larman, M., Martínez Ubago, J. L., & Díez, J. (2004). Increased collagen type I synthesis in patients with heart failure of hypertensive origin: Relation to myocardial fibrosis. *Circulation*, *110*(10), 1263–1268. https://doi.org/10.1161/01.CIR.0000140973.60992.9A

Razmara, E., & Garshasbi, M. (2018). Whole-exome sequencing identifies R1279X of MYH6 gene to be associated with congenital heart disease. *BMC Cardiovascular Disorders*, *18*(1), 1–7. https://doi.org/10.1186/s12872-018-0867-4

Richards, D. J., Li, Y., Kerr, C. M., Yao, J., Beeson, G. C., Coyle, R. C., Chen, X., Jia, J., Damon, B., Wilson, R., Starr Hazard, E., Hardiman, G., Menick, D. R., Beeson, C. C., Yao, H., Ye, T., & Mei, Y. (2020). Human cardiac organoids for the modelling of myocardial infarction and drug cardiotoxicity. *Nature Biomedical Engineering*, *4*(4), 446–462. https://doi.org/10.1038/s41551-020-0539-4

Ricklin, D., Lambris, J. D., Ricklin, D., & Lambris, J. D. (2013). *Complement in Immune and Inflammatory Disorders: Therapeutic Interventions*. https://doi.org/10.4049/jimmunol.1203200

Rogers, J. D., Holmes, J. W., Saucerman, J. J., & Richardson, W. J. (2021). Mechano-chemo signaling interactions modulate matrix production by cardiac fibroblasts. *Matrix Biology Plus*, *10*, 100055. https://doi.org/10.1016/j.mbplus.2020.100055

Saito, Y., Nakamura, K., Yoshida, M., Sugiyama, H., Akagi, S., Miyoshi, T., Morita, H., & Ito, H. (2022). Enhancement of pacing function by HCN4 overexpression in human pluripotent stem cell-derived cardiomyocytes. *Stem Cell Research and Therapy*, *13*(1), 1–13. https://doi.org/10.1186/s13287-022-02818-y

Sakamiya, M., Fang, Y., Mo, X., Shen, J., & Zhang, T. (2020). A heart-on-a-chip platform for online monitoring of contractile behavior via digital image processing and piezoelectric sensing technique. *Medical Engineering and Physics*, *75*, 36–44. https://doi.org/10.1016/j.medengphy.2019.10.001

Saleem, U., Mannhardt, I., Braren, I., Denning, C., Eschenhagen, T., & Hansen, A. (2020). Force and Calcium Transients Analysis in Human Engineered Heart Tissues Reveals Positive Force-Frequency Relation at Physiological Frequency. *Stem Cell Reports*, *14*(2), 312–324. https://doi.org/10.1016/j.stemcr.2019.12.011

Sandell, L. L., Sanderson, B. W., Moiseyev, G., Johnson, T., Mushegian, A., Young, K., Rey, J., Ma, J., Staehling-hampton, K., & Paul, A. (2007). *RDH10 is essential for synthesis of embryonic retinoic acid and is required for limb , craniofacial , and organ development*. 1113–1124. https://doi.org/10.1101/gad.1533407.binding

Santana, L. F., Cheng, E. P., & Lederer, W. J. (2010). How does the shape of the cardiac action potential control calcium signaling and contraction in the heart? *Journal of Molecular and Cellular Cardiology*, *49*(6), 901–903. https://doi.org/10.1016/j.yjmcc.2010.09.005

Shaffer, F., McCraty, R., & Zerr, C. L. (2014). A healthy heart is not a metronome: an integrative review of the heart's anatomy and heart rate variability. *Frontiers in Psychology*, *5*(September), 1–19. https://doi.org/10.3389/fpsyg.2014.01040

Shao, S., Cai, W., Sheng, J., & Yin, L. (2015). Role of SDF-1 and Wnt signaling pathway in the myocardial fibrosis of hypertensive rats. *American Journal of Translational Research*, *7*(8), 1345–1356.

Sharma, V. K., Colecraft, H. M., Wang, D. X., Levey, A. I., Grigorenko, E. V, Yeh, H. H., & Sheu, S.

(n.d.). *Molecular and Functional Identification of nil Muscarinic Acetylcholine Receptors in Rat Ventricular Myocytes*. https://doi.org/10.1161/01.RES.79.1.86

Shen, J. Z., Morgan, J., Tesch, G. H., Fuller, P. J., & Young, M. J. (2014). CCL2-dependent macrophage recruitment is critical for mineralocorticoid receptor-mediated cardiac fibrosis, inflammation, and blood pressure responses in male mice. *Endocrinology*, *155*(3), 1057–1066. https://doi.org/10.1210/en.2013-1772

Shull, S. A., Rich, S. K., Gillette, R. L., & Manfredi, J. M. (2021). Heart Rate Changes Before, During, and After Treadmill Walking Exercise in Normal Dogs. *Frontiers in Veterinary Science*, *8*(April), 1–7. https://doi.org/10.3389/fvets.2021.641871

Siddique, I., Kamble, K., Gupta, S., Solanki, K., Bhola, S., & Ahsan, N. (2023). *ARL6IP5 Ameliorates α -Synuclein Burden by Inducing Autophagy via Preventing Ubiquitination and Degradation of ATG12*.

Simó-Vicens, R., Kirchhoff, J. E., Dolce, B., Abildgaard, L., Speerschneider, T., Sørensen, U. S., Grunnet, M., Diness, J. G., & Bentzen, B. H. (2017). A new negative allosteric modulator, AP14145, for the study of small conductance calcium-activated potassium (KCa2) channels. *British Journal of Pharmacology*, *174*(23), 4396–4408. https://doi.org/10.1111/bph.14043

Skorska, A., Johann, L., Chabanovska, O., Vasudevan, P., Kussauer, S., Hillemanns, M., Wolfien, M., Jonitz-Heincke, A., Wolkenhauer, O., Bader, R., Lang, H., David, R., & Lemcke, H. (2022). Monitoring the maturation of the sarcomere network: a super-resolution microscopy-based approach. *Cellular and Molecular Life Sciences*, *79*(3), 1–16. https://doi.org/10.1007/s00018-022-04196-3

Solaro, R. J. (2007). Mechanisms of the Frank-Starling law of the heart: The beat goes on. *Biophysical Journal*, *93*(12), 4095–4096. https://doi.org/10.1529/biophysj.107.117200

Song, J. J., & Ott, H. C. (2011). Organ engineering based on decellularized matrix scaffolds. *Trends in Molecular Medicine*, *17*(8), 424–432. https://doi.org/10.1016/j.molmed.2011.03.005

Stone, R. C., Pastar, I., Ojeh, N., Chen, V., Liu, S., Garzon, K. I., & Tomic-Canic, M. (2016). Epithelial-mesenchymal transition in tissue repair and fibrosis. *Cell and Tissue Research*, *365*(3), 495–506. https://doi.org/10.1007/s00441-016-2464-0

Strauss, D., Jacqueline, S., Nelson, C., & Raghuwanshi, R. (2022). *Advancing Alternative Methods for Regulatory Use Presentation to the FDA Science Board on Behalf of Thank You to FDA New Alternative Methods Group Members*.

Streckfuss-Bömeke, K., Wolf, F., Azizian, A., Stauske, M., Tiburcy, M., Wagner, S., Hübscher, D.,

Dressel, R., Chen, S., Jende, J., Wulf, G., Lorenz, V., Schön, M. P., Maier, L. S., Zimmermann, W. H., Hasenfuss, G., & Guan, K. (2013). Comparative study of human-induced pluripotent stem cells derived from bone marrow cells, hair keratinocytes, and skin fibroblasts. *European Heart Journal*, *34*(33), 2618–2629. https://doi.org/10.1093/eurheartj/ehs203

Sun, Z., Zhao, J., Leung, E., Flandes-iparraguirre, M., Vernon, M., Silberstein, J., De-juan-pardo, E. M., & Jansen, S. (2023). *Three-Dimensional Bioprinting in Cardiovascular Disease : Current Status and Future Directions*.

Szklarczyk, D., Kirsch, R., Koutrouli, M., Nastou, K., Mehryary, F., Hachilif, R., Gable, A. L., Fang, T., Doncheva, N. T., Pyysalo, S., Bork, P., Jensen, L. J., & Mering, C. Von. (2023). *The STRING database in 2023 : protein – protein association networks and functional enrichment analyses for any sequenced genome of interest*. *51*(November 2022), 638–646.

Takahashi, K., & Yamanaka, S. (2006). Induction of Pluripotent Stem Cells from Mouse Embryonic and Adult Fibroblast Cultures by Defined Factors. *Cell*, *126*(4), 663–676. https://doi.org/10.1016/j.cell.2006.07.024

Tang, S., Li, R., Ma, W., Lian, L., Gao, J., Cao, Y., & Gan, L. (2023). Cardiac - to - adipose axis in metabolic homeostasis and diseases : special instructions from the heart. *Cell & Bioscience*, 1–15. https://doi.org/10.1186/s13578-023-01097-1

Tani, H., & Tohyama, S. (2022). Human Engineered Heart Tissue Models for Disease Modeling and Drug Discovery. *Frontiers in Cell and Developmental Biology*, *10*(March), 1–21. https://doi.org/10.3389/fcell.2022.855763

Taylor, D. A., Sampaio, L. C., Cabello, R., Elgalad, A., Parikh, R., Wood, R. P., Myer, K. A., Yeh, A. T., & Lee, P. F. (2018). Decellularization of whole human heart inside a pressurized pouch in an inverted orientation. *Journal of Visualized Experiments*, *2018*(141), 1–11. https://doi.org/10.3791/58123

Thomas, P. D., & Mushayahama, T. (2022). *PANTHER : Making genome-scale phylogenetics accessible to all*. *October 2021*, 8–22. https://doi.org/10.1002/pro.4218

Thompson, B., Katsanis, N., Apostolopoulos, N., Thompson, D. C., Nebert, D. W., & Vasiliou, V. (2019). *Genetics and functions of the retinoic acid pathway , with special emphasis on the eye*. 1–15.

Thomsen, M. B., & Calloe, K. (2016). Human atrial fibroblasts and their contribution to supraventricular arrhythmia. *Physiological Reports*, *4*(3), 3–5. https://doi.org/10.14814/phy2.12711

Tiburcy, M. (2014). *Collagen-Based Engineered Heart Muscle*. *1181*, 61–68. https://doi.org/10.1007/978-1-4939-1047-2

Tirziu, D., Giordano, F. J., & Simons, M. (2010). Cell Communications in the Heart. *Circulation.*, *122*(9), 928–937. https://doi.org/10.1161/CIRCULATIONAHA.108.847731.Cell

Tohyama, S., Hattori, F., Sano, M., Hishiki, T., Nagahata, Y., Matsuura, T., Hashimoto, H., Suzuki, T., Yamashita, H., Satoh, Y., Egashira, T., Seki, T., Muraoka, N., Yamakawa, H., Ohgino, Y., Tanaka, T., Yoichi, M., Yuasa, S., Murata, M., … Fukuda, K. (2013). Distinct metabolic flow enables large-scale purification of mouse and human pluripotent stem cell-derived cardiomyocytes. *Cell Stem Cell*, *12*(1), 127–137. https://doi.org/10.1016/j.stem.2012.09.013

Toyoda, Y., Okada, M., & Kashem, M. A. (1998). A canine model of dilated cardiomyopathy induced by repetitive intracoronary doxorubicin administration. *Journal of Thoracic and Cardiovascular Surgery*, *115*(6), 1367–1373. https://doi.org/10.1016/S0022-5223(98)70221-1

Uscategui Calderon, M., Gonzalez, B. A., & Yutzey, K. E. (2023). Cardiomyocyte-fibroblast crosstalk in the postnatal heart. *Frontiers in Cell and Developmental Biology*, *11*(April), 1–12. https://doi.org/10.3389/fcell.2023.1163331

Van Den Heuvel, N. H. L., Van Veen, T. A. B., Lim, B., & Jonsson, M. K. B. (2014). Lessons from the heart: Mirroring electrophysiological characteristics during cardiac development to in vitro differentiation of stem cell derived cardiomyocytes. *Journal of Molecular and Cellular Cardiology*, *67*, 12–25. https://doi.org/10.1016/j.yjmcc.2013.12.011

Vasquez, C., Benamer, N., & Morley, G. E. (2011). The cardiac fibroblast: Functional and electrophysiological considerations in healthy and diseased hearts. *Journal of Cardiovascular Pharmacology*, *57*(4), 380–388. https://doi.org/10.1097/FJC.0b013e31820cda19

Vega-Hernández, M., Kovacs, A., de Langhe, S., & Ornitz, D. M. (2011). FGF10/FGFR2b signaling is essential for cardiac fibroblast development and growth of the myocardium. *Development*, *138*(15), 3331–3340. https://doi.org/10.1242/dev.064410

Vliegen, H. W., Van Der Laarse, A., Cornelisse, C. J., & Eulderink, F. (1991). Myocardial changes in pressure overload-induced left ventricular hypertrophy: A study on tissue composition, polyploidization and multinucleation. *European Heart Journal*, *12*(4), 488–494. https://doi.org/10.1093/oxfordjournals.eurheartj.a059928

von Bibra, C., Shibamiya, A., Geertz, B., Querdel, E., Köhne, M., Stüdemann, T., Starbatty, J., Schmidt, F. N., Hansen, A., Hiebl, B., Eschenhagen, T., & Weinberger, F. (2022). Human engineered heart tissue transplantation in a guinea pig chronic injury model. *Journal of Molecular and Cellular Cardiology*, *166*(January), 1–10. https://doi.org/10.1016/j.yjmcc.2022.01.007

Wadman, M. (2023). FDA no longer has to require animal testing for new drugs. *Science*, *379*(6628), 127–128. https://doi.org/10.1126/science.adg6276

Walklate, J., Ferrantini, C., Johnson, C. A., Tesi, C., Poggesi, C., & Geeves, M. A. (2021). Alpha and beta myosin isoforms and human atrial and ventricular contraction. *Cellular and Molecular Life Sciences*, *78*(23), 7309–7337. https://doi.org/10.1007/s00018-021-03971-y

Warkman, A. S., Whitman, S. A., Miller, M. K., Garriock, R. J., Schwach, C. M., Gregorio, C. C., & Krieg, P. A. (2012). Developmental expression and cardiac transcriptional regulation of Myh7b, a third myosin heavy chain in the vertebrate heart. *Cytoskeleton*, *69*(5), 324–335. https://doi.org/10.1002/cm.21029

Watanabe, Y., Seya, D., Ihara, D., Ishii, S., Uemoto, T., Kubo, A., Arai, Y., Isomoto, Y., Nakano, A., Abe, T., Shigeta, M., Kawamura, T., Saito, Y., Ogura, T., & Nakagawa, O. (2020). Importance of endothelial Hey1 expression for thoracic great vessel development and its distal enhancer for Notch-dependent endothelial transcription. *Journal of Biological Chemistry*, *295*(51), 17632–17645. https://doi.org/10.1074/jbc.RA120.015003

Watanabe, Y., Wang, Y., Tanaka, Y., & Iwase, A. (2023). *Hey2 enhancer activity defines unipotent progenitors for left ventricular cardiomyocytes in juxta- - cardiac field of early mouse embryo*. 1–10. https://doi.org/10.1073/pnas.

Weisbrod, D. (2020). Small and Intermediate Calcium Activated Potassium Channels in the Heart: Role and Strategies in the Treatment of Cardiovascular Diseases. *Frontiers in Physiology*, *11*(November), 1–18. https://doi.org/10.3389/fphys.2020.590534

Wiesinger, A., Boink, G. J. J., Christoffels, V. M., & Devalla, H. D. (2021). Retinoic acid signaling in heart development: Application in the differentiation of cardiovascular lineages from human pluripotent stem cells. *Stem Cell Reports*, *16*(11), 2589–2606. https://doi.org/10.1016/j.stemcr.2021.09.010

Wobus, A. M., Kaomei, G., Shan, J., & Wellner, M. (1997). *Retinoic Acid Accelerates Embryonic Stem Cell-Derived Cardiac Differentiation and Enhances Development of Ventricular Cardiomyocytes*. *1539*, 1525–1539.

World Health Organization. (2021). *Cardiovascular diseases (CVDs)*. https://www.who.int/news-room/fact-sheets/detail/c.

Wu, H., Lee, J., Vincent, L. G., Wang, Q., Gu, M., Lan, F., Churko, J. M., Sallam, K. I., Matsa, E., Sharma, A., Gold, J. D., Engler, A. J., Xiang, Y. K., Bers, D. M., & Wu, J. C. (2015). Epigenetic Regulation of Phosphodiesterases 2A and 3A Underlies Compromised β-Adrenergic Signaling in an iPSC Model of Dilated Cardiomyopathy. *Cell Stem Cell*, *17*(1), 89–100. https://doi.org/10.1016/j.stem.2015.04.020

Xiao, Y., Zhang, B., Liu, H., Miklas, J. W., Gagliardi, M., Pahnke, A., Thavandiran, N., Sun, Y., Simmons, C., Keller, G., & Radisic, M. (2014). Microfabricated perfusable cardiac biowire: A platform that mimics native cardiac bundle. *Lab on a Chip*, *14*(5), 869–882. https://doi.org/10.1039/c3lc51123e

Yamada, N., Asano, Y., Fujita, M., Yamazaki, S., Inanobe, A., Matsuura, N., Kobayashi, H., Ohno, S., Ebana, Y., Tsukamoto, O., Ishino, S., Takuwa, A., Kioka, H., Yamashita, T., Hashimoto, N., Zankov, D. P., Shimizu, A., Asakura, M., Asanuma, H., … Takashima, S. (2019). Mutant KCNJ3 and KCNJ5 Potassium Channels as Novel Molecular Targets in Bradyarrhythmias and Atrial Fibrillation. *Circulation*, *139*(18), 2157–2169. https://doi.org/10.1161/CIRCULATIONAHA.118.036761

Yang, X., Pabon, L., & Murry, C. E. (2014). Engineering adolescence: Maturation of human pluripotent stem cell-derived cardiomyocytes. *Circulation Research*, *114*(3), 511–523. https://doi.org/10.1161/CIRCRESAHA.114.300558

Yang, X., Rodriguez, M., Pabon, L., Fischer, K. A., Reinecke, H., Regnier, M., Sniadecki, N. J., Ruohola-Baker, H., & Murry, C. E. (2014). Tri-iodo-l-thyronine promotes the maturation of human cardiomyocytes-derived from induced pluripotent stem cells. *Journal of Molecular and Cellular Cardiology*, *72*, 296–304. https://doi.org/10.1016/j.yjmcc.2014.04.005

Yoo, B., Lemaire, A., Mangmool, S., Wolf, M. J., Curcio, A., Mao, L., & Rockman, H. A. (2009). *1 -Adrenergic receptors stimulate cardiac contractility and CaMKII activation in vivo and enhance cardiac dysfunction following myocardial infarction*. *240*. https://doi.org/10.1152/ajpheart.00504.2009.

Zebrowski, D. C., Becker, R., & Engel, F. B. (2016). Towards regenerating the mammalian heart: Challenges in evaluating experimentally induced adult mammalian cardiomyocyte proliferation. *American Journal of Physiology - Heart and Circulatory Physiology*, *310*(9), H1045–H1054. https://doi.org/10.1152/ajpheart.00697.2015

Zhang, Q., Jiang, J., Han, P., Yuan, Q., Zhang, J., Zhang, X., Xu, Y., Cao, H., Meng, Q., Chen, L., Tian, T., Wang, X., Li, P., Hescheler, J., Ji, G., & Ma, Y. (2011). Direct differentiation of atrial and ventricular myocytes from human embryonic stem cells by alternating retinoid signals. *Cell Research*, *21*(4), 579–587. https://doi.org/10.1038/cr.2010.163

PUBLICATIONS

Work published during the PhD studies:

- Kałużna, E., **Nadel, A**., Zimna, A., Rozwadowska, N., Kolanowski, T.J. (2022). Modeling the human heart ex vivo - current possibilities and strive for future applications. *J Tissue Eng Regen Med*.16(10):853 - 874.doi: 10.1002/term.3335. IF - 4.3

- Yépez, V.A., Gusic, M., Kopajtich, R., Mertes, C., Smith, N.H., Alston, C.L., Berutti, R., Blessing, H., Ciara, E., Fang, F., Freisinger, P., Ghezzi, D., Hayflick, S.J., Kishita, Y., Klopstock, T., Lamperti, C., Lenz, D., Makowski, C.C., Mayr, J.A., Mosegaard, S., Müller, M.F., Muñoz - Pujol, G., Murayama, K., **Nadel, A**., (…), Meitinger, T., Gagneur, J., Prokisch, H.(2022).Clinical implementation of RNA sequencing for Mendelian disease diagnostics. *Genome Med*, 4(1): 38.doi: 10.1186/s13073 - 022 - 01019 - 9. IF - 10.7

- Kopajtich, R., Smirnov, D., Stenton, S.L., Loipfinger, S., Meng, C., Scheller, I.F., Freisinger, P., Baski, R., Berutti, R., Behr, J., Bucher, M., Distelmaier, F., Gusic, M., Hempel, M., Kulterer, L., Mayr, J ., Meitinger, T ., Mertes, C ., Metodiev, M.D., **Nadel, A.,** (…), Gagneur, J., Prokisch, H.(2021).Integration of proteomics with genomics and transcriptomics increases the diagnostic rate of Mendelian disorders. *MedRxiv*.doi: 10.1101/2021.03.09.21253187.

- Madeja, Z.E., Podralska, M., **Nadel, A.,** Pszczoła, M., Pawlak, P., & Rozwadowska, N. (2021). Mitochondria Content and Activity Are Crucial Parameters for Bull Sperm Quality Evaluation. *Antioxidants (Basel)*, 10(8): 1204.doi: 10.3390/antiox10081204. IF - 7.7

- Yépez, V.A., Kremer, L.S., Iuso, A., Gusic, M., Kopajtich, R., Koňaříkova, E., **Nadel, A.,** Wachutka, L., Prokisch, H., & Gagneur, J. (2018). OCR - Stats: Robust estimation and statistical testing of mitochondrial respiration activities using seahorse xf analyzer. *PLoS ONE*, 13(7), 1–18.doi: 10.1371/journal.pone.0199938. IF - 3.2